Synthesis and Characterization of Functional Diblock Copolymers

Dissertation

zur Erlangung des Doktorgrades

der Naturwissenschaften

im Fachbereich Chemie

der Universität Duisburg-Essen

vorgelegt von

Sachin Borkar

aus Pune (Indien)

November 2003

Statement

The work described in this thesis was carried out in the laboratories of the University of Duisburg-Essen, Department of Physical Chemistry, Essen, Germany, and The Danish Polymer Centre, Technical University of Denmark, Kgs. Lyngby, Denmark, between January 2001 and October 2003. Except for the elemental analysis and the optical anisotropy measurements (Chapter 4.4) this work is entirely that of the author.

Date of the oral examination: November 11, 2003
Referee: Prof. Dr. H. W. Siesler
Coreferee: Prof. Dr. M. Ulbricht

Dedicated
to my
Parents

Preface

The thesis entitled "Synthesis and Characterization of Functional Diblock Copolymers" is submitted to the University of Duisburg-Essen, Germany, for the award of a PhD degree in Chemistry.

The work reported here was carried out under the guidance of Prof. Dr. H. W. Siesler (Department of Chemistry, University of Duisburg-Essen, Essen) and Prof. Dr. S. Hvilsted (The Danish Polymer Centre, Technical University of Denmark, Lyngby, Denmark).

I am sincerely thankful to Professor Heinz Siesler, for his timely help and giving me an opportunity to work under his guidance. I am also grateful for his great care not only in academic but also for kind help for social life during my stay in Germany.

I am deeply thankful to Professor Søren Hvilsted for his guidance and immense cooperation during my stay at the Technical University of Denmark. Also I am very much thankful for the fruitful discussions and his great help during the process of publications and thesis writing.

Special thanks are due to Dr. Katja Jankova, for her helpfulness during my stay in the Danish Polymer Centre. And also to Professor Mathias Ulbricht for providing me the synthetic facility at the Technical Chemistry Department of the University of Duisburg-Essen.

I am very much thankful to my elder brother Mr. Praveen Borkar, for his inspiration and support.

The staff at The Danish Polymer Centre, Denmark and Department of Physical Chemistry and Department of Organic Chemistry at the University of Duisburg-Essen, is thanked for providing a very friendly and cooperative atmosphere. Special thanks to Dr. P.S. Ramanujam and Lian Nedelchev for optical anisotropy measurements.

Also, I am gratified to all my friends and colleagues for their moral support during my academic or non-academic life.

Finally I would like to express my most sincere indebtedness to my parents, other family members and research colleagues from National Chemical Laboratory, Pune, India, for their encouragement and support throughout my career. The financial support from the Ministry of Science and Education of North-Rhein Westfalia, Dusseldorf and the Danish Polymer Centre, Lyngby, Denmark are gratefully acknowledged.

Sachin Vinayak Borkar

Contents

Summary

In search of materials for high-density optical data storage by irradiation with polarized laser light liquid crystalline polymers containing azobenzene functionalities in the side chains have attracted great attention. These azobenzene groups generate different photoisomerization phenomena which can be exploited for optical data storage by using holographic techniques.

In this PhD study a new strategy for the synthesis of side chain liquid crystalline block copolymers is employed. SC-LC block copolymers with different composition of the mesogenic block and with different side chain spacer lengths were synthesized. The first approach used was the recent and most accepted radical polymerization technique Atom Transfer Radical Polymerization (ATRP). A side chain azobenzene containing styrene monomer was synthesized and successfully polymerized by ATRP technique. The second method used was the synthesis of template polystyrene block polybutoxystyrene (PS-*b*-PBS) copolymers by living anionic polymerization technique and successive deprotection to give PS-*b*-PHS. These polymers were then functionalized with azobenzene containing bromo precursors attached through a flexible alkyl spacer. The mesogenic monomers and block copolymers were characterized by ^{1}H-, ^{13}C-NMR spectroscopy and also by DSC. The molecular weight of the polymers was determined by SEC. Furthermore, the stability of the induced anisotropy in the mesogenic block copolymers was studied by optical analysis.

In order to synthesize thermally stable SC-LC polymers highly fluorinated styrene polymers were used as templates. The highly fluorinated new monomer 2,3,5,6-tetrafluoro-4-methoxystyrene (TFMS) was synthesized by a nucleophilic substitution reaction between 2,3,4,5,6-pentafluorostyrene (FS) and sodium methoxide. This monomer was then successfully polymerized in high yield and with low PDI by the ATRP method. The homopolymers were functionalized by demethylation and successive alkylations under phase transfer catalysis reactions with bromo precursors bearing different substituents. The ATRP of TFMS was comparatively faster than that of styrene and its highly fluorinated analogue FS. These results and the potential nucleophilic substitution in the *para* position of FS prompted us to attempt the preparation of novel FS monomers with 4-fluoroalkoxy side chains and subsequently investigate their polymerization potential with a view to the self assembly process of these materials at surfaces.

In this context materials with a fluorine content varying in a large range have been synthesized and characterized by different techniques. The ATRP technique was found as a suitable tool to control the M_n and also the PDI of the polymers.

Materials with low fluorine content were synthesized by use of fluorine containing initiators leaving the fluorine cluster at one end. Highly fluorinated materials were prepared by use of fluorine rich monomers TFMS, 2,3,5,6-tetrafluoro-4-(2,2,3,3,3-pentafluoropropoxy)styrene [TF(F_5)S] and 2,3,5,6-tetrafluoro-4-(2,2,3,3,4,4,5,5,6,6,7,7,8, 8,8-pentadecafluorooctaoxy)styrene [TF(F_{15})S], resulting in both homopolymers as well as block copolymers. Materials with an intermediate fluorine content were achieved by copolymerization of these monomers with styrene.

The TF(F_5)S and TF(F_{15})S are another two new monomers subjected for ATRP. These monomers were synthesized by a nucleophilic substitution reaction between FS and its corresponding alcohol. The structures of the monomers were confirmed by ^{1}H-, ^{13}C-, ^{19}F-NMR and also by FT-IR spectroscopy. The ATRP of these monomers results in fast polymerization and high yields. Polymers with relatively low PDI and in a broad range of M_n were synthesized. The block copolymers phase separate into PS/PFS phases as evidenced by two T_gs when the shortest block constitutes more than 10 mol %. A preliminary surface characterization of these polymers was performed by XPS and by measurement of the contact angle with water. Both analyses provide evidence for the segregation of fluorinated blocks resulting in low energy surfaces.

Abbreviations

A	absorbance
AcS	acetoxystyrene
an	anhydrous
ATRP	atom transfer radical polymerization
bipy	bipyridine
BuOSt	tertiary butoxystyrene
Bz	benzyl
C	concentration
CA	contact angle
CN	nitrile
Conv.	conversion
CRP	controlled radical polymerization
d	doublet
DCC	dicyclohexyl carbodiimide
DCM	dichloromethane
dd	double doublet
DMAP	dimethyl amino pyridine
DMSO	dimethyl sulfoxide
dnNbipy	dinonylbipyridine
DP	degree of polymerization
DSC	differential scanning calorimetry
$\bar{E}$	electric field vector
E_b	binding energy
E_k	kinetic energy
eq	equation
FS	2,3,4,5,6-pentafluorostyrene
FT-IR	fourier transform infrared
h	hour
HMTETA	1,1,4,7,10,10-hexamethyltriethylenetetraamine
I	initiator
k_a	rate constant for activation
k_d	rate constant for deactivation
k_{eq}	equilibrium constant
k_p	rate constant for propagation
k_t	rate constant for termination
LC	liquid crystal
LCP	liquid crystalline polymer
m	multiplet
M	monomer
MC-LCP	main chain liquid crystalline polymer
ME_6TREN	tris[2-(dimethylamino)ethyl]amine
MEK	methylethylketone
min	minute
MMA	methylmethacrylate
M_n	number average molecular weight
M_w	weight average molecular weight
MW	molecular weight
NMR	nuclear magnetic resonance
ODCB	1,2-dichlorobenzene

PAP	photoaddressable polymer
PBS	poly(*tert*-butoxystyrene)
PCPimine	2-pyridinecarboxaldehyde pentylimine
PDI	polydispersity index
PDMS	poly(dimethoxysiloxane)
PFS	poly(pentafluorostyrene)
PHS	poly(hydroxystyrene)
PIA	photoinduced anisotropy
PMDETA	1,1,4,7,7-pentamethyldiethylenetriamine
PMMA	poly(methylmethaacrylate)
$P_n^{\bullet}$	active polymer radical
ppm	parts per million
PS	polystyrene
PTFE	poly(tetrafluoroethylene)
q	quartet
Rec	receding
RI	refractive index
R_p	rate of propagation
RT	room temperature
s	singlet
S	smectic
SC-LCP	side chain liquid crystalline polymer
SEC	size exclusion chromatography
St	styrene
T	temperature
t	triplet
T_c	crystallization temperature
TEA	triethylamine
TEMPO	2,2,6,6-tetramethylpiperidinyl-1-oxy
TF(F_{15})S	2,3,5,6-tetrafluroro-4-(2,2,3,3,4,4,5,5,6,6,7,7,8,8,8-pentadecafluorooctaoxy) styrene
TF(F_5)S	tetrafluoro-4-(2,2,3,3,3-pentafluoropropoxy) styrene
TFMS	2,3,5,6-tetrafluoro-4-methoxystyrene
T_g	glass transition temperature
TGA	thermogravimetric analysis
TLC	thin layer chromatography
T_m	melting temperature
TMS	tetramethylsilane
UV	ultraviolet
XPS	X-Ray photoelectron spectroscopy
δ	phase shift
ν	wavenumber
λ	wavelength

Chapter I

Introduction

Abstract

Macromolecules including synthetic polymers and biopolymers have entered in every aspect of our daily live. Many modern functional materials, electronic devices, automobile parts, pharmaceutical equipments etc. have polymers as integral parts. Due to their low cost and special applications the polymers are unique materials to replace traditional materials. Our live has thoroughly changed by new odds and ends. E.g. mobile phones, computers, refrigerators, electrical domestic appliances, TV, video etc. all these made of synthetic materials to a large extent. Polymeric materials are also of great use in houses - floor carpeting, glue, pipes, paint, wallpaper, foils, electric insulation and moldings are examples of components based on synthetic materials.

Man has from time immemorial collected and used natural fibers, e.g. cotton, silk and wool, but the use of synthetically manufactured polymers started already before realizing the chemical structure of the polymers. Shortage of ivory led to the development of celluloid - the first synthetic plastic. This was a very popular material and many things were made of celluloid, e.g. billiard-balls, dentures, combs, spectacle frames and knife handles. Later the shortage of silk led to the development of nylon. When consumption increased, substitute materials were needed. In turn the development of various polymers has provided new materials with novel properties for advancement of other branches of science. Not surprisingly, roughly 30% of all scientists in the chemical industry work in the field of polymers.

The polymers are mainly classified in two major categories: elastomers and plastics. Elastomers or rubbery materials have a loose cross-linked structure. This type of chain structure causes elastic properties and these compounds are known as elastomers. Natural and synthetic rubbers are both the common examples of elastomers. Plastics are polymers, which under appropriate conditions of temperature and pressure can be molded or shaped (such as blowing to form a film). In contrast to elastomers, plastics have a greater stiffness and lack reversible elasticity. The plastics such as polyethylene and poly(vinyl chloride) have replaced traditional materials like paper and copper for a wide variety of applications. Furthermore, special polymers like liquid crystalline polymers (LCPs), biodegradable polymers and several others also belong to the plastic family. These polymers have applications in the field of electronic and medical sciences. Almost all the modern electronic equipments have digital display windows as one of their components. These displays are basically fabricated by using liquid crystals. Keeping in mind all these modern applications

this thesis is devoted to the synthesis and characterization of novel functional polymers. The remainder of this chapter is subdivided in different sections to give a brief overview of liquid crystals (LC), liquid crystalline polymers (LCPs), and the polymerization techniques employed to synthesize novel materials and finally the fluorinated polymeric materials.

1.1 Liquid Crystals

The discovery of liquid crystals by Reinitzer[1] in 1888 gave a new pavement in chemical and physical science. Further contributions of Lehmann in characterization of liquid crystals attracted the attention of researchers.[2-3] Liquid crystals are the compounds which have a tendency to show intermediate phases between the solid and the liquid phase. These intermediate phases are known as mesophases. Based on the mode of actions to induce the phase transitions LCs are basically classified into thermotropic liquid crystals (dependent on the temperature) and lyotropic liquid crystals (dependent on the concentration of solvent). Figure 1.1 shows the typical arrangement of molecules in the crystalline phase, the liquid phase and the intermediate liquid crystalline phase.

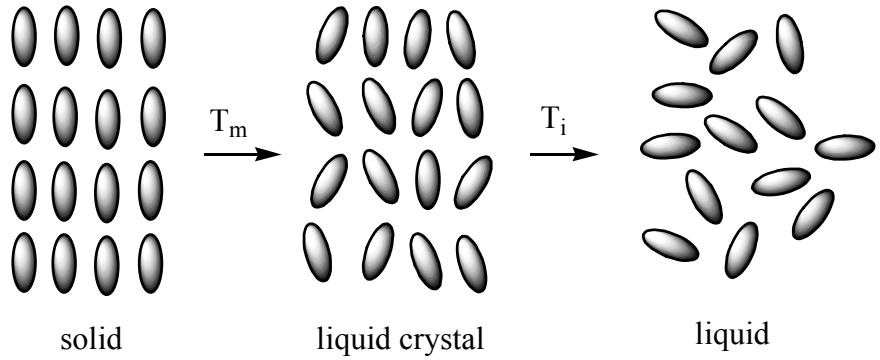

Figure 1.1 Schematic presentation of the liquid crystalline state. T_m and T_i are the melting and isotropization temperature (clearing point), respectively.

Several LC compounds show more than one intermediate phase. Depending upon the extent of orientation with respect to the preferential direction they are further classified in subtypes. The extent of orientation is represented by the order parameter "S" as defined by the expression[4]:

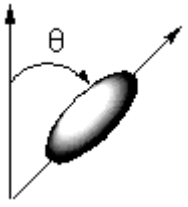

$$S = \frac{3\langle \cos^2 \theta \rangle - 1}{2} \qquad (1)$$

Here, θ is the angle between the molecular axis and the preferred direction while < > indicates an average value. The order parameter can vary from +1 for perfectly parallel-aligned molecules to –1/2 for perfectly perpendicular-aligned molecules with respect to a preferential direction through zero for isotropic molecules that are placed randomly.

A brief classification of liquid crystalline mesophases is given as follows.

1.1.1 Smectic LC Phase: This is a more ordered LC phase than the nematic LC phase. In the smectic state, the molecules maintain the general orientational order of nematics, but also tend to align themselves in layers or planes. This phase is more solid-like than the nematic. This smectic phase is further classified into several subtypes.

1.1.2 Nematic LC Phase: The nematic phase is less ordered than the smectic phase. This phase consists of microscopic threadlike structures and does not separate into layers. The spontaneous alignment towards the long axis generates highly birefringent material with dissimilar refractive index for polarized light propagating along and perpendicular to the optical axis. An orientation of nematic liquid crystals may be achieved easily in electric or magnetic fields.

1.1.3 Cholesteric LC Phase: This phase is termed so since a large number of cholesterol derivatives exhibit this phase. Most of the properties of the cholesteric phase resemble those of the nematic phase. An important characteristic of the cholesteric mesophase is the *pitch.* The pitch *p* is the distance which is needed for the director of a cholesteric liquid crystal to go through one complete rotation of 360 degrees. A byproduct of the helical structure of the chiral nematic phase is its ability to selectively reflect the light of wavelengths equal to the pitch length, so that a color will be reflected when the pitch is equal to the corresponding wavelength of light in the visible spectrum.

1.1.4 Columnar LC Phase: This phase is named columnar because stacking the discotic molecules into a column makes this mesophase. The columns are packed together to form a two-dimensional crystalline array. The arrangement of the molecules within the columns and the arrangement of the columns themselves lead to new mesophases.

1.1.5 Effect of Substituent and Spacer Length on the Properties of LC

The properties of low molecular weight liquid crystals are mainly influenced by several parameters.

a) Nature of Terminal Substituent: The transition temperature and mesophases of liquid crystals have been studied for different substituents in para position.[5]

A simplified group efficiency order in promoting liquid crystalline properties has been reported by Dave and Dewar.[6,7]

Nematics: $NO_2 > MeO > NMe_2 > Me > Cl > Br > H$

Smectics: $Br > Cl > F > NMe_2 > Me > H > > NO_2 > MeO$

b) Flexible Spacer Length: Kuhfuss and Jackson[8] first studied the effect of spacer length on the properties of LCPs. Two years later, Roviello and Sirigu[9] illustrated the first academic example of spacer length effect. The salient features are:

I) the transition temperature decreases with increasing alkyl spacer length II) a change in micro molecular packing structure III) the liquid crystalline polymers (LCPs) with short spacers show a nematic phase whereas with long spacers they tend to show smectic phases.

In the last two-three decades light sensitive polymers in which photochromic molecules have been incorporated in organic or polymeric materials have attracted considerable interest for many industrial applications. The large number of potential applications such as reversible optical data storage, diffraction and holography stimulated a great deal of experimental and theoretical work for photochromic materials. Among these, mainly photochromic azobenzene containing polymeric materials capable for storing optical information are thoroughly studied.[10-12] This is owing to their unique optical properties and high possibility of molecular engineering. The outstanding work of Ringsdorf et al.[10] promoted the researchers to study polymeric liquid crystals for optical information storage. Computer technology, credit cards, identity cards etc. are a few examples, which evidence the development of polymeric liquid crystal materials in electronic devices for the past few years.[13]

1.2 Liquid Crystalline Polymers (LCPs)

LCPs are materials which combine the properties of polymer macromolecules and low molecular weight liquid crystals (mesogens). Depending on the placement of the mesogen they are primarily classified into two subtypes: main chain LCPs [MC-LCPs] and side chain LCPs [SC-LCPs]. In MC-LCPs the mesogen is part of the main chain, whereas in SC-LCPs the mesogen is attached to the backbone through a flexible spacer.

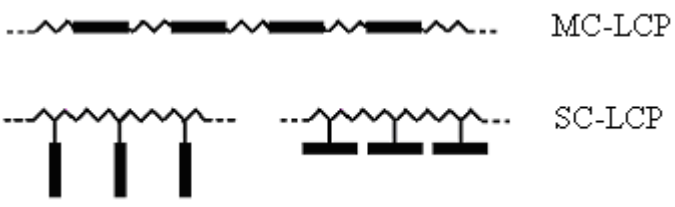

Figure 1.2 Schematic classification of LCPs

Finkelmann[14] et al. in 1978 first analyzed the structure of an SC-LCP based on a polymer backbone having pendant mesogenic groups connected via a flexible spacer.

The SC-LC copolymer systems containing azobenzene chromophores and mesogenic side groups are known as photoaddressable polymers (PAPs). The well known photo-induced reorientation ability of the azo group has revitalized the interest for the PAPs and made them potential candidates for optical information storage.

1.3 Results of Experimental Work on Azobenzene Containing Polymers

Depending on the relative energetic order of (n-π^*) and (π-π^*) states there are three different classes of azobenzenes: pseudo-stilbene-type, aminoazobenzene type and azobenzene type. The azobenzene type is characterized spectroscopically by a low intensity n-π^* band in the visible region, well separated from a high intensity π-π^* band in the UV.[11] In these molecules the back thermal cis-trans transition is very slow. In the interpretation of photo-induced phenomena in azo group containing polymers and in optical information storage the metastability of the cis state of azobenzene plays an important role. Ichimura et al.[15] have shown that the stable cis isomer of azo compounds is used for the induction of the molecular alignment of liquid crystals by light, whereas the stable trans state is preferred for optically induced birefringence and dichroism for a long period.

Two different mechanisms are suggested for photoisomerization: 1) Azo aromatic groups isomerize by rotation about the -N=N- bond. 2) Inversion of one or both of the nitrogen's. The first photochromic polymer used as an optical recording medium contained an azo dye (methyl red or methyl orange) dispersed in a matrix of poly(vinyl alcohol).[16] In this system, optical dichroism and birefringence have been observed, however, the photo induced anisotropy (PIA) only lasts a few tenths of seconds. Afterwards Wendorff et al[10] have shown that LCPs, whose structure is depicted in figure 1.3.1, can be used to perform optical storage experiments by irradiation with linearly polarized light at room temperature. The stored images were stable until the samples were heated above the isotropization temperature. Since this report there has been a lot of development in this area and different structures of LC nematic polyesters, polyacrylates, polysiloxanes[17-25] have been studied.

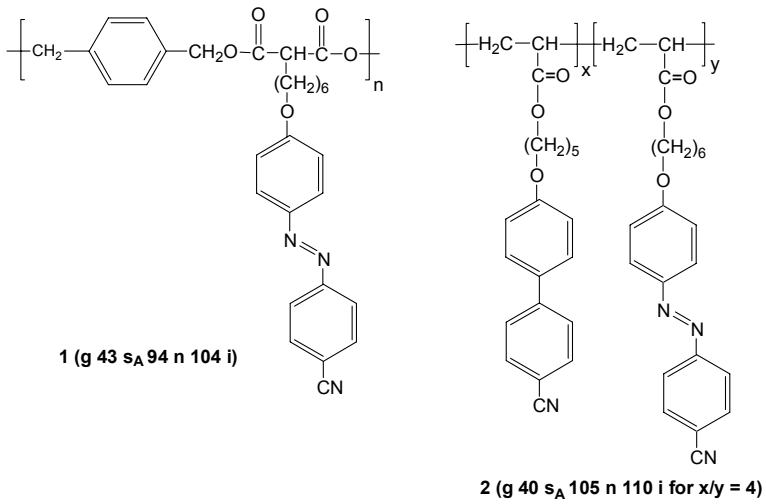

Figure 1.3.1 Structure of PAPs studied for optical information storage[11]

Ringsdorf et.al[26] reported that in azodye containing liquid crystalline copolymers the orientation could be frozen below the glass transition temperature resulting in a clear polymer film exhibiting optical dichroism. The film exhibits the maximum color intensity when the polarization plane of polarized light is parallel to the homogeneous orientation and the minimal intensity when the polarization plane is perpendicular. Shibaev et al.[27] and Ringsdorf et al.[28] have shown that in an electric field the SC-LCP can be oriented like low molecular weight liquid crystals. The behavior of the liquid crystalline copolymers is identical with the effects of low molecular weight guest-host systems.[26] Due to the high application temperatures and high viscosities the use of LCPs in displays is complicated; this problem can be overcome by using mixtures of SC-LCPs with low molecular weight LCs.[29,30]

Different techniques were developed for polymer synthesis during the last decade. Living anionic polymerization,[31] cationic polymerization,[32] controlled "living" radical polymerization,[33] group transfer polymerization[34] are just a few of them. All these techniques have their own advantages and disadvantages.

The following section gives a brief overview of the two different polymerization techniques used for polymerization during this PhD study.

1.4 Living Anionic Polymerization

In 1956 Szwarc[35] has discovered the living anionic polymerization technique. This polymerization technique is the most acceptable method for synthesis of well-defined polymers due to the living nature of the end groups. This method has important advantages like good control over molecular weight and molecular weight distribution. The following schematic presentation explains the mechanism of living anionic polymerization. After a relatively fast initiation chains only propagate and chain transfer or termination reactions are negligible.

$$M + In^{\ominus} \xrightarrow{\text{Initiation}} In\text{-}M^{\ominus} \qquad \text{eq (1.1)}$$

$$In\text{-}M^{\ominus} + nM \xrightarrow{\text{Propagation}} In\text{-}M_{n+1}^{\ominus} \qquad \text{eq (1.2)}$$

then

$$In\text{-}M_{n+1}^{\ominus} + T \xrightarrow{\text{Termination}} In\text{-}M_{n+1}\text{-}T \qquad \text{eq (1.3)}$$

When the proper initiator is chosen and the polymerization conditions like absence of moisture, oxygen and other impurities have been maintained, the resulting polymer has a predictable molecular weight and a narrow molecular weight distribution. By this technique polymers with relatively high molecular weights can also be prepared. The proper combination of monomer-initiator ratio controls the molecular weight of the polymer.[33]

$$\text{molecuar weight } (M_n) = \frac{\text{moles of monomer}}{\text{moles of initiator}} * \text{MW of monomer} \qquad \text{eq (1.4)}$$

This technique also has great advantage for the synthesis of block copolymers with defined block lengths. One of the characteristic features of block copolymers is the tendency for microphase separation in the solid state. It is the separation, which imparts many of the interesting and desirable properties displayed by this group of macromolecules. Many specific polymers are synthesized by this technique.

The homo polymerizations as well as block copolymerization of styrene by this technique using different initiators and solvents are well studied. The choice of initiator, solvent and temperature mainly influences the properties of the polymer. The quantitative conversion of styrene or several other monomers can be achieved within relatively short time by this method.

Unlike other techniques the living polymerization also has some disadvantages:

1) the functional groups have to be protected
2) the monomers and reagents should be highly pure
3) very stringent drying is required
4) handful to limited number of monomers are available and
5) low temperature is required (-70 °C).

1.5 Controlled Radical Polymerization (CRP)

Because of the above mentioned difficulties many commercial polymers and copolymers (almost 50% of synthetic polymers) are prepared by radical processes. The major success of radical polymerization was the large number of monomers that can undergo free radical polymerization, the convenient temperature range and the minimal requirement for purification of monomers and solvents, which should only be deoxygenated. But until recently it was not possible to prepare well-defined polymers and copolymers by the radical methods. This was due to unavoidable radical terminations. In order to minimize the terminations, the radicals are slowly and continuously generated by thermal or photo-induced decomposition of suitable initiators. This approach enables the synthesis of ill-defined polymers, but not block copolymers. The controlled radical polymerization (CRP) method has fascinated the attention of polymer chemists due to its novelty for well controlled block copolymers. The past few years have witnessed the growth in the development of CRP.[36] Three different approaches seem to be the most successful for CRP:

a) Thermal homolytic cleavage of the C-X bond of the P_n-X in a covalent species, which reversibly provides a growing radical $P_n^{\bullet}$ and a less reactive radical $X^{\bullet}$. The common examples are nitroxide[37, 38] and some bulky organic radicals, e.g. trityl.[39]

b) Formation of active radical $P_n^{\bullet}$ by reversible cleavage of C-X bond in the dormant species through a redox process. The atom transfer between growing chains and a catalyst is the key step for control. This technique is known as atom transfer radical polymerization (ATRP).[33]

c) The third approach is the thermodynamically neutral exchange between growing radicals present at low concentrations and dormant species. This degenerative transfer process can use alkyl iodides and also unsaturated methacrylate esters and thioesters. The latter two processes operate by addition-fragmentation chemistry.

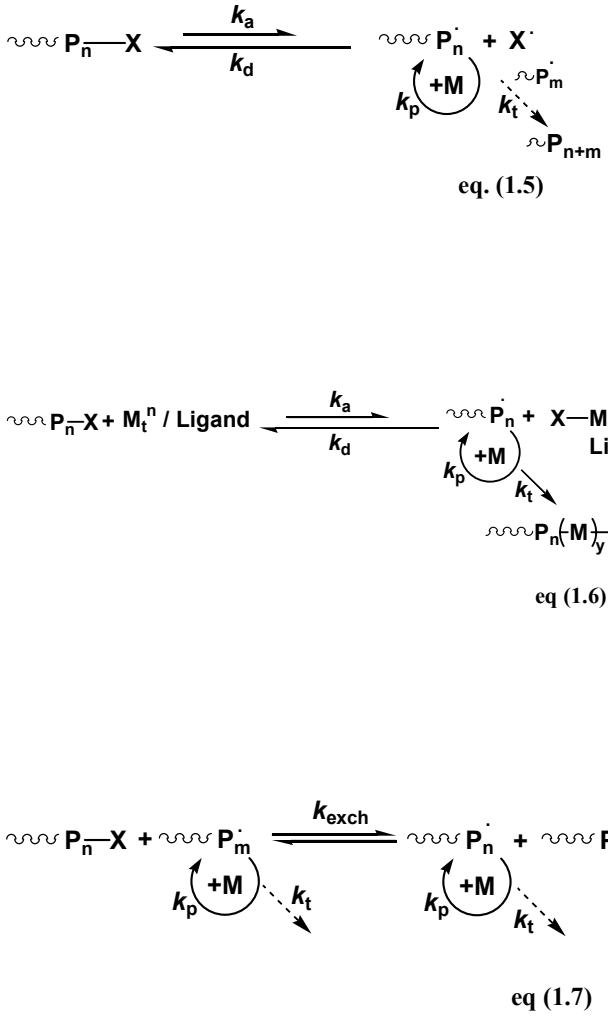

Figure 1.5.1 Schematic mechanisms of CRP. a) homolytic; b) ATRP; C) thermodynamic exchange of neutral radicals.

The following section deals only with the ATRP technique, which has been used during this PhD study.

1.6 Atom Transfer Radical Polymerization (ATRP)

ATRP is a process in which a vinyl monomer may be polymerized by a controlled/ "living" radical reaction under the influence of a transition metal halide. The ATRP has its origin in metal catalyzed atom transfer radical addition (ATRA), which is nothing, but a modified Kharasch addition. This addition usually occurs in the presence of light or conventional radical initiators.[40,41] The name ATRP is derived as the halogen atom of an organic halide moiety transfers to the transition metal complex to form the reactive radicals.

This active radical then adds to the alkene and then transfers back from the transition metal to the resulting polymer chain end.

The mechanism of ATRP is not completely certain, the proposed and most accepted radical mechanism is shown in figure 1.6.1.

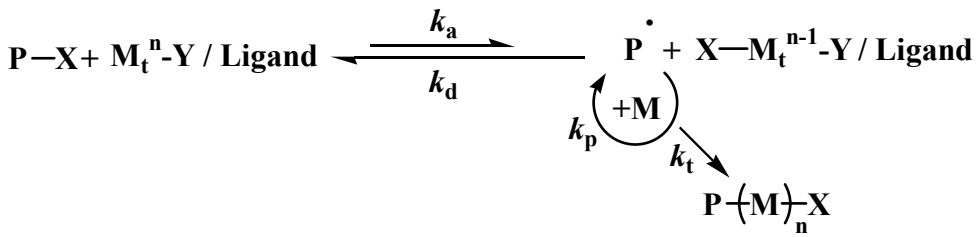

Figure. 1.6.1 Proposed mechanism of ATRP. (k_a, k_d, k_p and k_t are the rate constants for addition, dissociation, propagation and termination reactions).

The propagating free radicals are formed as the Cu/ligand complex acts as halogen atom transfer reagent between dormant and active polymer chains. During this exchange process the Cu/ligand complex undergoes an one-electron-oxidation. The resulting radical either adds to another monomer unit or reacts with the oxidized transition-metal complex to abstract the halogen and the metal complex undergoes an one-electron-reduction.[42-43] The possibility of chain termination reactions like radical-radical combination ($PM^{\bullet}$-$PM^{\bullet}$) or disproportionation in which formation of olefinic chain ends or hydrogenated chain ends ($PM^{=}$/PM^{H}) takes place. These termination reactions can be suppressed by maintaining the radical concentration. During the fast equilibrium process the chain propagation of the vinyl monomer is effectively controlled and chains initiated at the same time will have a uniform size distribution.

Matyjaszewski et. al[44] have first shown that the PS synthesized by ATRP has relatively narrow PDI and good control over molecular weight. The figure 1.6.2 shows the SEC overlay of the PS synthesized by three different techniques. The termination reactions can be minimized by reduction of the polymeric radical concentration. The termination reactions are second order with respect to the growing radical concentration and the propagation reaction is only of first order.[43]

$$R_t = k_t[P^{\bullet}]^2 \qquad \text{eq (1.8)}$$

$$R_p = k_p[M][P^{\bullet}] \qquad \text{eq (1.9)}$$

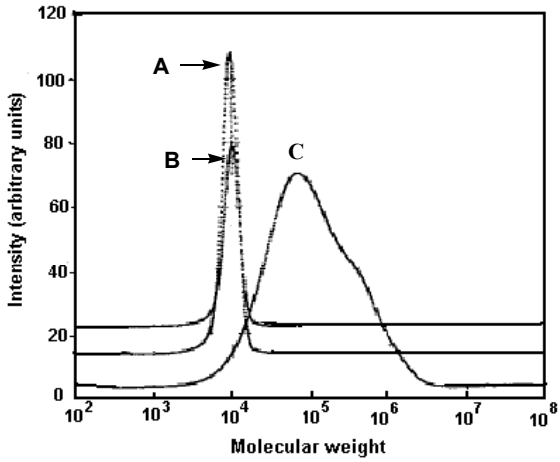

Figure 1.6.2 SEC diagram of PS synthesized by A) living anionic; B) ATRP; C) free radical technique[44]

If the reversible exchange between growing radicals ($PM_n^{\bullet}$) and dormant species (P-M_n-X) is fast, the molecular weight of the polymer can be predetermined by the ratio of the concentration of consumed monomer to the dormant chains and the PDI may remain narrow.

Moreover, in well controlled ATRP the M_n observed by SEC is in close agreement with the theoretical M_n. By monitoring the monomer and initiator concentrations the molecular weight can be predetermined,

$$M_n = ([M]/[P\text{-}X]_0) * (MW)_0 + MW_{P\text{-}X} \qquad \text{eq (1.10)}$$

where, M_n, [M], $[P\text{-}X]_0$, $(MW)_0$ and $MW_{P\text{-}X}$ represent the number average molecular weight, the concentration of consumed monomer, the initial concentration of initiator, molecular weight of monomer and molecular weight of initiator.

Therefore, a successful ATRP will have a small contribution of terminated chains and also a uniform growth of all the chains, which is achieved through fast initiation and rapid reversible deactivation. Hence, the PDI in ATRP in the absence of chain termination and transfer is dependent on the concentration of initiator (P-X) and deactivator (D), the rate constants of propagation (k_p) and deactivation (k_d), and the monomer conversion (p).

$$\frac{M_w}{M_n} = 1 + \left(\frac{([PX]_0 - [PX]_t)\, k_p}{k_d\,[D]} \right) \left(\frac{2}{p} - 1 \right) \qquad \text{eq (1.11)}$$

Thus, for the same monomer a catalyst that deactivates the growing chains faster will result in polymers with a narrow PDI (smaller k_p/k_d).[33]

Taking into consideration all the above factors the controlled/"living" nature of ATRP is dependent on the catalyst system, the type of monomer, initiator, and the type of solvents. The remainder of this section will give a brief summary on the individual components. A detailed discussion is beyond the scope of this PhD thesis.

1.6.1 Catalyst System

As mentioned earlier the catalyst is an active complex of transition metal halide and nitrogen containing ligand. The catalyst plays an important role for generating the active radicals by a redox process. A number of transition metal complexes have been studied for ATRP. The transition metal needs to have a flexible oxidation state/valency to undergo the redox process. The ideal catalyst for well controlled ATRP should fulfill a few requirements like: it should not participate in a reaction other than the radical formation, it must have an adjustable activation rate constant (k_a) to reach the particular requirement of specific monomers and it should deactivate extremely fast. Figure 1.6.3 shows a few complexes of Cu with nitrogen containing ligands. Various different transition metal complexes have been employed viz. Mo(V), Re(VI), Ru(II), Fe(II), Ni(II), Cu(I) and Cu(II).[33]

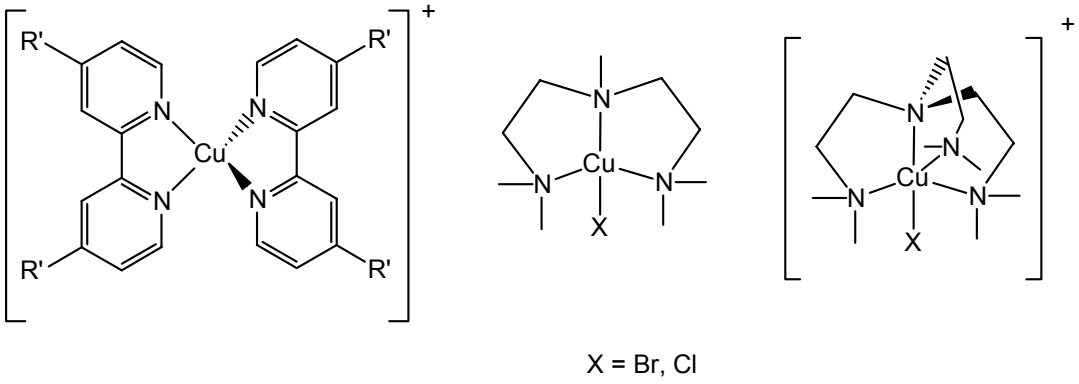

Figure 1.6.3 Structure of copper catalyst systems used for ATRP

Among all these different transition metals copper catalysts are superior in cost and versatility. Matyjaszewski et. al in 1995 first reported the styrene polymerization using cuprous halide complex.[43] At the same time Sawamoto et. al reported the polymerization of MMA and showed that the $RuCl_2(PPh_3)_3$ can also be used as an ATRP catalyst.[45] The activity of catalyst and its selectivity is mainly dependent on the type of suitable ligand.

The major role of the ligand is: a) to form a complex with the transition metal and adjust to force the metal center to undergo one electron transfer, b) the complex should be soluble in a suitable solvent and ensure stability of the complex in different monomers at

different temperatures, c) their should be no side reactions and d) to facilitate the removal and recycling of the catalyst.

The coordination chemistry for copper based ATRP greatly affects the catalyst activity. Even though the monodentate ligands are suitable for other transition metal salts in ATRA, they do not promote controlled copper mediated ATRP. Therefore, different multidentate nitrogen ligands have been developed. A few examples of the most commonly used nitrogen containing ligands are shown in figure 1.6.4.

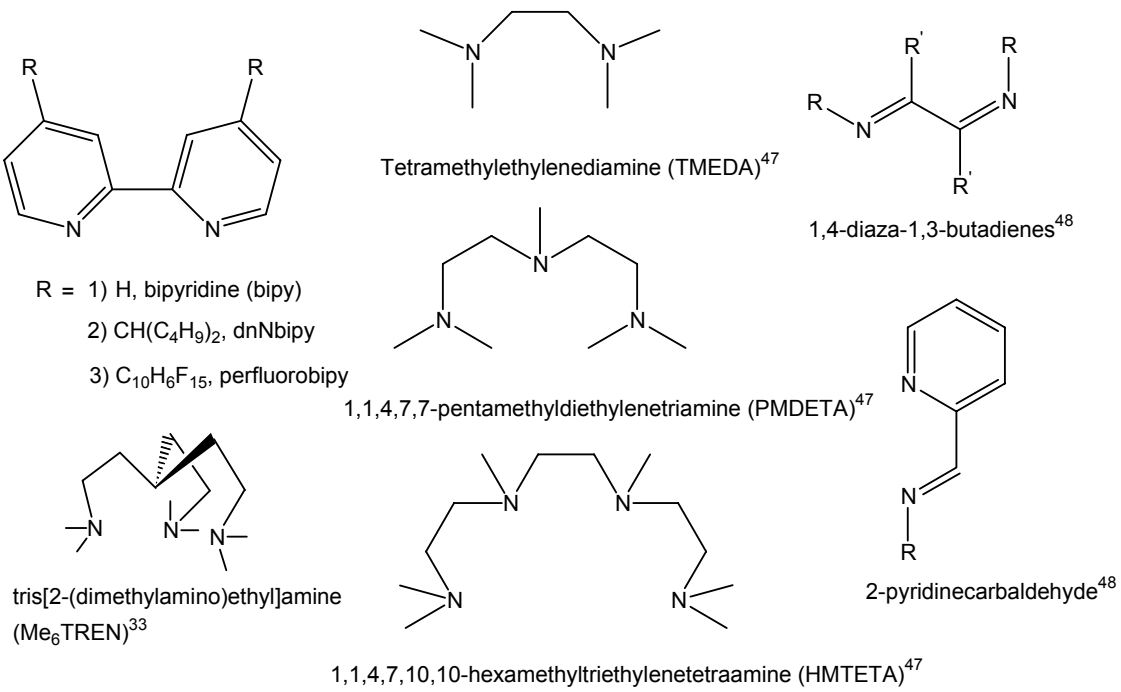

Figure1.6.4 Examples of ligands used in copper mediated ATRP

Matyjaszewski et. al [43] first reported the use of 2,2'-bipyridine (bipy) as a ligand in ATRP. They have also studied the effect of the ratio of the components in the initiating system on the kinetics and the level of the control of polymerization. The plot of $ln[M_0]/[M]$ against time (t), allows the calculation of k_p which changes with variation of external orders of initiator, catalyst and ligand. Further, the plot of k_p^{app} against concentration of initiator, catalyst and

$$k_p^{app} = d\, ln[M]/dt = k[PX]_0^x\, [CuX]_0^y\, [bipy]_0^z \qquad \text{eq (1.12)}$$

ligand shows the fractional orders (x, y and z) 1, 0.4 and 0.6 respectively. This shows that the kinetic order is less than one with respect to CuX and bipy. The only explanation provided is the catalyst system was not completely homogeneous. Several different ligands were developed to obtain the homogeneous catalyst system.

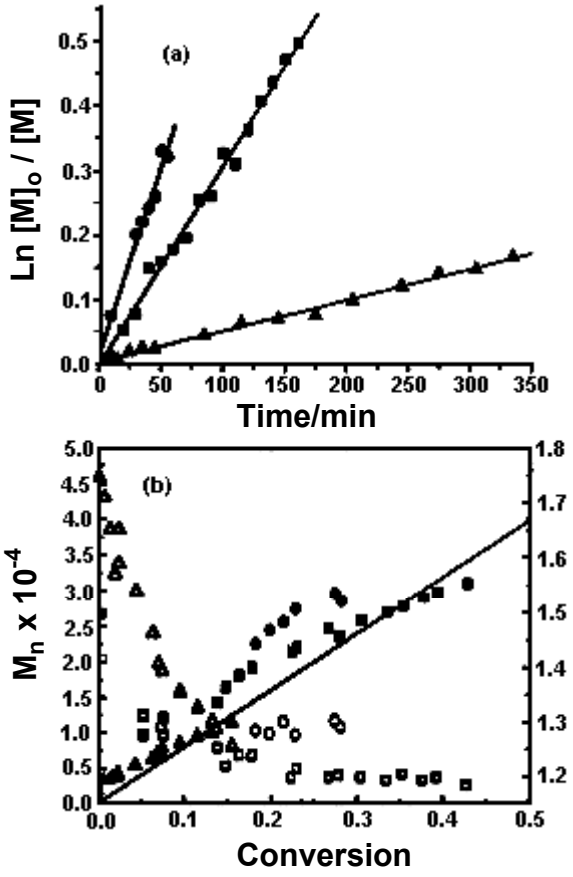

Figure 1.6.5 Comparison of ligands PMDETA(circle), dnNbipy (square) and PCPimine (triangle) during ATRP of MMA at 90°C with catalyst CuCl at [M]:[I]:[CuCl]:[L] = 800:1:1:2. a) First order kinetic plots; b) Dependence of M_n (filled symbols) and PDI (open symbols) on monomer conversion. Line represents theoretical values for living polymerization.[46]

A recent report by Agarwal et. al shows the effect of three different ligands and their concentration on the ATRP of MMA.[46] The catalyst system with PMDETA results in a higher k_p^{app} as compared to dnNbipy and 2-pyridinecarboxaldehyde pentylimine (PCP imine). Figure 1.6.5 shows that the M_n increases linearly with monomer conversion for dnNbipy and the PCPimine systems in accordance with theoretical prediction. But the M_n increase in the PMDETA system deviates from the theoretical prediction indicating early termination by radical-radical coupling caused by fast initiation. Furthermore, they observed that the apparent polymerization rate increases with increase in ligand concentration using dnNbipy ligand.

Matyjaszewski et. al studied multidentate linear amine like HMTETA, PMDETA and TMEDA as the ligands for copper mediated ATRP of St, MA and MMA.[47] All three monomers with three ligands gave linear increase in M_n with low PDI polymers. They observed that the polymerization rates were faster by the use of tridentate PMDETA and tetradentate HMTETA than by the use of bipy system. These results suggest that the coordination complex between simple amines and copper have lower redox potentials than the Cu/bipy complex, and also the steric factor of the ligand has an effect on the solubility. Later the use of Me_6TREN with Cu(I)X gave the highest rate of polymerization for ATRP of styrene so far as shown by Matyjaszewski.[47] The 0.2 equivalent of CuBr/Me_6TREN gave 82% conversion in 45 minutes whereas 480 min were required to reach the same level even though 1 equivalent of CuBr/dnNbipy was used.[47]

Haddleton et. al.[48] used the imines for copper based ATRP of styrene. These ligands were easily soluble in organic solvents and successfully used for ATRP of MMA. These

ligands were also stable in an aqueous solution even at 50 °C for 1 hour and around 10 hours at 25 °C.

1.6.2 ATRP Monomers

Styrenes, dienes, methacrylates, methylmethacrylates, acrylonitrile, vinyl pyridines and various other monomers have been successfully polymerized by ATRP.[33] As mentioned earlier ATRP has a tolerance for polar functionality, hence functional monomers containing acidic or basic substituents have been polymerized by ATRP. The presence of electron donating or withdrawing substituents plays a significant role because polymerizability is dependent upon the steric and electronic properties of the substituent. In other words the electronic effect due to the substituents on the monomers alters the electron density by inductive and resonance effects and stabilizes the active species.

The effect of different substituents on the polymerization of styrene by ATRP was investigated by Matyjaszweski.[49] The styrene monomers having a series of substituents, namely 4-CF_3, 3-CF_3, 4-Br, 4-Cl, 4-F, 3-Me, 4-Me, 4-CMe_3, 4-OMe were employed for the ATRP. Table 1.6.1 gives the detailed overview of the obtained results. They observed that the presence of electron withdrawing groups on the styrene enhances the polymerization rate and the polymers with defined characteristics have been synthesized. The probable explanation given for this observation was supported by the Hammet relation (ρ).

Table. 1.6.1 Apparent rate coefficients in ATRP and absolute propagation rate constants of substituted styrenes[49]

Substituent	σ	$k_p^{app}(S^{-1}) * 10^4$ [a]	$k_p^{app}(S^{-1}) * 10^5$ [b]	k_p (mol^{-1} L S^{-1}) [c]
4-CN	0.66			219
4-CF_3	0.54	1.25	5.47	
3-CF_3	0.43	1.44		
4-Br	0.23	1.06		186
4-Cl	0.23	0.97	2.56	150
4-F	0.06	0.39		
4-H	0.00	0.44	1.50	110
3-Me	-0.07	0.28		
4-Me	-0.17	0.16	0.36	84
4-CMe_3	-0.20	0.10		
4-OMe	-0.27	0.21		71

[a]Heterogeneous system at 110°C. $[M]_0$=4.37 M, $[M]_0$:$[I]_0$:$[CuBr]_0$:$[bipy]_0$=100:1:1:3. [b]Homogeneous system with 5% added $CuBr_2$ at 110°C.$[M]_0$ = 4.37 M;$[M]_0$:$[I]_0$:$[CuBr]_0$:$[bipy]_0$:$[CuBr_2]_0$=100:1:1:3: 0.05. [c] Absolute propagation rate constant at 30°C

The Hammet relation is useful to determine the influence of a substituent on the rate of a reaction. The styrenes bearing electron withdrawing substituents have a higher Hammet value than the styrenes in presence of electron donating substituents. Therefore, the higher ρ value can attribute to equilibrium constant (k_{eq}). Hence the monomers having electron withdrawing substituents have a greater k_{eq} than the monomers with electron donating substituents.

Furthermore, ATRP of 2,3,4,5,6-pentaflurorostyrene has k_p^{app} value 3.0 * 10^{-4} s^{-1} at 110 °C maintaining $[M]_0$:$[I]_0$:$[CuBr]_0$:$[bipy]_0$ = 100:1:1:2 as reported by Hvilsted.[51] These observed rates evidence that the presence of five electron withdrawing fluorine substituents

on styrene have a dramatic influence on the rate of polymerization. Figure 1.6.6 lists few monomers polymerized by ATRP.

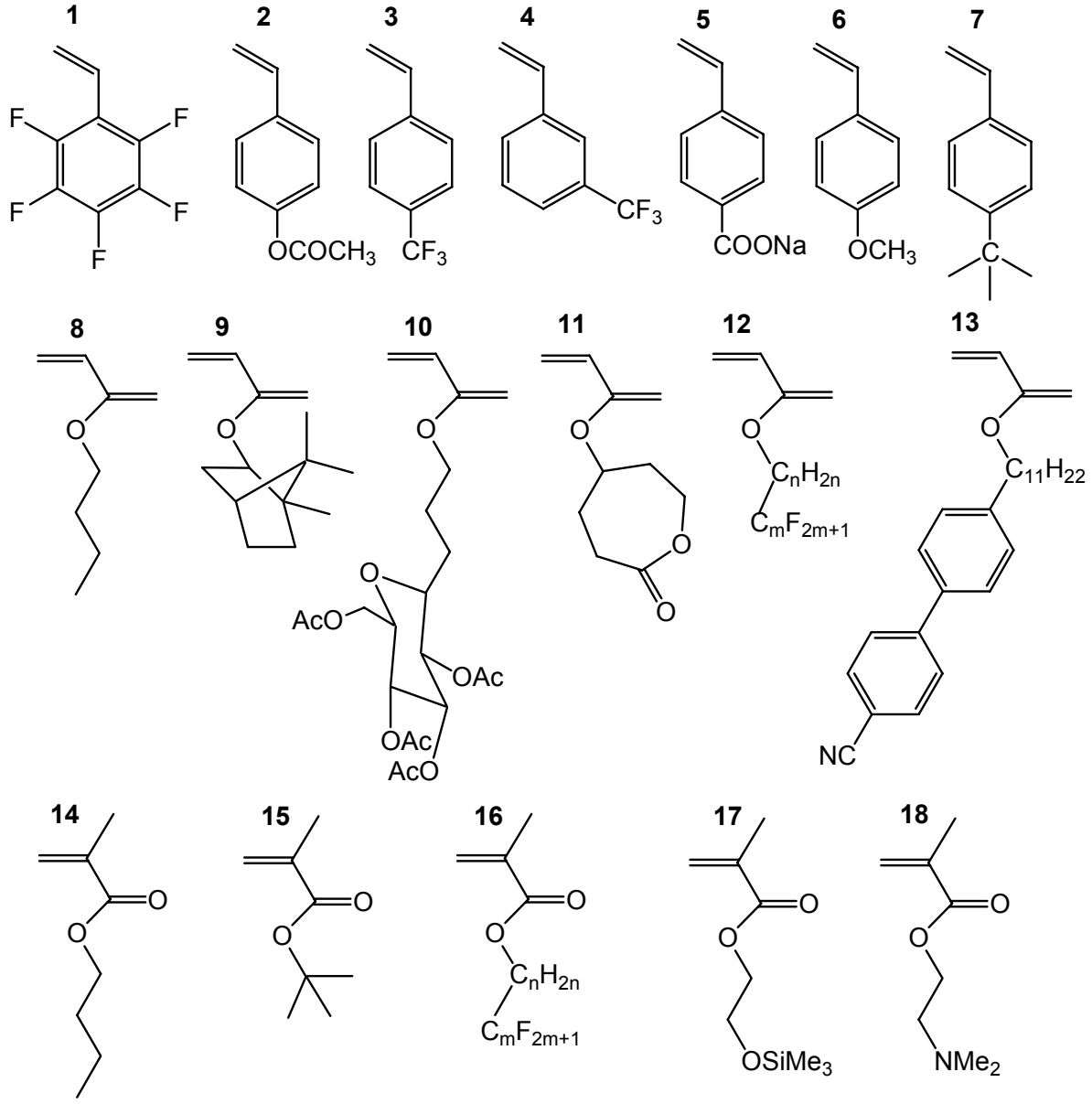

Figure 1.6.6 Example of monomers polymerized by ATRP

Armes et. al have shown that the monomer bearing a carboxylic acid (4-COOH) as substituent on styrene can also be successfully polymerized by ATRP at ambient temperature in aqueous media with controlled fashion.[50] The quantitative conversion was achieved within 1 hour. Kops and coworkers have polymerized acetoxystyrene in a controlled and living fashion even though it has -$OCOCH_3$ as a substituent.[52] The hydrolysis of these acetoxy containing polymers gave a new route to synthesize polyhydroxy styrene with specific properties, as the hydroxystyrene does not exist due to tautomerism.

The acrylates and methacrylates having pendant groups like 1,1-dihydroperfluorooctyl methacrylate (FOMA), 1,1-dihydroperfluorooctyl acrylate (FOA)[53] etc. were also polymerized by ATRP using supercritical carbon dioxide as a solvent. The different amphiphilic polymers have attracted attention due to their use as surfactants and as biopolymers. Star-like polymers from poly(propyleneglycol)methacrylate (PPGM) with defined molecular weight and low PDI have also been reported.[54]

1.6.3 Initiators

Different initiators were used for ATRP. The initiator concentration has a direct relation to the molecular weight. Bifunctional or multifunctional initiators can also be used to synthesize block or star copolymers. The major role of the initiator is to determine the number of growing polymer chains. An initiator in ATRP must undergo fast initiation to obtain well defined and low PDI polymers:

$$DP = \{[M]_0 / [I]_0\} * Conv. \qquad \text{eq (1.13)}$$

where DP is the degree of polymerization and Conv. stands for conversion.

In ATRP the activated alkyl halides (having an allyl, aryl or carbonyl group at the α-position) or the sulfonyl halides were potentially used as initiators. The alkyl halide can only be employed as an efficient initiator, when the halogen group undergoes rapid migration between the growing chain and the metal complex. The tertiary alkyl halides are better initiators than the secondary and the primary halides. The bond strength between the carbon and the halogen in an alkyl halide is also dependent on the type of halogen atom. The energy required for the dissociation of a C-X bond is in the order: C-F > C-Cl > C-Br > C-I. The dissociation energy required for the C-F bond cleavage is higher as compared to other C-X bonds, which limits its use as an initiator. Whereas the iodine containing initiators were suitable only for the copper mediated MMA polymerization and the ruthenium and rhenium based polymerization of styrene.[33] However, the initiation is better when the bromides and a copper(I) chloride was used as a catalyst.[56] This is due to the relatively high difference in the dissociation energies of the carbon-chlorine bond and the copper-halide bond, in which the halide exchange takes place right after the initiation.

One of the advantages of ATRP is that the structure of the initiator can be compatible with the structure of the polymer. Therefore, the initiator having almost identical structure to that of the monomer can be utilized for the polymerization. Furthermore, the use of functional initiators can result in chain-end functional polymers. These chain-end functionalities

generated from the initiator moiety can be activated in the post-polymerization reaction. Hence, the use of a functional initiator is the tool to introduce the functionality in the polymer chain end.

Matayjaszewski has employed a series of initiators bearing different functionalities for the styrene polymerization.[33] Figure 1.6.7 shows a few examples of initiators used for ATRP. Carbon tetrachloride (CCl_4) and chloroform ($CHCl_3$) also act as bifunctional initiators in CuCl/$(bipy)_3$ mediated ATRP of styrene. The obtained polymers with molecular weights deviating from the expected values suggest a bad control of the polymerization. The polymerization of MMA with CCl_4 and Ni {*o,o'*-$(CH_2NMe_2)_2C_6H_3$} Br as a catalyst shows a control at lower conversion but again a deviation was observed at high conversions.

The benzylic halides were found to be suitable initiators for the polymerization of various monomers.[33] The initiator efficiency varies from monomer to monomer. For example the 1-PhEBr was an active initiator with CuCl/dnNbipy for styrene polymerization, whereas it failed when employed for MMA polymerization under identical conditions. The PMMA obtained has shown a broad PDI and higher molecular weights than expected.[56]

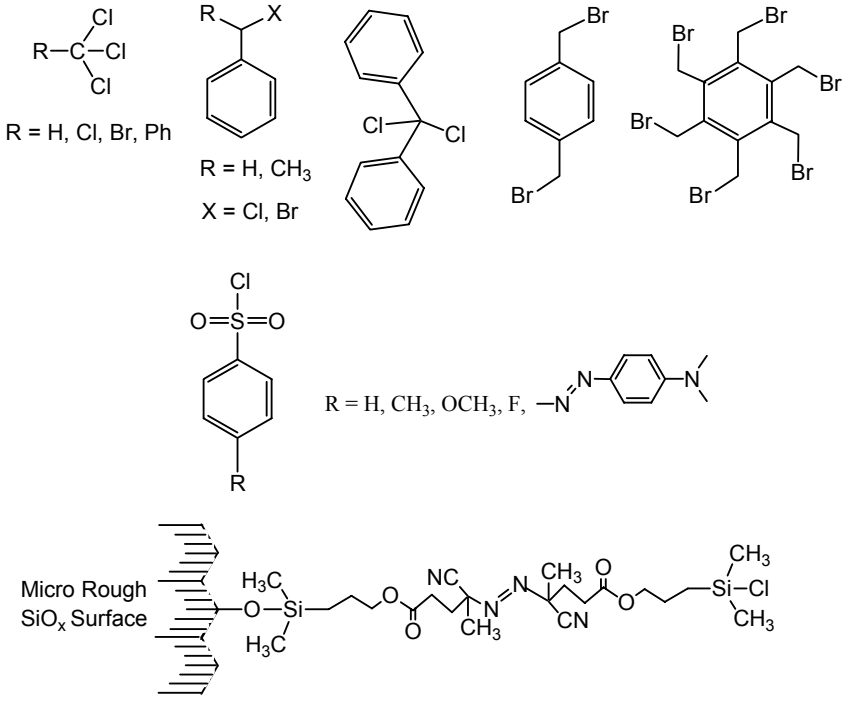

Figure 1.6.7 Structure of some representative commercial[33] and synthesized initiators.[55]

Haddleton and coworkers used initiators having an acid functionality for the polymerization of MMA.[57] Furthermore, they also studied the effect of carboxylic acid on MMA polymerization. The M_n observed were consistent but three times greater than the

theoretical M_n. Nevertheless the PDI was less than 1.2. The figures 1.6.8 a and b show the kinetics of ATRP of MMA in the presence of a carboxylic acid functionality.

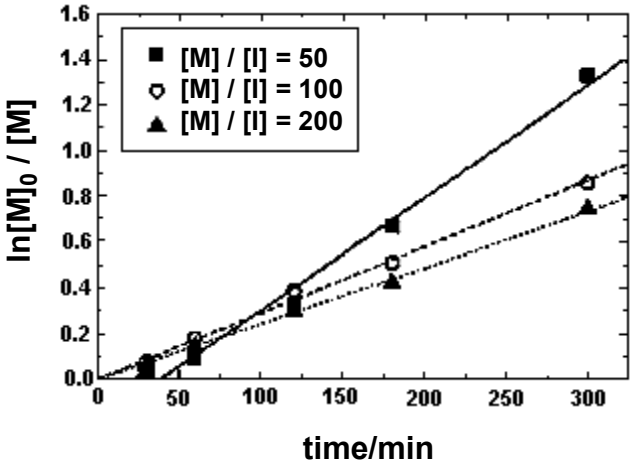

Figure 1.6.8 a) The first order kinetic plot for ATRP of MMA initiated by 2-bromo-2-methylpropionic acid.[57]

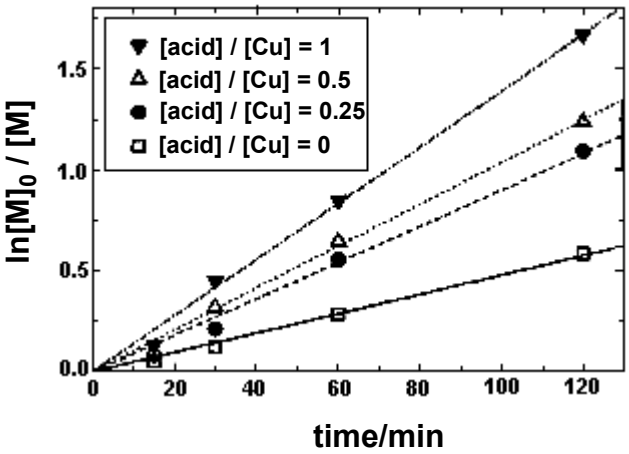

Figure 1.6.8 b) The first order kinetic plot for ATRP of MMA in the presence of benzoic acid initiated by ethyl 2-bromoisobutyrae.[57]

The polymers or inorganic compounds having one or more hydroxyl or amine functionalities can also be used as ATRP initiators by esterifying them with a halo acid having an activated halide. This approach can be applied to modify the surface of the material. Ruhe et. al have shown the modification of a hydrophilic silica surface to a hydrophobic surface by converting it to ATRP initiator and then polymerizing the perfluorinated acrylate on it.[55]

The halogen atoms migrated to the polymer chain ends allow to use the isolated polymer as a macroinitiator for block copolymerization reactions. This approach gives a relatively good control over the composition of the individual blocks. The sequential addition process for the block copolymerization by addition of the monomers one after another is not advisable. Since the ATRP is a radical process, in order to obtain the block copolymer the second monomer must be added before 100% conversion of the first monomer. The addition of the second monomer can kill/quench the growing radical and may terminate the active growing chain ends. Furthermore, the radical-radical combination at higher conversions can also be possible. The use of the bifunctional initiator results in a polymer having the halogen functionality at both chain ends. The polymerization using these isolated polymers can be useful for the synthesis of triblock copolymers. Pan[58] has used a discotic hexafunctional initiator for the synthesis of a hexaarm polystyrene.

1.6.4 Solvents

The solvents in ATRP have a few functions. As the polymerization progresses the viscosity of the reaction mixture increases. Hence the use of solvent can be helpful to form a homogeneous mixture and to reduce the viscosity. Sometimes a solvent is also necessary if the obtained polymer is insoluble in its monomer. During the polymerization reaction several bond breaking and bond forming exothermic reactions occur, which may increase the reaction temperature. Therefore, the solvents are used for industrial scale polymerizations not only to reduce the viscosity but also to increase the heat capacity of the reaction. The polymerizations of several monomers in bulk, in solution or in emulsion by ATRP are reported.[33] These results evidence the versatility of ATRP.

A variety of polar or non-polar solvents, such as xylene, benzene, toluene, tetrahydrofuran, anisole, ethylacetate, 1,2-dichlorobenzene, acetone, alcohols, dimethylformamide, carbon dioxide, water and several other have been successfully

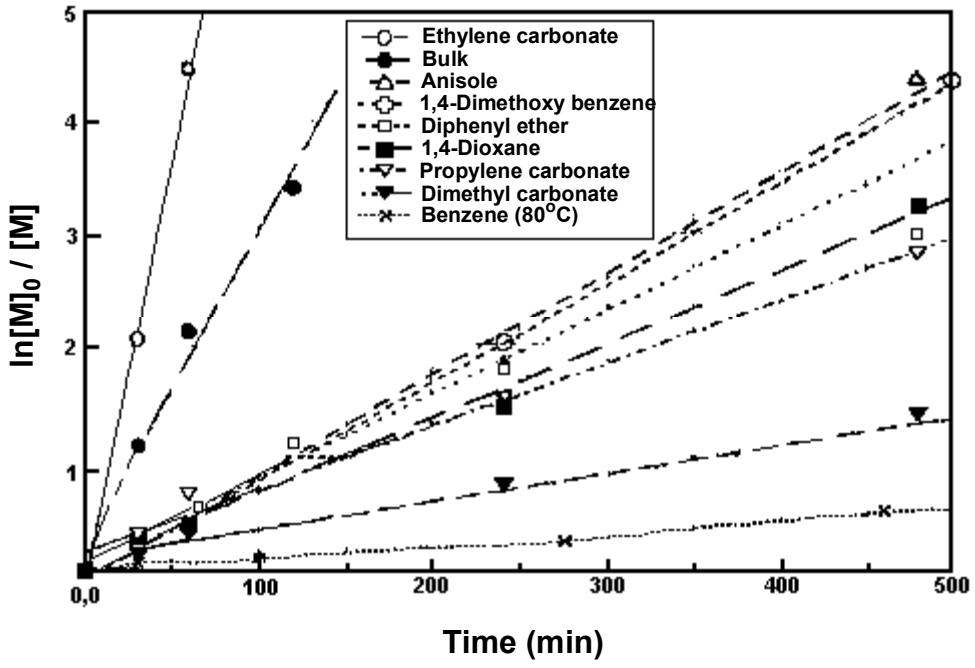

Figure 1.6.9 The first order kinetic plots for ATRP of n-butyl acrylate in various solvents.[60]

employed during ATRP of various monomers. The choice of a suitable solvent is based on the following considerations: the catalyst system has to be soluble and form a uniform solution, the catalyst poisoning by solvent assisted side reactions should be minimized,[59] the polymer formed should not precipitate, and the solvent should not participate in any side reactions. Matyjaszewski and coworkers have studied the polymerization of n-butyl acrylate in different

solvents as depicted in figure 1.6.9. They observed that the polymerization in ethylene carbonate had good control and was comparatively faster than in the other solvents or the bulk polymerization, in which the catalyst system was partially soluble.[60] Armes et. al have shown that the polymerization of sodium-4-vinylbenzoate and of few other monomers can be performed using water as a solvent.[50] Water is the most cheapest and easily obtainable environmentally friendly solvent. The catalyst system Cu(I)Br/Cu(I)Cl with bipy is soluble in water. By maintaining the pH of the water they observed surprisingly higher rates with good control over the polymerization of sodium-4-vinylbenzoate.

1.7 Fluoropolymers

1.7.1 Historical Perspective

The serendipitous discovery of poly(tetrafluoroethylene) (PTFE) by Plunkett and co-workers at DuPont opened a new era for special materials.[61] Commercially this polymer is also named Teflon®. The outstanding properties of Teflon® such as the high thermal stability, the low surface energy and the resistance to various chemicals made it a very attractive material. Non-stick coatings, pipes, valves, packaging are just a few examples of its commercial usage. PTFE polymers are commonly synthesized by the emulsion method using peroxide initiators and tetrafluoroethylene as a starting material. The structure of Teflon® is shown below.

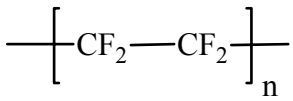

The weak intermolecular forces and the strong carbon-fluorine bond are the important features, which made PTFE a special polymer. PTFE is a highly crystalline polymer with a melting point around 330°C. The mechanical stability of this polymer remains practically unchanged over a wide range of temperature from -100 to +350°C. Furthermore, this polymer has a very low dielectric constant. It does not dissolve in strong acids, including hot fuming nitric acid and it is also resistant to a variety of known organic solvents. It should also be noted that the conventional techniques used for the processing of other polymers could not be applied to PTFE because of its very low melt flow rates. Several unattractive features challenged researchers striving for materials with comparable properties but more flexible processing. Hence various new fluorinated comonomers have been introduced to alter the properties of Teflon®.

During the last decade the discovery of ATRP[43] has given a new strategy to synthesize well defined polymers. (Also refer section 1.5). The use of a functional initiator or a

macroinitiator gives not only a well controlled polymerization but also a well defined architecture. Hence the ATRP technique has been used in this work for the synthesis of fluorinated homo as well as block copolymers.

One aspect about fluoropolymer research involves polymerization and polymer modification in supercritical CO_2 ($scCO_2$). This is of great interest due to the solubility of fluorinated systems in $scCO_2$, the chemical advantages of reactions in $scCO_2$, and the environmental friendliness of $scCO_2$ processing versus the standard practice of using organic solvents.[62, 63] The chain transfer to solvent side reactions are a big issue in any radical chain polymerization, which no longer has to be considered with the use of $scCO_2$. The radical synthesis of this type has been utilized to synthesize the novel perfluoropolyethers and fluorinated acrylate polymers.[53] Certain polymer composites have been produced via anionic polymerization with $scCO_2$ to produce new surface-modified composites. This method is easier than the previous methods with much less exposure to harsh chemical processes and organic solvents.[62]

1.7.2 Fluorinated Polymer Systems in Membrane Science and Coatings

Membrane science is a fast developing field that utilizes polymer and material knowledge to produce viable membranes for chemical separation and protection of surfaces. It has been clearly observed that the introduction of fluorine containing materials into polymers dramatically changes the material properties. Recently Miyata et. al[64] have shown that the addition of PFA-*g*-PDMS polymers into MMA-*g*-PDMS changes the surface properties relative to PFA. The removal of volatile organic compounds from waste water is an important issue from an environmental point of view. These surface modified membranes were effective to remove the benzene from a water solution. This property is may be due to the exclusive aggregation of perfluorinated blocks at the surface of the membrane and the hydrophobicity of the fluorinated system.

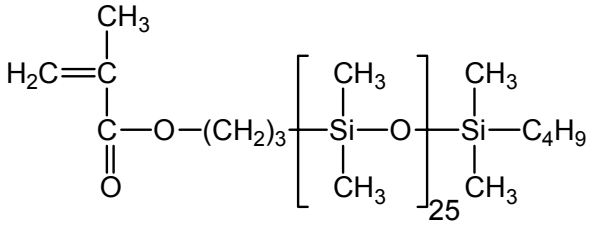

Methylmethacrylate grafted poly(dimethylsiloxane)
MMA-g-PDMS

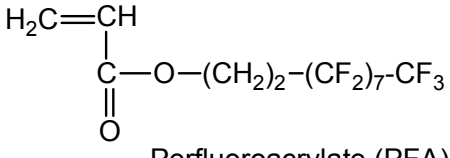

Perfluoroacrylate (PFA)

Figure 1.7.1 Structure of monomers used by Miyata et. al.[64]

These two copolymer systems MMA-g-PDMS and PFA-g-PDMS were produced via radical polymerization. Further MMA and PFA graft copolymer of PDMS were also reported and analyzed to determine possible parameters in microphase separated membranes.[64]

There are surfaces, which have lower surface tension than PTFE. These surfaces are often dominated by fluorinated methyl (CF_3) groups as compared to fluorinated methylene (CF_2) groups. The bulky -CF_3 groups lead to a lower density of attractive centers per unit area at the surface than in chain CF_2 groups. Zisman[65] established that the surface tension depends on the constituent groups and decreases in the order of $CH_2 > CH_3 > CF_2 > CF_3$.

Hirao et. al[31, 66] showed for the first time that the degree of surface enrichment increases with an increase in number of the terminal perfluorooctyl (C_8F_{17}) groups. They have synthesized and studied the chain ends and in chain functionalized styrene polymers with one, two, three and four C_8F_{17} groups with various architectures. They have also observed that the surface enrichment of the C_8F_{17} group is strongly dependent on the number and the placement of C_8F_{17} groups as well as the molecular weight of the functionalized polymer. The degree of surface enrichment in polymers increases with the increase in C_8F_{17} groups and decreases with the increase in molecular weight. Furthermore, they have also shown that the terminal C_8F_{17} groups are more mobile in molecular motion and have more tendency to go towards the surface than the internal groups.

Gas permeable membranes using the fluorinated systems poly(1,1'-dihydroperfluorooctyl methacrylate) and polystyrene-*b*-(1,1'-dihydroperfluorooctyl methacrylate) block copolymers have been synthesized and the effect of fluorinated block incorporation on the permeability of the membranes was studied by Arnold and coworker.[67] In general they have observed that PFOMA possesses a lower gas permeability and higher selectivity than PFOA. This observation was explained by the mobility of side groups, which affects the T_g. The activation energy for penetration of larger gas molecules like ethane and propane increases as T_g is

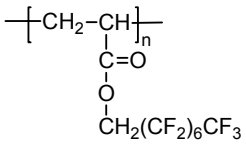

poly(1,1'-dihydroperfluorooctyl acrylate) PFOA

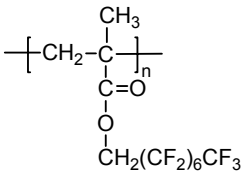

poly(1,1'-dihydroperfluorooctyl methacrylate) PFOMA

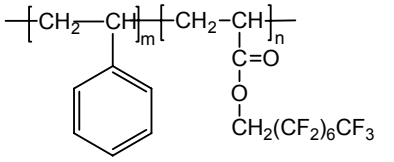

Polystyrene-*b*-poly(1,1'-dihydroperfluorooctyl acrylate) PS-*b*-PFOA

Figure 1.7.2 Structure of monomers used to synthesize gas permeable membranes[67]

approached. The gas permeabilities of PS-*b*-PFOA copolymers tend to decrease with the decrease in PFOA content. The structures of the fluorinated homo and block copolymers used for this study are shown in figure 1.7.2. A gas permeability study of pure PFOA and PS was performed and has shown that the tunability of gas permeability is possible by varying the copolymer structure and morphology.[67]

Chiellini et. al[68] used two different routes to synthesize polystyrene based di and tri-block copolymers having a fluorinated aromatic side chain as a substituent: a) TEMPO-mediated controlled radical polymerization of the fluorinated styrene monomer and b) The introduction of fluorinated side chains in the anionically synthesized diblock copolymer by post polymerization reactions. The block copolymers showed phase separation at the molecular level, the $(CF_2)_8$ side chain block copolymers had a stronger tendency to form the smectic mesophases than the block copolymers having $(CF_2)_4$ or $(CF_2)_6$ in the side chain. Furthermore, it was also reported that the contact angle measurements of these derivatized polymers as a function of immersion time in water evidences the segregation of fluorinated blocks at the surface resulting in highly hydrophobic surfaces.

As discussed in the earlier sections, the electron withdrawing nature of the fluorine has a great effect on radical stabilization and ultimately on the rate of ATRP.[49] A very recent report by Hvilsted[51] has shown that pentafluorostyrene polymerizes faster than the other substituted styrenes by the ATRP technique. Furthermore, the observed thermal stability of PFS is 50-60 °C higher than the normal PS. Also the partial solubility of PFS and its block copolymers in the common organic solvents supports the statement about the chemical resistance of these polymers. They have exploited different solvents to study the solubility parameter and found fluorobenzene as a good solvent for PFS but on the other hand poor solvent for PS.

These unique properties of the fluorinated polymers allow their utilization in surface coatings. The surfaces of these polymers have chemical inertness, relatively low permeability for most gases, low friction coefficients and extremely low surface energy. The various random or multiphase fluorinated copolymers have been used either as a pure compound or as additives to base polymers in film formation. This results in hydrophobic surfaces on hydrophilic substrates such as metals, inorganic compounds, polymers and so forth.[69,70] Rühe et. al have shown the building of a perfluorinated polymer monolayer on porous silica giving the materials ultra hydrophobic and oil-repellent properties.[55]

Chapter II

Characterization Methods

Abstract

In this chapter some considerations of the experimental characterization techniques are described which have been used frequently in this PhD study. Besides a short introduction, the basic conditions employed to study different properties of fluorinated and azobenzene containing mesogenic monomers as well as polymers will be given.

2.1 Size Exclusion Chromatography (SEC)

The investigations of molecular weights were performed with a Viscotek 200 instrument equipped with a PL guard and 2 PLgel Mixed-D columns in series from Polymer Laboratories (PL) and a Shimadzu refractive index (RI) detector. The measurements were performed in THF at room temperature with a flow rate of 1 mL/min. The M_n and M_w values were based on near monodisperse known molecular weight PS standards in the range of 7 x 10^2 to 4 x 10^5 from Polymer Laboratories.

2. 2 Differential Scanning Calorimetry (DSC)

The DSC analysis was performed on a DSC Q1000 TA instrument under a flow of dry nitrogen. The system was calibrated and the empty pan was used as a reference. Each sample was analysed by heat-cool-heat method using a controlled heating/cooling rate. The glass transition, the melt transition and the crystallization temperatures were determined automatically by the instrument from the second heating trace and are reported as the midpoint of the thermal transition.

2.3 Thermo Gravimetric Analysis (TGA)

The TGA analysis was performed on a TGA Q500 TA instrument measuring the total weight loss with approximately 10 mg sample from 30 to 600 °C in dry nitrogen with a flow rate of 90 mL/min. The heating and cooling rates were controlled depending on the sample type.

2.4 ^{1}H, ^{13}C and ^{19}F Nuclear Magnetic Resonance (NMR) Spectroscopy.

The NMR spectra were recorded on a Bruker 250 MHz spectrometer. All the spectra for ^{1}H NMR (250 MHz) and ^{19}F NMR (235 MHz) are recorded using 16 to 128 number of scans and the ^{13}C NMR (62.9 MHz) are recorded using 1000 to 10000 number of scans depending on the signal to noise ratio. The NMR analysis was performed in $CDCl_3$ or DMSO-d_6 as the solvent in 5 mm i.d. tubes at 25°C. The chemical shifts were assigned with internal standards TMS in ^{1}H NMR (0 ppm), $CDCl_3$ in ^{13}C NMR (76 ppm) and C_6F_6 in ^{19}F NMR (-162.90 ppm).

2.5 UV-visible Spectroscopy

The UV-visible absorption spectra of the azo precursors and the mesogenic polymers were performed on a Perkin Elmer UV spectrophotometer. The THF (spectroscopy grade) was used as solvent as well as reference for the measurements. The analysis was performed in quartz

cuvettes. The λ_{max} values determined by the Lambda 16 software and the ε_{max} values calculated were always the average of three solutions.

2.6 Fourier Transform Infrared Spectroscopy (FT-IR)

The FT-IR spectra of the monomers and polymers are recorded on a Perkin-Elmer Spectrum One spectrometer with a resolution of 4 cm^{-1} and 32 to 128 scans depending on the signal to noise ratio. The FT-IR absorption signals were assigned by means of literature values.

2.7 Contact Angle (CA) Measurements

The contact angle measurements were performed on a KL 1500 LCD (Schott, Germany) contact angle goniometer. The advanced (when the drop had the maximum volume allowable for liquid-solid interfacial area) and receded (when the liquid-solid interfacial area was decrease by removing water from drop) contact angles with a water droplet towards the air side were calculated by the VCA 2500 software. The CA values reported here are averaged over three measurements with an accuracy of $\pm$ 2°. The polymer solutions were passed through the alumina column and precipitated in methanol before spin coating. The single layer polymer thin films were prepared by spin coating of 3-5 % (w/v) tetrahydrofuran or hexafluorobenzene polymer solutions on glass slides, evaporating slowly for few hours and then drying in a vacuum oven at room temperature for 24 h. Figure 2.7.1 shows the principle of contact angle measurement.

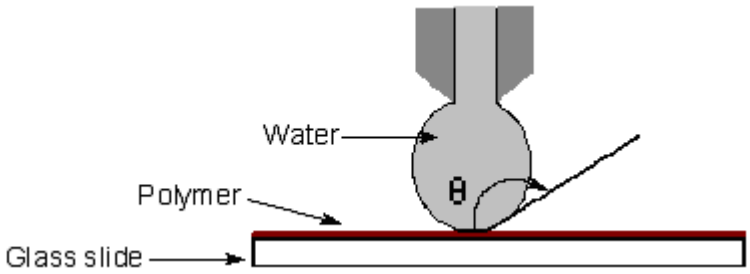

Figure 2.7.1 Schematic representation of contact angle measurement of a water droplet

2.8 X-Ray Photoelectron Spectroscopy (XPS)

X-ray photoelectron spectroscopy, also known as electron spectroscopy for chemical analysis (ESCA), is a widely used technique to study the chemical composition of polymer surfaces. The technique is based on the photoelectrical effect, which provides information on the elemental and the functional group composition and oxidation state. In the XPS experiment

the surface is irradiated with X-rays. The energy of the incident X-ray photons is high enough to eject the electrons from electron shells of surface atoms. These ejected electrons are referred to as photoelectrons. From the difference between the known energy of the X-ray photons and the measured kinetic energy of the photoelectrons, the binding energy can be calculated according to the following equation:

$$E_b = h\nu - E_\kappa - \varphi \qquad \text{eq (2.1)}$$

where, E_b denotes the binding energy of the photoelectron in the excited electron shell, E_κ the kinetic energy of the photoelectron, h Planck's constant ($6.626 * 10^{-34}$ J s), ν the frequency of the X-ray, and φ the work function of the spectrometer. The elements can be recognized by their binding energy, which depends slightly on the oxidation state and the chemical environment.

The spectra were recorded using a Sage 100 (SPECS, Berlin, Germany) instrument operated at a pressure of $<10^{-7}$ Torr. The analysis was performed using an Al K_α X-ray source operated at 300 W at a take-off angle of 90° from the surface plane. Atomic concentrations of each element were calculated by determining the relevant integral peak intensities using a linear type background. The absolute error is estimated to be in the order of 3-5%.

2.9 Optical Anisotropy Measurements

Figure 2.9.1 shows a typical set-up* for the optical anisotropy investigation of polymer thin films (25 mg in 200 μl chloroform spin coated at 800 rpm). The argon ion laser having a linearly polarized beam with a wavelength of 488 nm (which is within the absorption band of the photochromic azo groups) was used to induce the anisotropy. A laser power of 50 mW corresponding to an intensity of approximately 700 mW/cm^2 was employed. A beam of a HeNe laser (633 nm with 5 mW intensity) linearly polarized at 45 º was used for read out. The photoinduced changes in the polymer films were monitored by a ThorLabs PA410-EC polarimeter with a wavelength range of 450-700 nm and a maximal data collection rate of approximately 30 measurements/sec.

* *Optical anisotropy measurements were performed by Lian Nedelchev at Risoe National Lab, Denmark.*

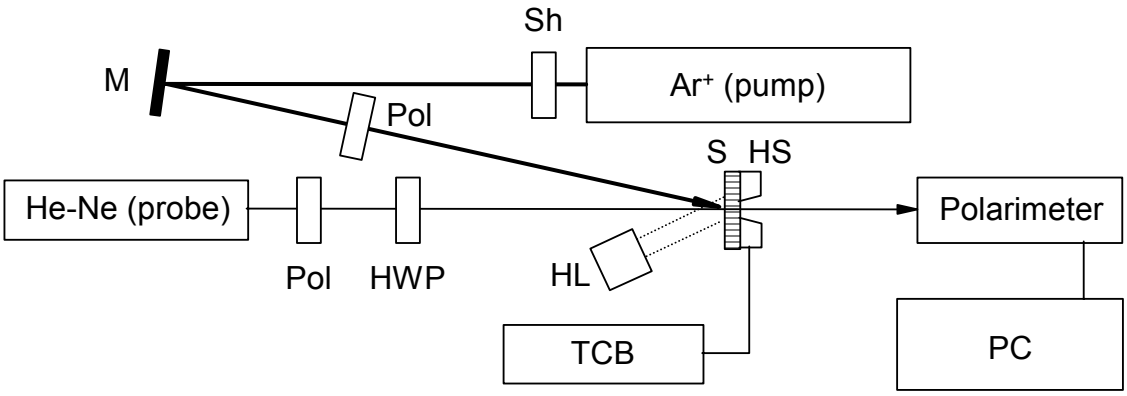

Figure 2.9.1 Experimental set-up for the measurement of the induced optical anisotropy. Sh: beam shutter; Pol: polarizer; M: mirror; HWP: half-wave plate; S: sample; HS: hot stage; TCB: temperature control block; HL: halogen lamp and PC: personal computer

The output from the polarimeter is an ASCII data file. Each line of the file is time stamped and includes the calculated Stokes parameters (S_0, S_1, S_2, S_3) as well as the degree of polarization, the ellipticity and the orientation of the polarization ellipse. S_1, S_2 and S_3 are the normalized intensities of the probe beam falling on the detector of the polarimeter and S_0 denotes total intensity, S_1 refers to the difference in intensities between horizontal and vertical linearly polarized components, S_2 refers to the difference in intensities between linearly polarized components oriented at + 45º and – 45º, and S_3 refers to the difference in intensities between left- and right-circularly polarized components. These Stokes parameters represent the state of polarization of light. From the Stokes parameters, the photoinduced phase shift δ can be calculated using the following equation:

$$\delta = \arctan\frac{S_3}{S_2} \qquad \text{eq (2.2)}$$

Chapter III

Polymerization of Styrenic LC Monomer by the ATRP Technique

Abstract

A new route for the synthesis of side chain liquid crystalline polymers (SC-LCP) is described. The azobenzene containing styrenic monomer is synthesized by esterification reaction using 4-vinylbenzoic acid, 4-[4-(6-hexyloxy)-phenylazo] benzonitrile and DCC as a coupling agent. The structure of the monomer is well confirmed by ^{1}H NMR, ^{13}C NMR and FT-IR spectroscopic measurements. The polymerization of this crystalline monomer was performed by ATRP technique using phenylethylbromide as an initiator and xylene as well as o-dichlorobenzene as the solvent. The polymers were prepared in controlled fashion with molecular weights (M_n) in the range of 2000 – 9000 and a polydispersity index (PDI) $\leq$1.2. The DSC analysis of the polymer reflects the glass transition (T_g) due to the amorphous polystyrene backbone and the melt transition (T_m) due to the side-chain azobenzene moieties. Furthermore, the homopolymer was also employed as a macroinitiator for the block copolymerization reaction with styrene (St) and pentafluorostyrene (FS).

3.1 Introduction

Azobenzene containing liquid crystalline polymers have attracted a considerable interest in recent years because of their potential applications in optical data storage.[1,2] The SC-LC azobenzene containing polymers have two advantages.[3] First, they have a much wider temperature range of the mesophase, and therefore a wide temperature range is available for optical applications. Secondly, they can function as image storage materials when they are operated at temperatures below their glass transition temperatures. Thus the azobenzene containing liquid crystalline polymers are potential materials for digital and holographic information storage.[4-6] Eich and coworkers[7,8] first reported that the image could be stored in the polymer liquid crystals as a hologram. A laser-beam-addressed recording has been achieved in SC-LCP. The most accepted mechanism for data storage is that the azobenzene groups align perpendicular to the applied electric field vector of the polarized laser radiation after several trans-cis-trans photoisomerization cycles.[9,10]

Block copolymers containing LC block(s) are fascinating systems and several reviews on this topic have appeared recently.[11-13] The most suitable method to synthesize the SC-LC copolymers with relatively narrow molecular weight distribution is a "living" polymerization. The LC monomers have been polymerized by different techniques like anionic, cationic, ring opening metathesis or group transfer polymerization.[11,13] Recently, controlled/living radical polymerization like nitroxide mediated radical polymerization[14] and atom transfer radical polymerization[15] have also been studied to synthesize SC-LC copolymers. Among all these methods the radical polymerization in controlled fashion has the greatest tolerance to moisture and a wide number of monomers can be polymerized. The ATRP is the most suitable method for polymerization of styrenic monomers[16] in a controlled manner and polymers with relatively narrow PDI can be prepared. To the best of our knowledge, this is the first report on the ATRP of side chain azobenzene containing styrenic monomer to synthesize these novel polymeric materials.

In this chapter the synthesis and characterization of monomer is described. The monomer is polymerized in a controlled manner with narrow PDI by the ATRP technique. The thermal properties of the polymers are also studied. The isolated homopolymers were employed as a macroinitiator for the block copolymerization with styrene (St) or pentafluorostyrene (FS).

3.2 Materials and Experimental

3.2.1 Materials

4-aminobenzonitrile, sodium nitrite ($NaNO_2$), phenol, 6-bromo-1-hexanol, dicyclohexylcarbodiimide (DCC), dimethylaminopyridine (DMAP), Cu(I)Br and bipyridine (bipy) were received from Aldrich and were used without further purifications. 4-vinylbenzoic acid was synthesized according to the procedure reported in the literature.[24] The anhydrous potassium carbonate (K_2CO_3) was dried at 150 °C and stored under nitrogen atmosphere. Methylethylketone (MEK) was dried over molecular sieves. All the other chemicals/solvents were used as received if not otherwise stated separately.

3.2.2 Experimental

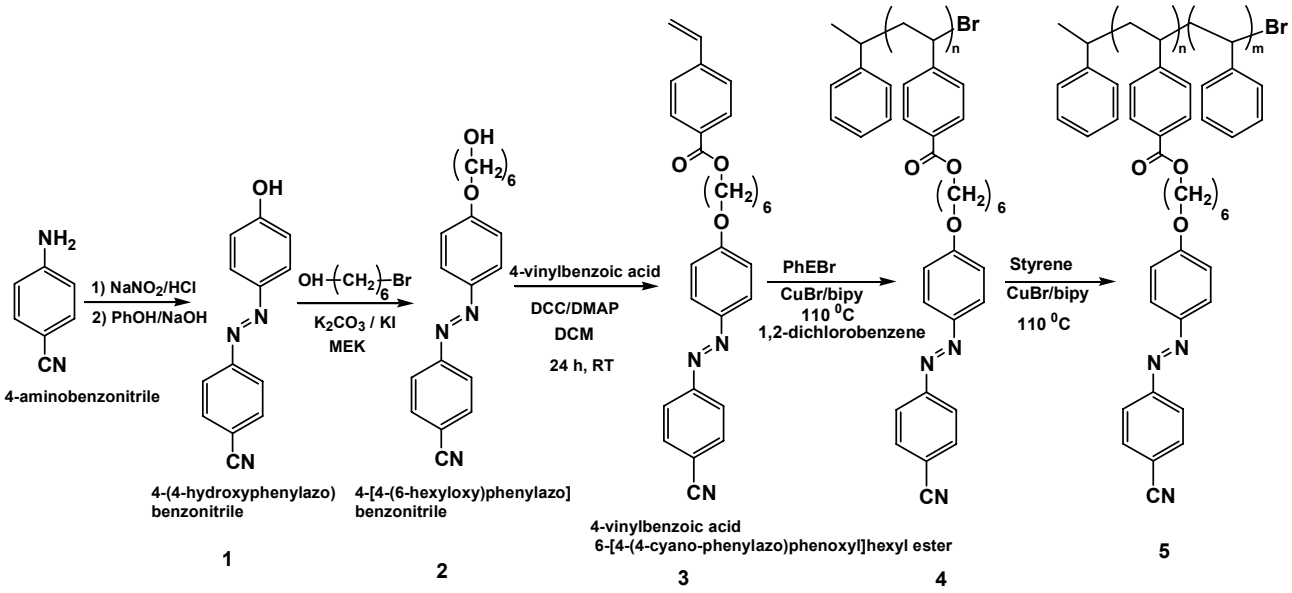

Scheme 3.1 Schematic presentation of the monomer synthesis and the subsequent polymerization

3.2.2.1 Synthesis of 4-(4-hydroxyphenylazo) benzonitrile (1)

The reported method of Ringsdorf et. al.[17] is modified and used for synthesis of 1. In a one-neck round bottom flask 2.76 g (23.4 mmol) of 4-aminobenzonitrile was dissolved in 30 ml of ethanol, to this 25 ml of 6N HCl was added slowly over a period of 30 min with vigorous stirring. The ethanol was evaporated slowly under reduced pressure on a rotary evaporator at 40 °C. This solution was then transferred to a three-neck 500 ml round bottom flask equipped with a mechanical stirrer and an addition funnel. To this mixture an ice-cold solution of 1.38 g (20 mmol) of $NaNO_2$ in 15 ml of water was added over a period of 20 min maintaining the temperature less than 5 °C. Then an ice-cold solution of 1.88 g (20 mmol) phenol and 6 g

(150 mmol) of NaOH in 30 ml of H_2O was added in 15-20 min with vigorous stirring. The temperature was maintained at less than 5 °C throughout the addition and then brought to room temperature. The reaction mixture was stirred for another 1 h and the precipitated azodye was isolated by filtration and washed several times with water. The residue was dissolved in 150 ml of 50% aq. EtOH and acidified with conc. HCl (37% w/v) to reprecipitate. The precipitate was filtered off and recrystallized using ethanol + water (2:1 v/v) as a solvent system to give brown-orange colored 4-(4-hydroxyphenylazo) benzonitrile. The purity of the recrystallized product was confirmed by OligoSEC, which shows a sharp single peak. Yield: 95%

Melting point: 198 °C

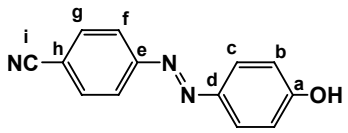

^{13}C NMR ($CDCl_3$) δ (TMS) = 116.5 (b); 118.5 (i); 119 (h); 124.4 (f); 125 (c); 133.3 (g); 142 (d); 153.4 (e); 162 (a).

Elemental analysis: theoretical: C (69.95 %), H (4.03%), N (18.83%)

observed: C (68.85%), H (3.92%), N (19.04%)

3.2.2.2 Synthesis of 4-[4-(6-hexyloxy)phenylazo] benzonitrile (2)

In a 500 ml one-neck flask equipped with a magnetic stirrer 10 g (46 mmol) of 4-(4-hydroxyphenylazo) benzonitrile (1), 12.56 g (69 mmol) of 6-bromo-1-hexanol, 12.79 g (93 mmol) of anhydrous K_2CO_3 and 50 mg of potassium iodide were dissolved in 300 ml MEK. The mixture was refluxed for 72 h under nitrogen and then cooled to room temperature. The excess K_2CO_3, KI and KBr formed were filtered and the filtrate was concentrated on a rotary evaporator. The product formed was purified by column chromatography using heptane/ethyl acetate (9:1 v/v) as an eluent. The purity was confirmed by OligoSEC and the structure was confirmed by FT-IR and ^1H NMR spectroscopy. Yield = 92 %

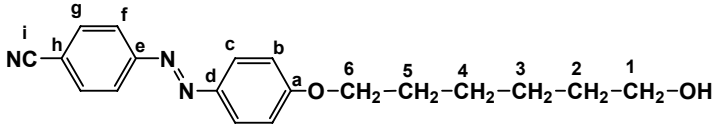

^1H NMR (DMSO) δ = 7.8-8.1(m, 6H, ^{b}C*H*, ^{c}C*H*, ^{f}C*H*); 7.15(dd, 2H, ^{g}C*H*); 4.28(t, 1H, -OH); 4.08(t, 2H, -^{6}CH_2-), 3.35(m, 2H, -^{1}CH_2-); 1.71(m, 2H, -^{5}CH_2-); 1.32(m, 6H, -^{2}CH_2-^{3}CH_2-^{4}CH_2-)

Elemental analysis: theoretical C (70.5 %), H (6.50%), N (13.00%)
observed C (70.09%), H (6.51%), N (13.20%)

3.2.2.3 Synthesis of 4-vinylbenzoic acid-6-[4-(4-cyano-phenylazo)phenoxyl]hexyl ester (3)

To a single-neck 250 ml round bottom flask equipped with a magnetic stirrer 5 g (34 mmol) of 4-vinylbenzoic acid and 400 ml of dry dichloromethane (DCM) were added. To these 10.9 g (34 mmol) of 4[4-(6-hexyloxy)phenylazo] benzonitrile (2), 9.5 g (46 mmol) of DCC and 1.5 g (12 mmol) of DMAP were added under nitrogen atmosphere and the mixture was stirred for 24 h at RT. The reaction mixture was poured in 15 ml of water and the layers were separated. The aqueous layer was extracted with fresh dichloromethane. The combined organic layer was washed twice with 10 % NaOH solution and three times with saturated solution of $NaHCO_3$ and finally with a brine solution. The DCM was evaporated on a rotary evaporator to give the crude ester. The resulting ester was purified by column chromatography using heptane: ethyl acetate (9:1 v/v) system. Yield = 70 %

Melting point: 111 °C.

Elemental analysis: theoretical C (73.46 %), H (6.12%), N (9.52%)
observed C (73.47%), H (6.09%), N (9.56%)

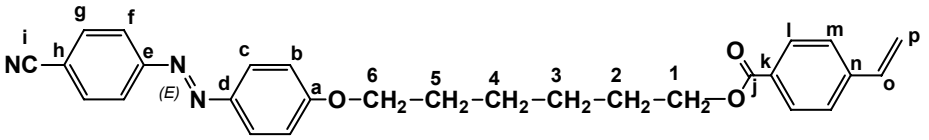

^{1}H NMR($CDCl_3$):δ = 7.8-8.1(m, 6H, ^{b}C*H*, ^{c}C*H,* ^{f}C*H*); 7.7(d, 2H, -^{l}CH_2-); 7.5(d, 2H, ^{m}C*H*); 7(d, 2H, ^{g}C*H*); 6.8(dd, 1H, -^{o}C*H*=); 5.8(d, 1H, ^{p}C*H*); 5.36(d, 1H, ^{p}C*H*); 4.37(t, 2H, -^{1}CH_2-); 4.07(t, 2H, -^{6}CH_2-), 1.8-2.0(m, 4H, -^{2}CH_2-^{5}CH_2-); 1.5-1.7(m, 4H, -^{3}CH_2-^{4}CH_2-)

^{13}C NMR ($CDCl_3$):δ = 166.34(j); 162.661(a); 154.83(e); 146.77(d); 141.89(o); 136.02(n); 133.11(g); 129.81(k); 129.58(L), 126.07(m); 125.43(c); 123.04(f); 118.58(i); 116.39(p); 114.87(b); 113.17(h); 68.23(6); 64.79(1); 29.01(2); 28.65(5); 25.79(3); 25.71(4)

3.2.2.4 Polymerization of 4-vinylbenzoic acid-6-[4-(4-cyano-phenylazo)phenoxyl]hexyl ester (4)

The ATRP of 4-vinylbenzoic acid-6-[4-(4-cyano-phenylazo)phenoxyl]hexyl ester (3) was carried out in *o*-dichlorobenzene (ODCB) as a solvent and under the conditions given in table 3.3.1. In a typical experiment a predried Schlenk tube was charged with 0.8 g (1.7 mmol) 4-vinylbenzoic acid-6-[4-(4-cyano-phenylazo)phenoxyl]hexyl ester and 1.5 ml

o-dichlorobenzene. To this 0.021 ml (0.16 mmol) PhEBr, 0.045 g (0.32 mmol) of CuBr and 0.075 g (0.48 mmol) bipy were added. The system was degassed three times with a freeze-pump-thaw cycle to remove oxygen and the polymerization was initiated by immersing the tube in an oil bath at 110 °C. The homopolymers were precipitated in methanol and the yield was determined gravimetrically after vacuum drying. The polymer was purified by soxhlet extraction in boiling methanol for 48 h.

The block co-polymerization reactions with St and FS were performed using poly 4-vinylbenzoic acid-6-[4-(4-cyano-phenylazo)phenoxyl]hexyl ester (4) as a macroinitiator and following the similar procedure as above.

3.3 Results and Discussion

The pioneering work of Matyjaszewski[18] and Sawamoto[19] on ATRP provided a new direction for the "controlled/living" radical polymerization. By this technique various functional monomers can be polymerized with living/controlled nature. In order to synthesize the liquid crystalline polymers we have also chosen the ATRP technique.

3.3.1 Synthesis of Precursor

The general strategy used for the synthesis is given in scheme 3.1.

The synthetic route used for the preparation of the mesogen is shown in the experimental section. The 4-(4-hydroxyphenylazo) benzonitrile was synthesized by electrophilic aromatic substitution reaction between the phenol and the diazonium cation. The diazonium cation was generated by diazotization reaction of 4-aminobenzonitrile and an aqueous solution of sodium nitrite in 6N hydrochloric acid solution[20] at a temperature less than 5 °C. This diazo cation is however, a weak electrophile and will normally only attack highly reactive aromatic compounds such as phenols and amines. The initial diazotization of aniline was carried out in strongly acidic media to ensure that, as yet unreacted amine is converted to the cation and so prevented from coupling with the diazonium salt as it was formed.

$$Ar-NH_2 + NaNO_2 + 2HCl \longrightarrow Ar-N\equiv N^{\oplus}\,Cl^{\ominus} + NaCl + 2H_2O \qquad \text{eq (3.1)}$$

The aqueous solution of phenol was added immediately with continuous stirring and maintaining the temperature always less than 5 °C.

The temperature of the reaction is an important parameter because even at lower temperatures the diazonium salt decomposes and results in unwanted side products.

The diazonium cation exists in acid and slightly alkaline solution (in strongly alkaline solution it is converted first into diazotic acids, Ph-N=N-OH, and then into the diazotate anions, Ph-N=N-O^-). Therefore, the coupling reaction with phenol was carried out at a slightly alkaline pH as it is PhO^-, and not the PhOH, that undergoes attack by ArN_2^+.

$$\text{Rate} = k\,[ArN_2^+]\,[PhO^-] \qquad \text{eq (3.2)}$$

Due to the various factors like electron density, strength of bond formed and bulk of the attacking electrophile, the coupling with the phenoxide ion preferably takes place on the carbon at para position as shown in figure 3.3.1.

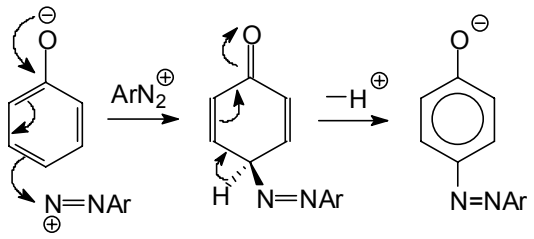

Figure 3.3.1 Mechanism of electrophilic substitution reaction of phenol

In order to avoid the multiplication of impurities the side products formed due to the unavoidable side reactions the azophenols were purified by recrystallization in aqueous ethanol. Thin layer chromatography using 8:2 mixtures of heptane and ethyl acetate revealed the presence of only one azophenol containing product. Furthermore, the percentage elemental analysis of the azophenols observed is in good approximation with the theoretical percentage of the elements.

The UV-visible spectroscopic analysis of the 4-(4-hydroxyphenylazo) benzonitrile shows strong absorption in the range of 350 nm to 380 nm. According to Rau,[21,22] there are three different types of azobenzene derivatives, depending on the relative energetic order of their (n-π*) and (π-π*) transitions: azobenzene-type, aminoazobenzene-type and pseudo-stilbene-type. The most stable trans conformation of the azobenzene has a characteristic low-intensity n-π* band and a high-intensity π-π* band as depicted in figure 3.3.2.

Nine different peaks were observed in the ^{13}C NMR spectrum of 4-(4-hydroxyphenylazo) benzonitrile performed in DMSO-d_6. The assignment of the chemical shifts of the individual carbon resonances is according to previous reports.[23] The ^1H NMR of the substituted azophenols also supports the structure shown in scheme 3.1.

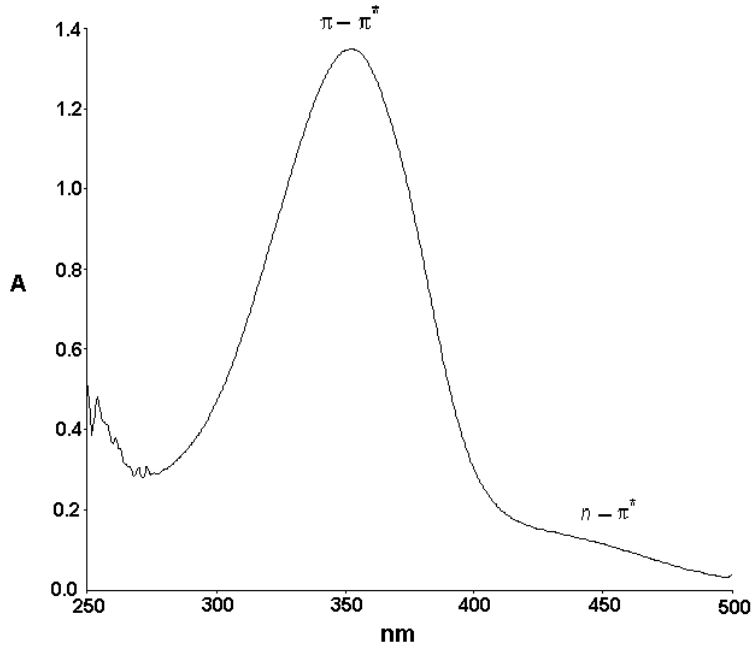

Figure 3.3.2 UV-visible spectrum of 4-(4-hydroxyphenylazo) benzonitrile

The melting point was determined by DSC to provide a more accurate determination. The melting point recorded for 4-(4-hydroxyphenylazo) benzonitrile (198 °C) is from the first heating because the compound decomposed after the first heating. The value observed is in good agreement with the reported value in the literature.[23]

This 4-(4-hydroxyphenylazo) benzonitrile (1) (scheme 3.1) was used as a base material for the synthesis of vinylic monomer. The Williamson etherification reaction of the compound (1) with 1:1.5 excess of 6-bromo-1-hexanol gave the 4[4-(6-hexyloxy)phenylazo] benzonitrile (2) in 92% yield.

The compound was purified by column chromatography using 9:1 (v/v) heptane and ethyl acetate as an eluent. The TLC analysis of the column fraction shows a single spot revealing the compound is pure enough. Furthermore, the OligoSEC analysis of the column fraction shows a sharp single peak.

The structure of the compound was confirmed by FT-IR and ^{1}H NMR spectroscopy. The ^{1}H NMR spectrum illustrates the resonance at 4.08 ppm due to the methylene protons next to phenolic oxygen separates from other aliphatic protons. The methylene protons next to the hydroxyl group appear at 3.35 ppm, which has the same resonance corresponding to the starting 6-bromo-1-hexanol. The hydroxyl proton resonance appears at 4.3 ppm. The D_2O treatment study supports the claim that the 4.3 ppm resonance is corresponding to the hydroxyl proton.

A few drops of deuterated water (D_2O) were placed in the NMR tube and the tube was shaken thoroughly. The ^1H NMR spectra of the sample after treatment with D_2O showed that the resonance at 4.3 ppm has disappeared. The figure 3.3.3 a and b shows the ^1H NMR spectrum of compound 2 before and after treatment with D_2O.

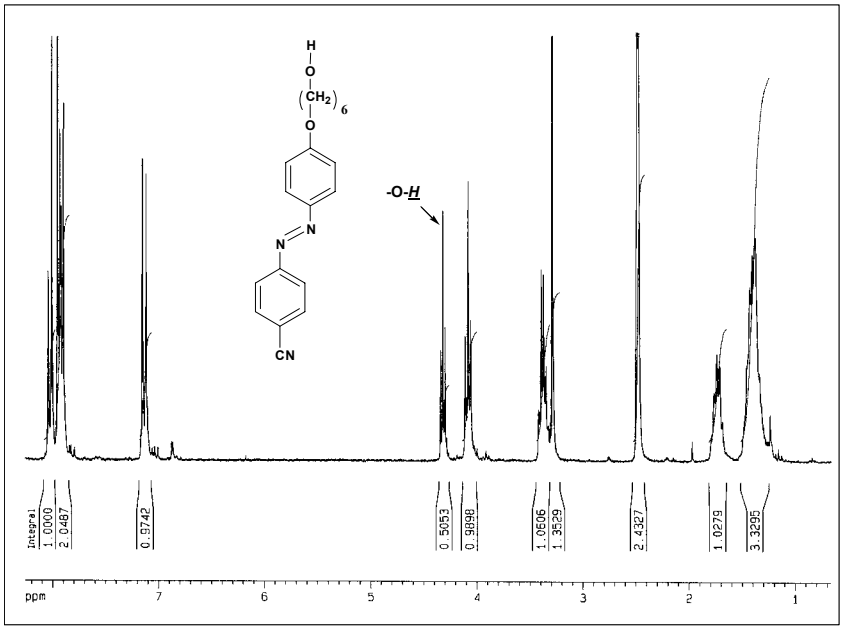

a

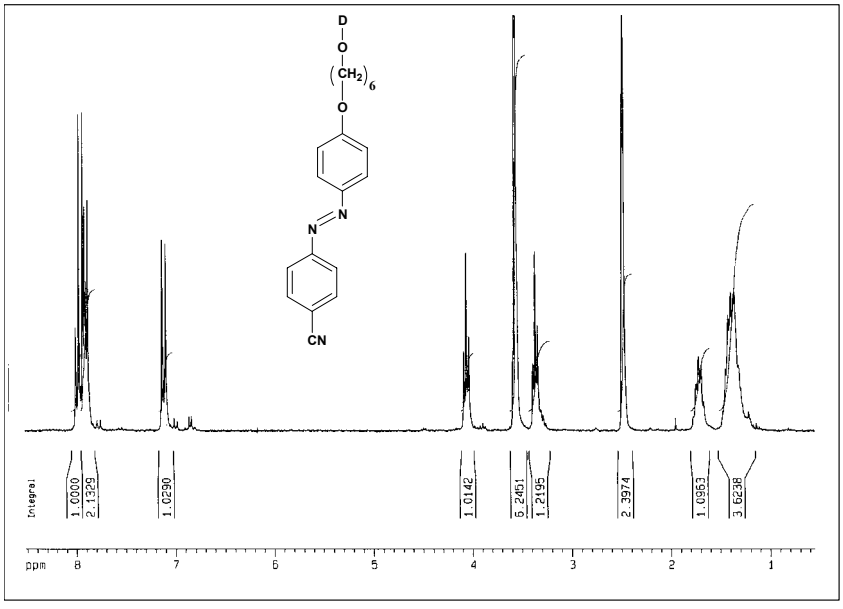

b

Figure 3.3.3 ^1H NMR spectrum of 4[4-(6-hexyloxy)phenylazo] benzonitrile 2 a) before D_2O treatment b) after D_2O treatment.

3.3.2 Synthesis of 4-vinylbenzoic acid

The 4-vinylbenzoic acid (synthesized by Tenna Nielsen, DTU, Denmark) was purified by recrystallization and used for the initial experiments. Due to the large number of experiments the surplus amount of 4-vinylbenzoic acid was synthesized from 4-methylbenzoic acid as described in the literature.[24] The yield observed was more than 80%. The structure of the 4-vinylbenzoic acid was confirmed by ^{1}H and ^{13}C NMR and it was in good agreement with the analysis reported in the literature.

The general scheme followed for the synthesis of 4-vinylbenzoic acid is given in figure 3.3.4.

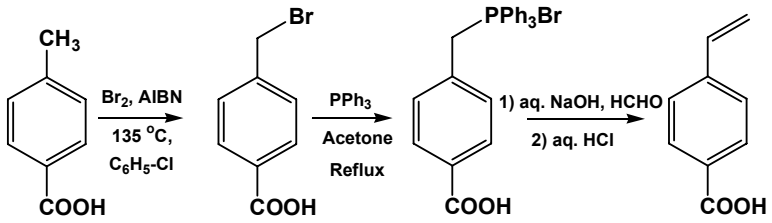

Figure 3.3.4 Synthesis of 4-vinylbenzoic acid

3.3.3 Synthesis of 4-vinylbenzoic acid-6-[4-(4-cyano-phenylazo)phenoxyl]hexyl ester (3) and its Polymerization

The vinylic monomer bearing the pendant alkoxyazobenzene group was synthesized by esterification reaction between 4-vinylbenzoic acid and the alkoxy terminated azobenzene 2 using DCC and DMAP.[25] The initial attempt was to make the corresponding 4-vinylbenzoyl chloride by treatment of oxalylchloride/thionylchloride with 4-vinylbenzoic acid and perform the esterification reaction with the compound 2 (scheme 3.1) in the presence of pyridine. But the esterification reaction between acid chloride and alkoxy azobenzene leads to some side products and also the reaction conditions required were very harsh. Therefore, the use of DCC avoids the handling of toxic oxalyl or thionyl chloride and yields the compound 3 (scheme 3.1) in one step with fairly quantitative conversion.

The mechanism of esterification reaction using DCC coupling is shown in figure 3.3.5. The DCC first forms the activated complex with a carboxyl functionality. Then the nucleophile attacks this activated carboxyl complex and yields the corresponding ester.

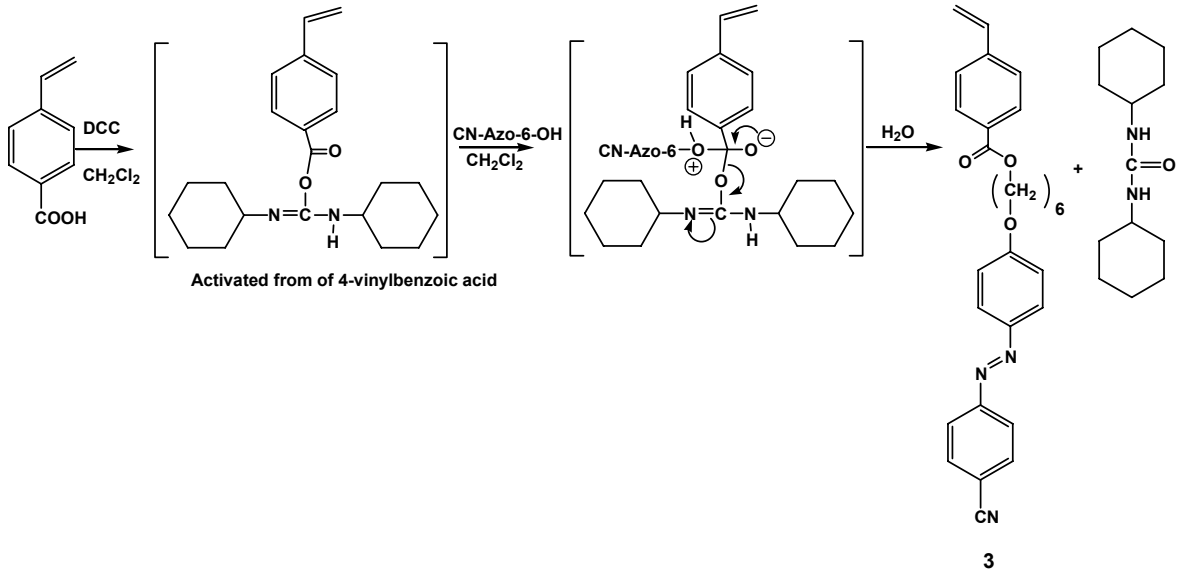

Figure 3.3.5 Mechanism of the esterification reaction using DCC

The side product formed during the reaction is dicyclohexyl urea, which has been removed during the work-up of the reaction. The esterification reaction was performed in dry DCM for 24 h at RT to ensure quantitative conversion. The reaction was monitored by TLC. After completion of the reaction 10-15 ml of water was added to quench the reaction. The organic layer was washed thoroughly with 10 % NaOH (w/v) solution to remove the unreacted 4-vinylbenzoic acid. Then it was washed with a saturated solution of $NaHCO_3$ and finally with the brine solution. The DCM layer was dried over anhydrous sodium sulphate and evaporated on a rotary evaporator. The solid product formed was then purified by column chromatography using heptane and ethyl acetate (9:1 v/v) as an eluent. The purity was confirmed by TLC (shows a single spot) and also by OligoSEC (shows a sharp single peak).

The structure of the compound 3 was illustrated by ^{1}H and ^{13} C NMR spectroscopy performed in $CDCl_3$. In ^{1}H NMR (not shown here) the two doublets at 5.36 and 5.8 ppm, respectively, elucidate the resonance due to geminal protons of the double bond whereas the dd at 6.8 ppm reflects the -C*H* proton of the vinylic double bond. The resonances in the aromatic region were complex and an individual assignment was difficult. The methylene protons next to the carboxyl group ($^{1}CH_2$) and phenoxyl group ($^{6}CH_2$) separate from the other aliphatic protons and appear as triplets at 4.37 and 4.07 ppm, respectively. The remaining eight aliphatic protons from the side chain appear as a multiplet between 1.8-2.0 and 1.5-1.7 ppm. The comparison of the integral area also confirmed the purity of the monomer.

Figure 3.3.6 shows the ^{13}C NMR of the compound 3. The assignments illustrated in the figure are based on a literature[23] report. The six aliphatic carbon atoms of the alkyl spacer

appear between 20 to 70 ppm whereas the aromatic carbon resonances appear between 110 to 165 ppm. The resonance at 118.58 ppm is characteristic of the nitrile substituent.

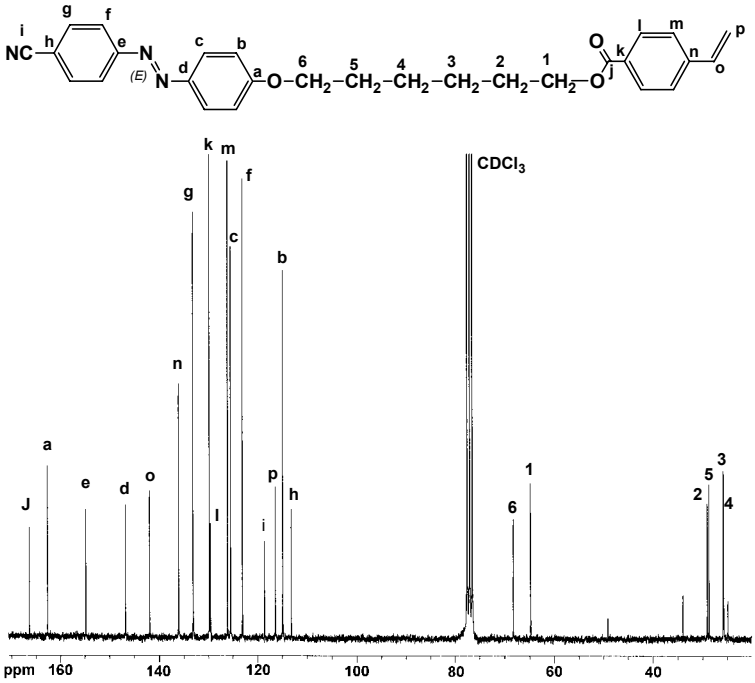

Figure 3.3.6 ^{13}C NMR spectrum of 4-vinylbenzoic acid-6-[4-(4-cyano-phenylazo)phenoxyl]hexyl ester

Both the ^{1}H NMR as well as the ^{13}C NMR spectrum strongly evidence the structure shown in the scheme 3.1. In the FT-IR spectrum the hydroxyl absorption at 3400 cm^{-1} of the alkoxy azo precursor disappears completely and a new ester carbonyl absorption at 1704 cm^{-1} was observed. Furthermore, the absorption at 2222 cm^{-1} also evidences the nitrile substituent of the starting azobenzene part of the alkoxy precursor.

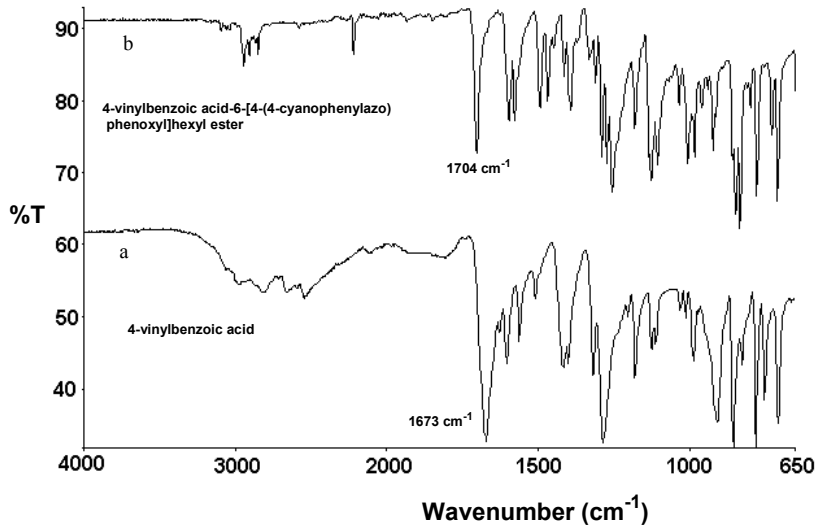

Figure 3.3.7 Comparative FT-IR spectra of 4-vinylbenzoic acid a) before esterification b) after esterification.

The DSC analysis of this monomer shows a melt transition at 108°C and 111°C. The transitions reported here are based on the first heating cycle.

This vinylic monomer was polymerized by the ATRP technique. As mentioned in chapter I ATRP is a versatile method with which polymers with a controlled molecular weight and a relatively narrow PDI can be prepared. Also, monomers bearing functional groups can be polymerized. The detailed mechanism of the ATRP is given in chapter I. The recent review by Matyjazewski[16] has shown that a wide range of vinylic monomers like substituted St, acrylates or methacrylates can be polymerized in a controlled fashion with narrow molecular weight distribution. Matyjaszewski[26] has also reported that long alkyl chain substituted acrylates with bulky pendant groups can also be polymerized by this technique.

Among the various substituted St, so far there was no report on ATRP of St bearing an azobenzene substituent as a pendant group. Therefore, this new vinylic monomer 3 was synthesized and polymerized by ATRP technique using phenylethylbromide (PhEBr) as an initiator and CuBr/bipy as a catalyst system in xylene as well as in *o*-dichlorobenzene solution. Homopolymers P(CN-Azo-6)S-Br (4) with molecular weights ranging from 2000 – 8000 have been synthesized. The molecular weights and PDIs calculated by SEC are based on PS-standards. A PDI as low as 1.11 can be obtained. The initial experiment was performed with 200 mg of monomer in 2 ml of *o*-dichlorobenzene targeting a molecular weight of 5000. This polymerization reaction resulted in the traces of the polymer within 8 h at 110°C. The M_n calculated by SEC showed that the molecular weight was 2200 with a PDI of 1.15. The observed low yield may be due to the early termination or the insufficient reaction time; therefore further reactions were performed for more than 18 h. The M_n and PDI of the homopolymers obtained by SEC analysis are given in table 3.3.1.

It has been observed that by increasing the reaction time the polymerization yield has improved. The maximum yield obtained was 69% within 18.5 h at 110°C using *o*-dichlorobenzene as solvent. Simultaneous experiments in 1,2-dichlorobenzene and xylene under similar conditions were performed. In both cases the molecular weight observed was more than 8000 and also the PDI was relatively narrow (<1.12).

When *o*-dichlorobenzene was used as solvent 69% yield was achieved whereas in xylene solution it leads to only 44% yield after 18.5 h. Furthermore, the experiment 1-80-4 from table 3.3.1 showed that the dilution of the reaction mixture gave a better control over the PDI but a low conversion even though the reaction was performed for 20 h.

Table 3.3.1 ATRP of 4-vinylbenzoic acid-6-[4-(4-cyanophenylazo)phenoxyl]hexyl ester

No.	M_n (Target)	M_n (SEC) and PDI	Solvent	Time h	Yield %
1-79-2	5000	2200,1.15	ODCB (7 %)	8	-
1-80-1	10000	8800,1.11	ODCB (27 %)	18.5	69
1-80-2	10000	8200,1.12	Xylene (22 %)	18.5	44
1-80-3	5000	6700, 1.14	ODCB (29 %)	20	56 [a]
1-80-4	5000	6820, 1.11	ODCB (20 %)	20	65

a = % yield calculated after soxhlet extraction

The DSC analysis of the homopolymer is shown in figure 3.3.8. The transformation of the styrenic monomer to the mesogenic polystyrene does not influence the melt transition of the mesogen. The backbone polystyrene polymer has a T_g of 60 °C and the mesophase transition due to the azobenzene mesogens was observed at 106 °C.

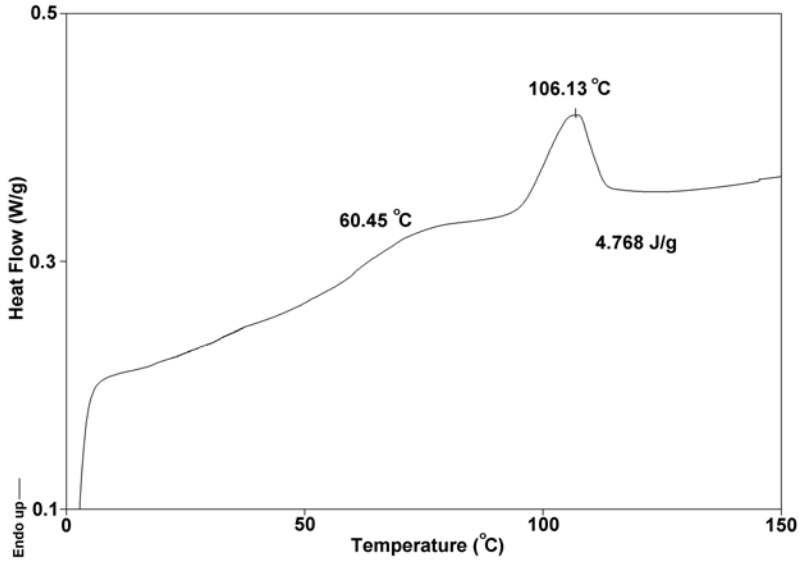

Figure 3.3.8 DSC chromatogram of P(CN-Azo-6)S

The homopolymer having an M_n 6700 (1-80-3 from table 3.3.1) was purified by a soxhlet extraction in boiling methanol to employ it as a macroinitiator. This polymer was characterized by ^{1}H NMR spectroscopy. The ^{1}H NMR illustrates that the resonances due to the olefinic protons between 5 to 6.5 ppm have disappeared and new resonances in the

aliphatic region between 1.1 to 2.3 ppm were observed. Not much information could be extracted from the aliphatic region because the protons of the polymer main chain and the side chain protons overlap and appear as a multiplet. Evidently, the methylene protons adjacent to oxygen from the side chain are well separated from the other aliphatic protons and appeared at 4 ppm.

One of the major advantages of the ATRP technique is that the halogen functionality migrates from the starting initiator moiety to the isolated homopolymer chain end. This halogen functionality of isolated homopolymers can be activated in a post-polymerization reaction and can be employed as a macroinitiator for the block copolymerization reactions. By this method the chain length or the composition of the individual blocks can be well controlled.

Therefore, this strategy of using a macroinitiator for the block copolymerization with St or FS was undertaken. The 1-80-3 was employed as a macroinitiator for the block copolymerization reactions. In addition CuBr/bipy were used as a catalyst system in *o*-dichlorobenzene and the polymerizations were performed at 110°C. The initial experiments were performed in bulk using St itself as a solvent as depicted in table 3.3.2 (entry 1 and 2). The obtained polymer had a shoulder towards the high molecular weight side instead of a clear shift in the elution volume as observed by SEC. A broadening of the PDI was observed with a slight increase in the molecular weight compared to the corresponding macroinitiator. Furthermore, the effect of catalyst concentration has also been studied. The strategy of using higher amounts of catalyst was to accelerate the initiation and hence ultimately the polymerization reaction. But these experiments also gave polymers with a slight increase in molecular weight and a big shoulder towards the high molecular weight side instead of a clear shift of the elution volume.

Table 3.3.2 Block copolymerization data of the mesogenic block copolymer with St and FS

No.	Polymer	M_n (Target)	Solvent	SEC		Time h
				M_n	PDI	
1/81/1	P(M)S-*b*-PS	50000	-	8070	1.49	20
1/81/2[a]	P(M)S-*b*-PS	50000	-	9300	1.55	22
1/81/3	P(M)S-*b*-PFS	50000	ODCB 1ml	9800	1.43	8
1/82/1[b]	P(M)S-*b*-PFS	50000	ODCB 1ml	6830[c] 24100[c]	1.12 1.08	4

[I]: [Cu]: [bipy] 1: 1.1: 3 Polymerization temperature 110°C, [a] [I]: [Cu]: [bipy] 1: 3: 7 [b] 4, 4 -dinonyl-2, 2 -bipyridine as a ligand, [c] M_n calculated for individual peak (refer to figure 3.3.10)

Hvilsted[27] et. al have shown that FS polymerizes much faster than St under ATRP conditions. The block copolymerization of P(CN-Azo-6)S-Br with FS using *o*-dichlorobenzene as a solvent under similar conditions clearly showed a bimodal distribution in the SEC analysis. Figure 3.3.10 shows the SEC overlay of the P(CN-Azo-6)S-Br macroinitiator and its block copolymer with FS.

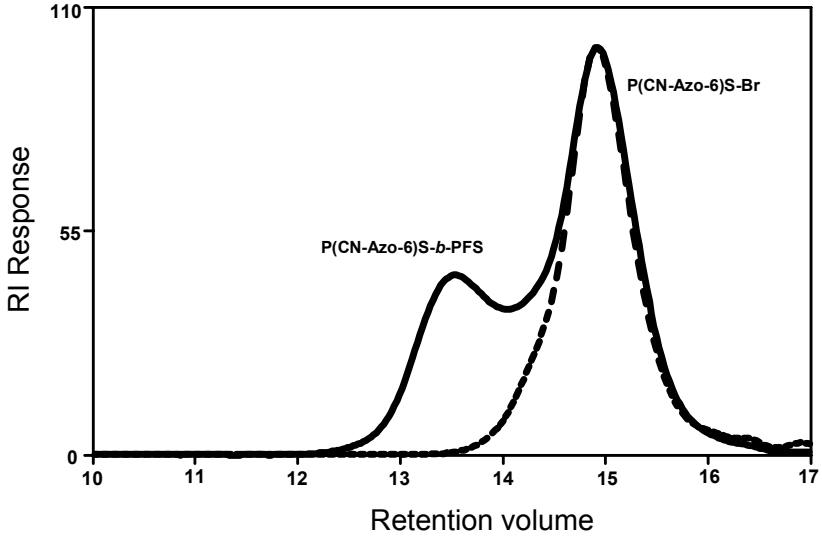

Figure 3.3.10 SEC overlay of P(CN-Azo-6)S-Br and its block copolymer with FS

From the SEC traces it was observed that the resulting polymer is a mixture of the macroinitiator and the block copolymer formed with FS. In order to confirm that the second peak observed is due to the block copolymer and not due to thermal polymerization of FS, the two fractions were separated on a SEC column and collected separately. This was the only possible method because no other easier alternative was found to separate these two fractions. Since the amount of polymer recovered from these fractions was relatively small, only an FT-IR analysis could be performed on these fractions. The FT-IR spectrum of the high molecular weight fraction (1st fraction) showed the absorption at 2222 cm^{-1} due to the nitrile functionality suggesting the presence of the mesogenic blocks. In addition, the absorption around 1204 cm^{-1} suggests the incorporation of FS. These results strongly evidence that the high molecular weight fraction is the block copolymer [P(CN-Azo-6)S-*b*-PFS] and not the thermally polymerized FS. Furthermore, the FT-IR analysis of the second fraction has an absorption only at 2222 cm^{-1} due to the nitrile functionality of the azobenzene part and no absorption due to the PFS block was observed.

From these observations it can be concluded that during the block copolymerization reaction only the part of the bromine functionality of the macroinitiator was initiated. It

resulted in a mixture of the starting homopolymer as well as the block copolymer with PFS. In general, to study the effect of various parameters on the properties of mesogenic block copolymers the polymer needs to be free from this mixture. In practice we found the separation of this mixture on quantitative basis to be very difficult. Therefore, another route to synthesize the mesogenic block copolymer was followed and is mentioned in the subsequent chapter.

3.4 Conclusions

The side chain azobenzene containing styrenic liquid crystalline monomer was synthesized successfully with high purity. The structure of the monomer was confirmed by ^{1}H and ^{13}C NMR spectroscopy. The monomer was successfully polymerized under ATRP conditions using PhEBr as an initiator and CuBr/bipy as a catalyst system. Homopolymers with a molecular weight in the range of 2000 to 9000 were prepared. A PDI of less than 1.2 was obtained for these polymers. The DSC analysis of the azobenzene containing homopolymers indicates the separation of the mesophase. Furthermore, these isolated homopolymers were employed as the macroinitiator for the block copolymerization reaction with St and FS but surprisingly they resulted in a mixture of two different polymers.

Chapter IV

Synthesis and Characterization of Photoaddressable Polymers

Abstract

The synthesis and characterization of a series of side chain liquid crystalline (SC-LC) block copolymers bearing azobenzene side chains have been carried out. The polystyrene block polyhydroxystyrene copolymer (PS-b-PHS) was used as template polymer and was achieved by deprotection of the tert-butoxy group from polystyrene block polybutoxystyrene (PS-b-PBS) copolymer. These PS-b-PBS copolymers were synthesized by living anionic polymerization and sequential addition of St and tert-butoxystyrene (t-BuOSt). Block copolymers with four different PS compositions have been synthesized. The resulting hydroxyl sites of PS-b-PHS were functionalized with azobenzene mesogens bearing four different alkyl spacers [-$(CH_2)_4$-, -$(CH_2)_6$-, -$(CH_2)_8$- and -$(CH_2)_{10}$-] under phase transfer catalysis reaction conditions. The mesogenic block copolymers were characterized by SEC, ^{1}H-NMR, DSC and also by a holographic technique. The effect of the side chain spacer length of the mesogens and also the effect of polystyrene content on the phase behavior, stability of anisotropy and thermal properties of the polymer were studied.

4.1 Introduction

The SC-LC diblock copolymers are a class of materials that have undergone tremendous development in the last few years.[1,2] These materials combine the properties of polymer macromolecules with the properties of liquid crystalline organic molecules. As mentioned earlier these materials have attracted severe attention due to their use in high-density optical data storage.[3]

Bignozzi et. al have shown the block copolymerization of 4-acetoxystyrene with [(4'-methoxyphenyl) 4-oxybenzoate]-6-hexyl (4-vinylbenzoate) by using benzoyl peroxide and 2,2,6,6-tetramethylpiperidinyl-1-oxy (TEMPO) as radical initiators.[2] These block copolymers were susceptible to show separate phases of amorphous blocks and segregated LC domains possessing a smectic mesophase. Ober and coworkers used the living anionic polymerization technique to synthesize coiled liquid crystalline diblock copolymers. They have synthesized a styrene-isoprene block copolymer and used several steps to introduce the liquid crystalline azobenzene substituent in the isoprene block.[1] These LC blocks had a tendency to form cylindrical domains bearing smectic-A mesophases. Furthermore, they have also reported that these smectic-A cylinders are embedded within a polystyrene matrix. These smectic cylindrical microdomains have a higher clearing transition than the lamellar structure. This may be due to the stabilization of the smectic mesophase within the cylindrical microdomains. The use of poly(methacrylate)-based side chain azobenzene containing polymers for optical storage has been well studied by Nathanson[21] and Hvilsted.[4] These materials possess large diffraction efficiency, which was stable at room temperature.

One hindrance to the commercial use of these SC-LC azobenzene polymers for optical data storage is the presence of liquid crystalline domains. On the one hand they are necessary for the permanent storage of the information but on the other hand the light scattering from these domains is the reason for background noise. This has led to the design of amorphous polymers with a high T_g.[5,6] In these polymers the formation of domains will be suppressed by having a high T_g and the stored information will be stable. However, it is reported that the induced anisotropy is not stable over a long period of time in glassy polymers.[7]

Hence the presence of domains for the stability of the stored information and the absence of domains for a good optical quality can be achieved by reducing the size of the domains. This can be possible by use of the block copolymers in which one block should contain the azobenzene functionality.

Among the library of polymeric materials for implanting azobenzene side chains for optical storage the materials based on polystyrene block copolymers were missing. The block

copolymer of St and hydroxystyrene is the class of material, which has never been investigated.

To investigate the influence of polymer block length, number of methylene units in the alkyl spacer, type of substituent etc. it is advisable to have polymers with relatively narrow PDI. In anticipation of several difficulties in the purification of the monomer and the polymers we have followed the anionic polymerization method to synthesize the template polymer. These SC-LC diblock copolymers were synthesized by introduction of side chain LC precursors by the phase transfer catalysis route.

4.2 Experimental

4.2.1 Materials

The St and t-BuOSt (Aldrich) were passed through an alumina column to remove inhibitor and stored under argon. 4-aminobenzonitrile, 4-fluoroaniline, 4-aminotrifluromethylbenzene, sodium nitrite, phenol and α,ω-dibromoalkanes were received from Aldrich and used as received. The anhydrous potassium carbonate was dried at 150 °C and stored under nitrogen atmosphere. The methylethylketone (MEK) was dried over molecular sieves and stored under nitrogen. All the other chemicals/solvents were used as received if not otherwise stated separately.

4.2.2 Synthesis of 4-(4-hydroxyphenylazo) benzonitrile (1)

The detailed procedure for the synthesis of azophenols is given in the experimental section of chapter III.

4-(4-hydroxyphenylazo) fluorobenzene and 4-(4-hydroxyphenylazo) trifluromethyl benzene were prepared by following a similar procedure. Both these *p*-anilines are liquids. Therefore, they were used directly without dissolving in ethanol.

Melting point: R = CN (198 °C), R = F (151 °C), R = CF_3 (128 °C)

^1H and ^{13}C-NMR in $CDCl_3$ were used to confirm the structures. In addition UV absorption measurements of the compounds are also reported.

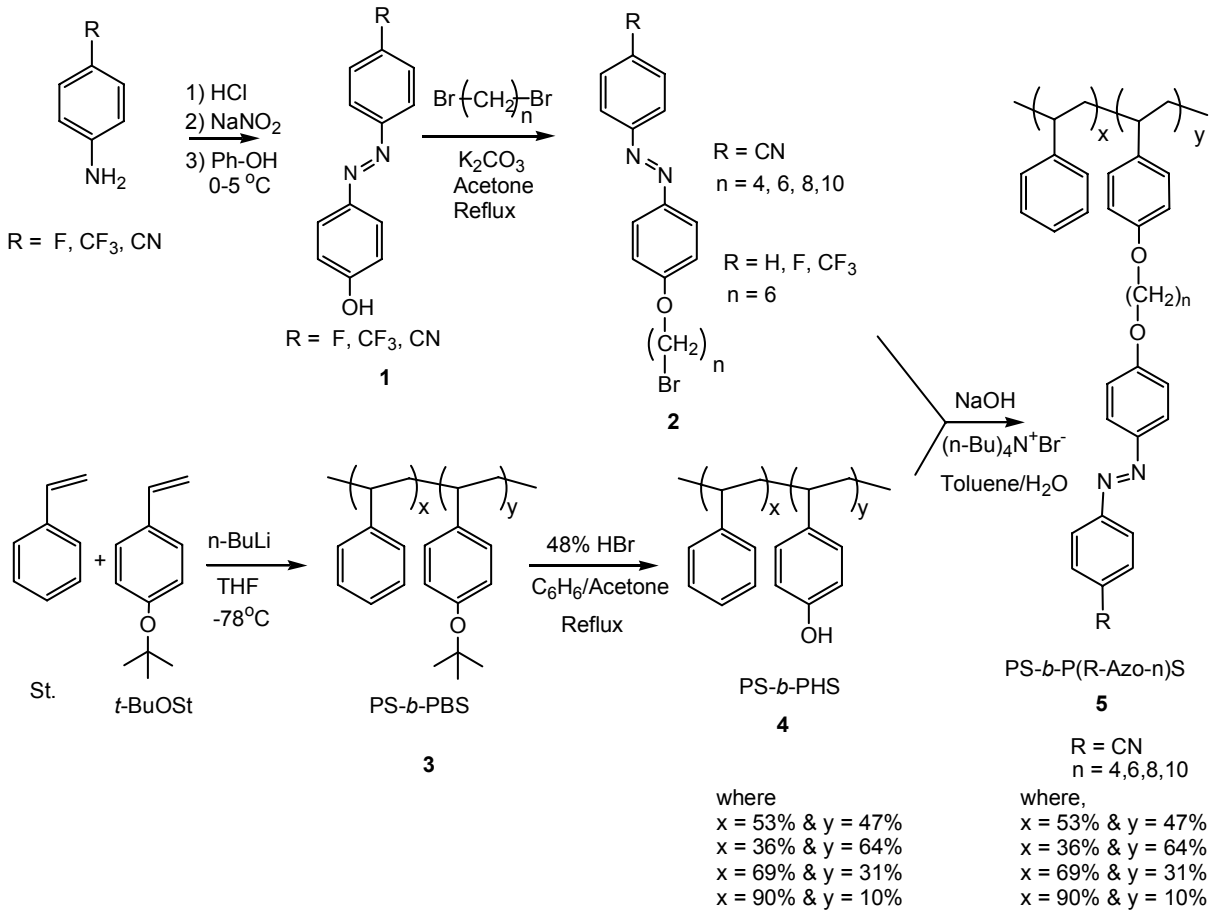

Scheme 4.1 Synthetic strategies used for the preparation of the mesogenic block copolymers

4.2.3 Synthesis of 4(ω-bromoalkoxy)-4'-cyanoazobenzenes (2)

The coupling reactions of 4-(4-hydroxyphenyl) azobenzenes with α,ω-dibromoalkanes were performed under Williamson etherification reaction conditions using MEK as a solvent.[8]

In a 250 ml one-neck round bottom flask equipped with a magnetic stirrer and a reflux condenser 13.4 mmol of 4-(4-hydroxyphenylazo) benzonitrile were dissolved in 70 ml of dry MEK. To this solution 268 mmol of the corresponding α,ω-dibromoalkane, and 21.44 mmol of anhydrous K_2CO_3 and 25 mg of KI were added. The reaction mixture was refluxed for 72 h under nitrogen and then cooled to room temperature. The mixture was filtered to remove the excess of K_2CO_3 and KBr formed. The MEK was evaporated under reduced pressure on a rotary evaporator. The residue was diluted with 30 ml hexane and the reaction mixture was cooled down to induce the crystallization. The resulting crystalline product was filtered off under suction and washed thoroughly with hexane to remove the excess of dibromoalkane. The formed orange color product was dried under vacuum and purified by column chromatography using silica gel (Aldrich, 70-270 mesh, 80 Å) in heptane and ethyl acetate (9:1 v/v) system.

The purity of the product was investigated by OligoSEC which showed a sharp single peak.

Yield: 70 %

Following the same procedure 4-(6-bromoalkoxy)-4'-fluoroazobenzene, 4(6-bromoalkoxy)-4'-trifluoromethylazobenzene were synthesized using the corresponding azophenol and 1, 6-dibromohexane. In both cases the yield was more than 70%.

Melting point: the melting points were determined by DSC, which were in close agreement with the literature report and are given in table 4.1.

The 4(ω-bromoalkoxy)-4'-cyanoazobenzenes were characterized by UV absorption measurements in THF solutions and ^{1}H-NMR as well as ^{13}C NMR in $CDCl_3$ (table 4.3 and 4.4 respectively). In addition, the results of the elemental analysis of the starting azophenol and the corresponding 4(ω-bromoalkoxy)-4'-azobenzene are given in table 4.2.

Table 4.1 Melting and crystallization temperatures of the azobenzene precursors.

R	**CN**	**CN**	**CN**	**CN**	**F**	**CF_3**	**H**
n	**4**	**6**	**8**	**10**	**6**	**6**	**6**
T_m (°C)	123	91 &101	81 & 97	103	79	n.d	n.d
T_c (°C)	106	68	64 & 61	87	43	n.d	n.d

Heating and cooling rate 5°C/min, n.d = not determined, T_m and T_c stands for melting and crystallization temperatures respectively.

Table 4.2 Elemental analyses of the azobenzene precursors

Azo phenol				**Theoretical (%)**			**Observed (%)**		
No	R	Mol. Formula	M Wt. (g/mol)	C	H	N	C	H	N
1	CN	$C_{13}H_9N_3O$	223	69.95	4.03	18.83	68.85	3.92	19.04
2	F	$C_{12}H_9FN_2O$	215	66.97	4.18	13.02	65.05	4.17	12.64
3	CF_3	$C_{13}H_9F_3N_2O$	263	58.6	3.38	10.5	57.4	3.43	9.45

Azo mesogens					**Theoretical (%)**			**Observed (%)**		
No	R	n	Mol. Formula	M Wt. (g/mol)	C	H	N	C	H	N
1	CN	4	$C_{17}H_{16}BrN_3O$	358	56.98	4.47	11.73	57.11	4.32	11.92
2	CN	6	$C_{19}H_{20}BrN_3O$	386	59.06	5.18	10.88	58.9	4.97	10.83
3	CN	8	$C_{21}H_{24}BrN_3O$	414	60.86	5.79	10.14	60.24	5.56	10.12
4	CN	10	$C_{23}H_{28}BrN_3O$	442	62.44	6.33	9.50	61.28	6.25	9.48
5	F	6	$C_{18}H_{20}FBrN_2O$	378	57.14	5.29	7.41	56.40	5.36	7.52
6	CF_3	6	$C_{19}H_{20}F_3BrN_2O$	429	53.14	4.66	6.53	52.69	4.72	6.6
7	H	6	$C_{18}H_{21}BrN_2O$	362	59.66	5.80	7.73	59.07	5.69	6.98

Table 4.3 ^{1}H NMR chemical shifts of azo compounds in $CDCl_3$

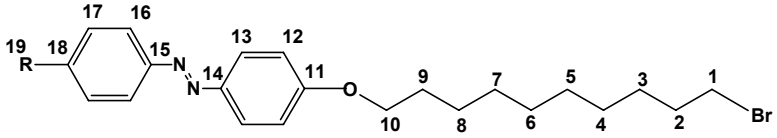

CN-azo-4-Br	δ=8.3(dd, 4H, ^{12}C*H*, ^{13}C*H*); 8.1(d, 2H, ^{16}C*H*); 7.3(d, 2, ^{17}C*H*); 4.45(d, 2H, -O-^{4}CH_2); 3.8(d, 2H, -^{1}CH_2-Br); 2.4(m, 4H, -^{2}CH_2-^{3}CH_2-)
CN-azo-6-Br	δ=7.95(dd, 4H, ^{12}C*H*, ^{13}C*H*); 7.8(d, 2H, ^{16}C*H*); 7.0(d, 2, ^{17}C*H*); 4.1(d, 2H, -O-^{6}CH_2); 3.55(d, 2H, -^{1}CH_2-Br); 1.9(m, 4H, -^{2}CH_2-^{5}CH_2-); 1.55(4H, -^{3}CH_2-^{4}CH_2-)
CN-azo-8-Br	δ=8.0(dd, 4H, ^{12}C*H*, ^{13}C*H*); 7.9(d, 2H, ^{16}C*H*); 7.0(d, 2, ^{17}C*H*); 4.1(d, 2H, -O-^{8}CH_2); 3.55(d, 2H, -^{1}CH_2-Br); 1.9(m, 4H, -^{2}CH_2-^{7}CH_2-); 1.55(8H, -^{3}CH_2-^{4}CH_2-^{5}CH_2-^{6}CH_2)
CN-azo-10-Br	δ=7.95(dd, 4H, ^{12}C*H*, ^{13}C*H*); 7.8(d, 2H, ^{16}C*H*); 7.0(d, 2, ^{17}C*H*); 4.1(d, 2H, -O-^{10}CH_2); 3.55(d, 2H, -^{1}CH_2-Br); 1.9(m, 4H, -^{2}CH_2-^{9}CH_2-); 1.5(10H, -^{3}CH_2-^{4}CH_2-^{5}CH_2-^{6}CH_2 -^{7}CH_2-^{8}CH_2)
F-azo-6-Br	δ=7.95(dd, 4H, ^{12}C*H*, ^{13}C*H*); 7.2(d, 2H, ^{16}C*H*); 7.0(d, 2, ^{17}C*H*); 4.1(d, 2H, -O-^{6}CH_2); 3.55(d, 2H, -^{1}CH_2-Br); 1.9(m, 4H, -^{2}CH_2-^{5}CH_2-); 1.5(4H, -^{3}CH_2-^{4}CH_2)
CF_3-azo-6-Br	δ=7.95(dd, 4H, ^{12}C*H*, ^{13}C*H*); 7.8(d, 2H, ^{16}C*H*); 7.0(d, 2, ^{17}C*H*); 4.1(d, 2H, -O-^{6}CH_2); 3.55(d, 2H, -^{1}CH_2-Br); 1.9(m, 4H, -^{2}CH_2-^{5}CH_2-); 1.55(4H, -^{3}CH_2-^{4}CH_2)
H-azo-6-Br	δ=7.9(dd, 4H, ^{12}C*H*, ^{13}C*H*); 7.45(d, 2H, ^{16}C*H*); 7.0(d, 2, ^{17}C*H*); 4.1(d, 2H, -O-^{6}CH_2); 3.45(d, 2H, -^{1}CH_2-Br); 1.9(m, 4H, -^{2}CH_2-^{5}CH_2-); 1.5(4H, -^{3}CH_2-^{4}CH_2)

Table 4.4 ^{13}C NMR Chemical shifts of R-Azo-$(CH_2)_n$-Br precursors in $CDCl_3$

R	CN	CN	CN	CN	F	CF_3	H
n	**4**	**6**	**8**	**10**	**6**	**6**	**6**
11	162.8	163.0	163.1	163.3	166.3	162.7	162.0
12	115.3	115.2	115.2	115.5	115.1	115.2	115.1
13	125.8	125.8	125.8	126.1	125.1	125.6	125.2
14	147.2	147.1	147.0	147.3	147.1	147.1	147.3
15	155.1	155.1	155.1	155.3	149.6(d)	155.0	153.2
16	122.9	123.4	123.4	123.6	124.8(d)	123.1	122.9
17	133.5	133.5	133.5	133.7	116.3(d)	126.5	129.4
18	113.5	113.5	113.5	113.7	162.1(d)	126.5	130.7
19	119.0	119.0	119.0	119.2	-	132.1(q)	-
1	33.7	34.1	34.3	34.6	34.1	34.1	34.1
2	29.7	33.0	33.1	33.4	33.0	33.0	33.0
3	28.2	29.3	29.5	29.3	29.4	29.4	29.4
4	67.7	25.6	29.5	29.6	25.6	25.6	25.7
5	-	28.3	29.0	29.9	28.3	28.3	28.3
6	-	68.6	26.3	29.9	68.5	68.1	68.1
7	-	-	28.4	30.0	-	-	-
8	-	-	68.8	26.6	-	-	-
9	-	-	-	28.7	-	-	-
10	-	-	-	69.09	-	-	-

where, n refers to the individual carbon atom

4.2.4 Synthesis of polystyrene-*b*-poly(*tert.*-butoxystyrene) [PS-*b*-PBS] Copolymer (3)

The block copolymers of St and *t*-BuOSt were synthesized by the living anionic polymerization technique as reported by Se[9] et.al. and Jannasch.[10] The St was passed through an inhibitor remover alumina column and distilled over CaH_2 and dibutyl magnesium prior to use. The *t*-BuOSt was also passed through an inhibitor remover alumina column and distilled twice over calcium hydride before polymerization. The n-butyl lithium (n-BuLi) (2.2M in hexane, Aldrich) was used as received. The tetrahydrofuran (THF) was passed through a basic alumina column and distilled over sodium before use. The typical procedure for the synthesis of the block copolymers is given as follows.

In a 1 l flame dried round bottom flask equipped with pressure gauze, a thermometer, a magnetic stirrer, septum and argon inlet, 200 ml of dry THF were added. The reaction flask was flushed with dry argon and then cooled down to –78 °C in a dry ice-isopropanol mixture. To this cooled solution a predetermined amount of n-BuLi and then St were added under vigorous stirring. The initiation of the reaction was observed since by formation of an orange color styryllithium anion. After continuing the reaction for one hour a predetermined amount of *t*-BuOSt was added slowly. No change in color was observed even after addition of the second monomer. The reaction was continued for additional 2 h and then quenched with 5 ml of degassed methanol. The polymer was precipitated in 2 l of methanol and filtered off under suction, washed thoroughly with methanol and dried under vacuum. The diblock copolymer was analyzed by SEC and ^{1}H NMR. The composition of PS and PBS was determined by using ^{1}H NMR. Yield: 99 % (gravimetrically)

^{1}H NMR (250 MHz, $CDCl_3$, TMS) (δ) ppm 6.3-6.9 (m, $7H_{ar}$); 6.9-7.25 (s_{br}, $3H_{ar}$); 1.1-2.3 (m, $3H_{ali}$)

Repeating the above procedure, four different block copolymers with four compositions of PS and PBS were synthesized.

4.2.5 Hydrolysis of PS-*b*-PBS (4)

The protective *t*-BuO group of PBS was cleaved by reacting PS-*b*-PBS with 48% HBr under reflux condition.[9] The detailed procedure of the deprotection of *t*-BuO group is as follows.

Approximately 1 wt% of the PS-*b*-PBS copolymer was dissolved in a mixture of benzene and acetone (1:3 v/v). To this 1 wt % of HBr solution (48% solution in water) was added and refluxed for 1 h. After 1 h the reaction mixture was poured in methanol. It has been observed that the resulting PS-*b*-PHS was partially soluble in methanol. Therefore, the polymers were precipitated in water and filtered off under suction with thorough washing with water and then they were dried carefully under high vacuum.

The SEC was used to explore whether cleavage of the *t*-BuO group accompanies hydrolysis without cross-linking. The apparent molecular weights of four pairs of samples before and after hydrolysis with different compositions of the St and *t*-BuOSt are compiled in table 4.6. The PS-*b*-PHS block copolymers were also characterized by ^{1}H-NMR and FTIR spectroscopy. The yield was more than 95% in all the cases.

^{1}H-NMR (250 MHz, DMSO-d_6) (δ ppm): 9 (S_{br}, -O*H*); 6.1-6.8 (S_{br}, H_{ar}); 0.9-2.1 (m, H_{ali})

FT-IR = ν(OH) at 3500 cm^{-1}

4.2.6 Functionalization of PS-*b*-PHS with 4(ω-bromoalkoxy)-4'-cyanoazobenzenes (5)

The synthesis of the mesogenic polystyrene diblock copolymers is performed by analogy with the St homopolymers as described by Crivello et. al.[8]

To a one-neck 100 ml round bottom flask equipped with a magnetic stirrer and a reflux condenser 2.5 mmol of PS-*b*-PHS (based on hydroxyl groups) were added. To this 2.7 mmol of 4(ω-bromoalkoxy)-4'-cyanoazobenzene, 0.25 mmol of *tetra*-n-butyl ammonium bromide [$(n\text{-}Bu)_4N^+Br^-$], 3.5 mmol of NaOH, 5 ml of water and 20 ml of toluene were added. The reaction mixture was refluxed for 24 h. The resulting mixture was cooled down to room temperature and diluted with 50-60 ml of dichloromethane. The solution was washed several times with water and extracted with dichloromethane. The dichloromethane was removed on a rotary evaporator and the glassy material formed was again dissolved in a small amount of dichloromethane and reprecipitated in methanol. The polymer formed was filtered and dried under vacuum. The unconsumed bromo-precursor was removed completely by extraction with methanol using a soxhlet extractor for 24h.

The yield was 90-95% in all the cases.

The molecular weight and the molecular weight distribution of the resulting polymers were determined by SEC and mentioned in table 4.5. The polymers were characterized by FT-IR, ^1H NMR and UV visible spectroscopic methods. The T_g, T_m and T_c were measured by DSC.

Table 4.5 SEC Data of mesogenic polystyrene

No.	Polymer	PS content (by ^{1}H NMR)	M_n	M_w/M_n
1-42	PS-*b*-PBS	50%	31700	1.12
1-43	PS-*b*-PHS	50%	26300	1.26
1-48	I-4-CN	50%	41100	1.15
1-45	I-6-CN	50%	42900	1.15
1-49	I-8-CN	50%	55100	1.44
1-50	I-10-CN	50%	47700	1.24
1-46	PS-*b*-PBS	33%	51300	1.43
1-47	PS-*b*-PHS	33%	39300	1.30
1-53	II-4-CN	33%	72400	1.38
1-52	II-6-CN	33%	72700	1.32
1-54	II-8-CN	33%	55200	1.74
1-55	II-10-CN	33%	54700	1.52
1-56	PS-*b*-PBS	69%	45700	1.13
1-57	PS-*b*-PHS	69%	43100	1.22
1-61	III-4-CN	69%	64900	1.19
1-58	III-6-CN	69%	54700	1.42
1-72	III-8-CN	69%	50100	1.38
1-77	III-10-CN	69%	78000	1.99
1-67a	PS-*b*-PBS	90%	63600	1.23
1-67	PS-*b*-PHS	90%	54900	1.19
1-69	IV-4-CN	90%	60000	1.20
1-68	IV-6-CN	90%	63900	1.28
1-70	IV-8-CN	90%	52800	1.20
1-71	IV-10-CN	90%	62100	1.23

4.3 Results and Discussion

4.3.1 Mesogen Synthesis

The synthetic route used for the preparation of the mesogen is given in the experimental section. The 4-substituted azophenols were synthesized by electrophilic aromatic substitution reaction between the phenol and the corresponding diazonium cation. The respective diazonium cations were generated by diazotization reaction of relevant aniline and an aqueous solution of sodium nitrite in 6N hydrochloric acid solution maintaining the temperature at less than 5 °C[11] as mentioned in the previous chapter III.

In case of 4-fluoroaniline and 4-trifluoromethyl aniline the presence of electron withdrawing groups enhances their electrophilic character by increasing the positive charge on the diazo group. However, several other side reactions like ortho coupling, formation of disubstituted phenol or replacement reaction in which nitrogen is lost as N_2 can be suppressed by controlling the temperature.

The azophenols were purified by recrystallization in an aqueous ethanol. The purity was confirmed by thin layer chromatography using a 8:2 (v/v) mixture of heptane and ethyl acetate. In all the cases the yields were quantitative. The percentage elemental analysis of the azophenols is given in table 4.2.

The UV–visible spectroscopic analysis of the azophenols was performed in THF solution.

The ^{13}C and ^{1}H NMR spectra of the azophenols were recorded in DMSO-d_6. When the substituent was CF_3, the ^{13}C NMR spectrum showed nine different peaks whereas eight peaks were observed when the substituent was fluorine. Furthermore, both the ^{1}H and the ^{13}C NMR spectra support the claim of structure shown in scheme 4.1 and confirm the purity of the compounds. The assignments of the chemical shifts are based on the previous report by Lycka and coworkers.[12]

The melting points reported here are from the first heating cycle of DSC. These fluoro and trifluoromethyl azophenols also decomposed after 200 °C as 4-cyano azophenol.

The bromo precursors of the 4-cyano azobenzenes with the spacer length 4, 6, 8 and 10 methylene units, 4-fluoro azophenol and 4-trifluoromethyl azophenol with a spacer length of 6 methylene units were prepared under the Williamson etherification reaction condition. This synthesis results in high yields by reaction of azophenols and corresponding α,ω-dibromoalkane using potassium carbonate and potassium iodide in MEK. The initial experiments were performed in acetone, but it has been observed that the etherification reaction needs longer time to result in quantitative conversions.[8] The use of MEK allowed to

raise the reaction temperature and the time needed to achieve quantitative conversions was ultimately reduced.

In the etherification reaction the α,ω-dibromoalkanes were used in 20 fold excess as compared to the azophenols (1,8-dibromooctane was used in 1:10 excess as it was more expensive). By using the excess of dibromocompounds the possible side reaction with the alkylation at both ends of the dibromocompound (figure. 4.1) can be suppressed. The reflux was continued for 72 h in order to ensure complete transformation of the azophenol to the corresponding product.

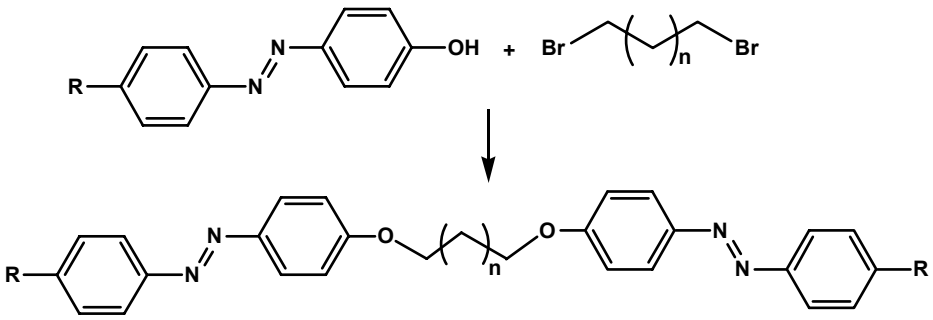

Figure 4.1 Possible structure of the side product formed by di-coupling

The excess of potassium carbonate and potassium bromide formed were filtered and the filtrate was concentrated on a rotary evaporator to remove MEK. The reaction mixture was then diluted with hexane and cooled in an ice bath to induce the crystallization. The crystalline product was suction filtered and washed thoroughly with n-hexane.

Despite the use of an excess of the dibromo alkane a close inspection of the OligoSEC chromatogram showed a small peak towards the high molecular weight side. Hvilsted has confirmed by ^{13}C NMR that the high molecular weight fraction is nothing but the disubstitued alkane[23]. This can be separated by column chromatography.

The nitrile-substituted azobenzene bromoprecursors bearing four different side chain spacer lengths (4, 6, 8 and 10) and the fluoro or trifluoromethyl substituted bromoprecursor having six carbon spacer lengths were synthesized. Since the 4(ω-bromoalkoxy)-4'-azobenzenes are the key compounds for the synthesis of side chain liquid crystalline polymers, a purification by column chromatography was desirable. The compounds were purified by a silica column and heptane–ethyl acetate (9:1 v/v) solvent system as an eluent. In all the cases the yields were in the range of 70-80 %.

The UV visible spectroscopic analysis of these bromo precursors was performed in THF solution. The λ_{max} values depend on the presence of the substituent on the azobenzene part: nitrile (368 nm), trifluoromethyl (356 nm) and fluoro (349 nm) as depicted in figure 4.2. The extinction coefficient (ε_{max}) values observed were in the range of 19000-26000 l/cm mol.

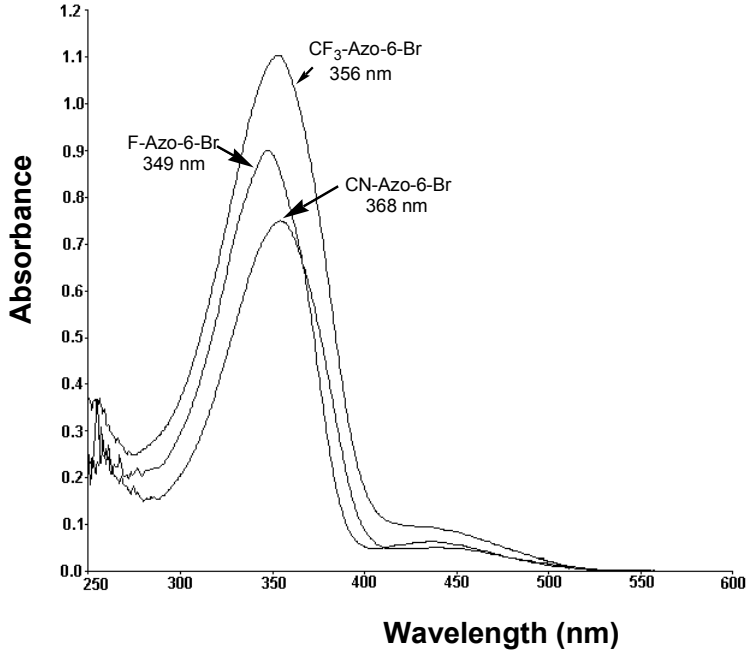

Figure 4.2 Overlay of UV spectra of CN, F and CF_3 substituted azoprecursors

The DSC measurements were performed using the heat-cool-heat method with a heating rate of 5 °C/min. The melting and crystallization temperatures were in good agreement with the values reported in the literature.[8] The nitrile substituted precursors bearing spacer length 6 and 8 showed two different melt transitions, whereas compounds having spacer length 4 and 10 showed only one melt transition. Crivello et. al have performed the polarizing optical microscopic and X-ray analysis on these precursors and reported that with the exception of the compound with the four carbon spacer, all exhibit liquid crystalline behavior. Furthermore, the compounds with six and ten carbon spacers have only a nematic mesophase and the compound with the eight carbon spacer has an additional smectic mesophase. In case of fluoro and trifluoromethyl substituted azobenzene precursors having a six methylene unit spacer only one melt transition temperature was observed.

The ^{1}H and ^{13}C NMR analysis of these bromo precursors is performed in $CDCl_3$ solution. Figure 4.3 is the representative example of a ^{13}C NMR spectrum of the CN-Azo-10-Br precursor. The assignments for individual carbons are based on a literature report.[12] The azobenzene part of the bromoprecursor showed resonances in the range from 119-164 ppm,

whereas the aliphatic carbons appear in the range from 25 to 70 ppm depending on the spacer length. In case of the nitrile and the trifluoromethyl substituted precursors extra peaks were observed because of the nitrile and the trifluoromethyl groups. When the substituent is CF_3, a quartet was observed at 132.1 ppm suggesting coupling of carbon with the three geminal fluorine atoms. The detailed chemical shift assignment is given in table 4.4. The peak assignments in the aromatic region are based on the 4-substituted-4-hydroxyazobenzenes and n-alkyls in the aliphatic region.

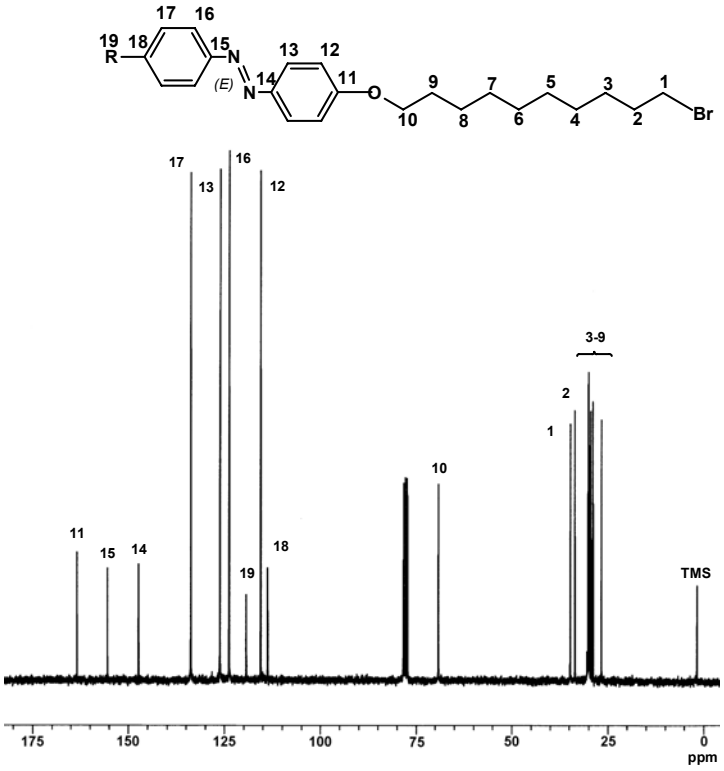

Figure 4.3 ^{13}C NMR spectrum of CN-Azo-10-Br precursor in $CDCl_3$

The ^{1}H NMR spectrum showed the methylene protons next to the phenoxy -($^{10}CH_2$)- and bromine -($^1CH_2$)- shift from other aliphatic protons and appear at 4.1 and 3.5 ppm, respectively. The other aliphatic proton peaks merge with each other and appear as a multiplet between 1.5 to 1.9 ppm. Also no much distinction was observed in the aromatic region. Nevertheless the relative integral area of the respective protons was in good agreement. It was employed to confirm the structure. Table 4.3 gives the detailed peak assignments with the splitting pattern of the ^{1}H NMR chemical shifts of the bromo precursors.

4.3.2 Synthesis of the PS Backbone Copolymer

The PS-*b*-PHS was chosen as a backbone copolymer. The hydroxyl functionality of the PS is attractive due to its availability in the post-polymerization reaction that allows the introduction of various pendant side groups. The monomer 4-hydroxystyrene does not occur due to tautomerism. Therefore, the template approach using the protected hydroxystyrene was selected. The initial strategy to synthesize these template copolymers was to use the block copolymers of St and acetoxystyrene (AcS). The homopolymer of St was synthesized by the ATRP technique using phenylethylbromide as an initiator and Cu(I)Br/bipy as catalyst system at 110 °C. Further, this homopolymer was employed as a macroinitiator for the block copolymerization reaction with AcS.

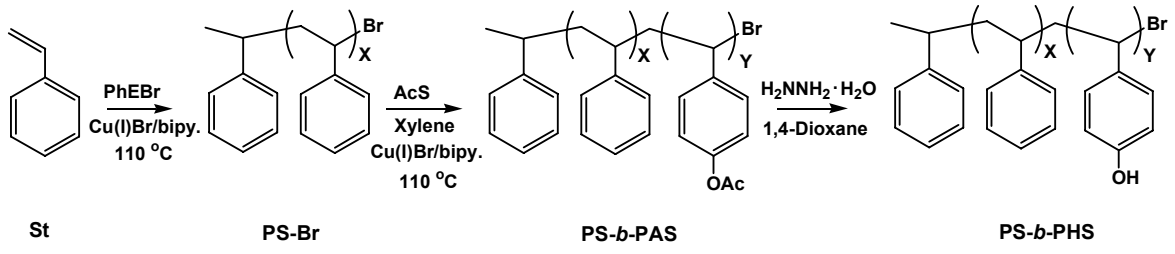

Figure 4.4 ATRP route to synthesize PS-*b*-PHS copolymer[13]

The quantitative deprotection of acetoxy group can be achieved using hydrazine monohydrate as a deprotecting agent.[13] The general scheme for the synthesis of PS-*b*-PHS by the ATRP pathway is given in figure 4.4. Great care is needed to avoid crosslinking reactions. But in our case this possibility was unavoidable because of the polymers we were targeting were higher in molecular weight.

Another strategy was to synthesize PS-*b*-PBS block copolymers using either PS-Br or PBS-Br as a macroinitiator. The previous reports[9,10] showed that the bulky *t*-BuO group could be cleaved easily without cross-linking under mild reaction conditions. The polymerization of *t*-BuOSt by the ATRP technique was very slow, only traces of the polymer were obtained within 20 h. Furthermore, the polymer obtained had a bimodal distribution as observed by SEC which may be due to early terminations. The use of different ligands like bipyridine or HMTETA also could not help to accelerate the rate of polymerization. As stated in chapter I, Matyjaszewski et. al have studied the ATRP of various different substituted St and showed that the monomers having electron donating substituents posses low Hammet (σ) values compared to electron withdrawing substituents. Hence the equilibrium constant for the atom transfer reaction, k_{eq}, and the absolute propagation rate constant k_p decrease for styrene with

electron donating substituents.[14] Also in the presence of electron donating substituents the active growing species can even change to a possible cationic nature.

Consequently, we explored another possibility and have chosen the living anionic polymerization technique. Recently Se et al[9] and Jannasch[10] reported the block copolymerization of St and *t*-BuOSt by the living anionic polymerization method. Following the similar procedure, the PS-*b*-PBS block copolymers with four different compositions of the PS and PBS were synthesized by sequential addition of St and *t*-BuOSt.

The St and *t*-BuOSt were passed through the inhibitor remover alumina column and distilled twice before use over the dibutylmagnesium and calcium hydride respectively. The distillations were performed in sealed ampoules under high vacuum. The cyclohexane was passed through the neutral alumina and distilled over dibutylmagnesium in the reaction flask prior to use.

The St and cyclohexane were added to the flame dried round bottom flask equipped with a teflon septum, stirring bar and thermocouple. The flask was heated up to 40 °C followed by the addition of initiator solution. The reaction mixture turned orange after addition of the initiator. It is an indication of the formation of styryllithium anion. The *t*-BuOSt was added slowly after 1 h and the polymerization reaction was continued for 3 h in total before quenching with degassed methanol. The polymer was precipitated in excess of methanol and then filtered under suction. The block copolymer formed was dried under high vacuum at room temperature.

The initial polymerizations were performed using *sec*-BuLi as an initiator and cyclohexane as a solvent at 40 °C. The yields were quantitative, but the SEC analysis of these block copolymers revealed a PDI $\geq$ 1.5. The only explanation we can offer for this observation is that at higher temperature there must be a reaction between the *t*-BuO group and the initiator. Therefore, further polymerizations were performed in THF using n-BuLi as an initiator at -78 °C.

The St and THF were distilled separately and stored under argon pressure. The THF was added to the polymerization reactor and the flask was then cooled to a temperature of -78°C by dipping it in a mixture of dry ice and isopropanol. The initiator solution was added with a syringe. Then the St was added slowly to the THF solution and immediately the mixture turned to slightly orange color suggesting the formation of styryllithiuim anion. It has been observed that the polymerization reaction was relatively faster in THF. Almost 100% conversion of St can be achieved within 30 to 40 min. In order to ensure that first monomer (St) has been consumed completely the *t*-BuOSt was added after 1 h. The polymerization was

quenched by addition of 5 ml of degassed methanol and precipitated in a surplus amount of methanol.

Following the same procedure four different template polymers with different compositions of PS and PBS were synthesized. The molar masses and the compositions of the individual blocks obtained are given in table 4.6. The molecular weights and PDIs are based on polystyrene standards. The polymers are abbreviated and designated as I, II, III and IV depending on the composition of PS. From here onwards the abbreviations I, II, III and IV will represent the corresponding PS block copolymer.

Table 4.6 Polymerization data of PS-*b*-PBS and PS-*b*-PHS

No	n-BuLi	S	*t*-BuOSt	Yield	M_n	PDI	%PS[a]	PS-*b*-PHS	
	mmol	mmol	mmol	(%)	(SEC)			M_n	PDI
I	0.715	68.7	61.27	98	31700	1.12	53	26300	1.26
II	0.395	38.0	67.29	99	51300	1.42	36	39300	1.30
III	0.700	182.9	79.71	98	45700	1.13	69	43100	1.22
IV	0.5	240	14.32	97	62600	1.26	90	54900	1.19

Solvent: 200 ml of THF; Temp. : -78 °C; Time: 3 h (1 h for Ist monomer, 2 h for IInd monomer);[a] by ^{1}H NMR

The ^{1}H NMR analysis of PS and PBS individual homopolymers was performed to confirm the corresponding proton resonances. The ^{1}H NMR of PBS showed a broad singlet resonance between 6.3 and 7 ppm due to four aromatic protons[15] whereas aromatic protons of PS have two different resonances. The peak between 6.3 and 7 ppm is due to the two meta protons and the peak between 7 and 7.25 ppm indicates the two ortho and one para proton.

Taking into consideration the individual ^{1}H NMR assignments, the two broad peaks of the block copolymers were assigned. The resonance between 6.3 and 7 ppm is due to 4 protons of *t*-BuOSt and two meta protons of the St. The other resonance is due to two ortho and one para proton of the St. The figure 4.5 shows the representative ^{1}H NMR spectrum of PS-*b*-PBS copolymer.

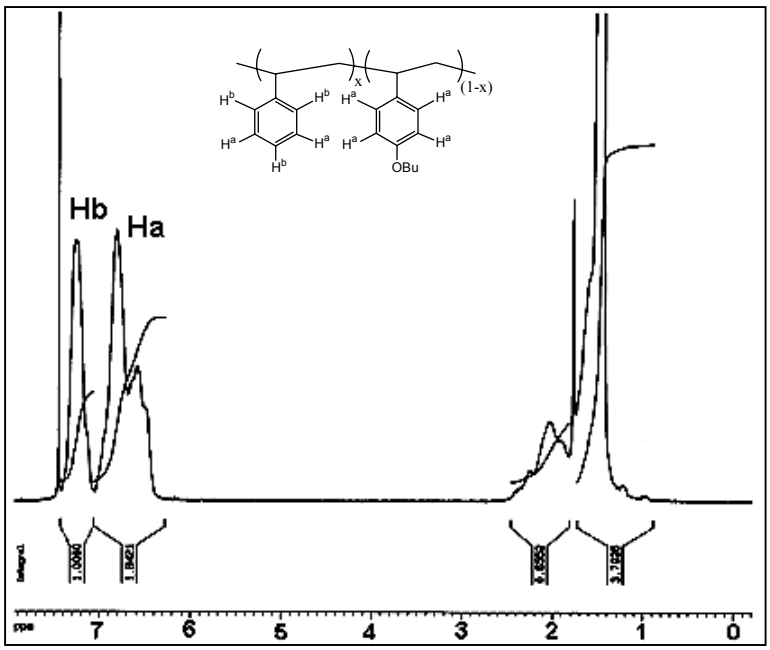

Figure 4.5 ^{1}H NMR spectrum of PS-*b*-PBS

By considering the above assignments a general equation is defined to determine the individual composition in the block copolymer,

$$A_1 = 3 * x * H \qquad \text{eq (4.1)}$$

Where A_1 is the integral area of the resonance between 7 to 7.25 ppm (see figure 4.5)

H stands for St protons (H^b)

and x for the composition of PS

By substituting the value of A_1 obtained by NMR the equation 4.1 can be simplified as

$$H = \frac{1}{3 * x} \qquad \text{eq (4.2)}$$

For the resonance between 6.3 to 7 ppm the following equation can be derived

$$A_2 = 2 * x * H + 4 * (1\text{-}x) * H \qquad \text{eq (4.3)}$$

Where A_2 is the integral area of the peak between 6.3 to 7 ppm

H stands for the St and *t*-BuOSt protons (H^a and H^b)

And (1-x) is the composition of *t*-BuOSt

By substituting the equation (4.2) in equation (4.3)

$$A_2 = 2 * \frac{1}{3 * x} * x + 4 * \frac{1}{3 * x} * (1 - x) \qquad \text{eq (4.4)}$$

Following the above defined equations the actual compositions of individual blocks in four different template polymers were determined.

The *t*-BuO group of PS-*b*-PBS block copolymers was cleaved by treatment with aq. HBr in 1:3 (v/v) mixtures of benzene and acetone to obtain the corresponding PS-*b*-PHS block copolymer.[9] The resulting hydroxyl polymers were precipitated in water, as they were partially soluble in methanol. Figure 4.6 shows SEC chromatograms of PS-*b*-PBS (before deprotection) and PS-*b*-PHS (after deprotection). All four samples showed a sharp single peak in the SEC diagram. The PDI value of the hydroxyl block copolymers was most likely the same as that of its butoxy analogue. The SEC elution peak of the resultant block copolymer shifted to the lower molecular weight side to that of the original block copolymer evidencing the removal of *t*-BuO group. The polymers were dried carefully at 50 °C under high vacuum for 72 h.

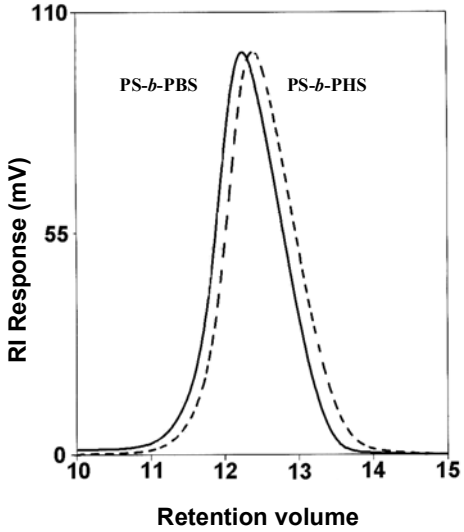

Figure 4.6 SEC overlay of PS-*b*-PBS (before deprotection) and PS-*b*-PHS (after deprotection)

The FT-IR analysis of the PS-*b*-PBS has shown no absorption in the vicinity of 3400 cm^{-1}, whereas the resultant hydroxyl block copolymer had a broad absorption around 3400 cm^{-1}. The figure 4.7 shows the FT-IR spectra of block copolymers before and after the deprotection. The ^{1}H NMR of the PS-*b*-PBS has a resonance at 1.2 ppm corresponding to the *t*-BuO group, which has disappeared in PS-*b*-PHS after deprotection. These observations also evidence the formation of the hydroxyl functionality in the block copolymers.

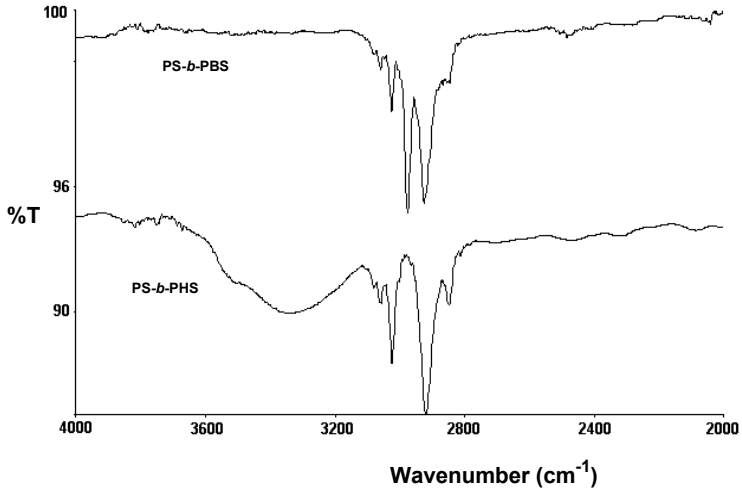

Figure 4.7 FT-IR spectra of the PS-*b*-PBS and PS-*b*-PHS copolymers

4.3.3 Functionalization Reactions

The hydroxyl sites of PS-*b*-PHS copolymers containing different compositions of PS were subjected to the reaction with mesogenic bromo precursors under the phase transfer catalysis conditions using NaOH and $(n\text{-}Bu)_4N^+Br^-$. The reactions were performed in a 1 : 3 (v/v) mixture of water and toluene under reflux conditions. The general procedure followed for the synthesis of the mesogenic polystyrene block copolymers is summarized in the experimental section. The PS-*b*-PHS block copolymer and the corresponding bromo precursors having different alkyl spacers [$-(CH_2)_4-$, $-(CH_2)_6-$,$-(CH_2)_8-$, $-(CH_2)_{10}-$] were dissolved in a toluene-water mixture in 1 : 1.1 molar ratio (based on the hydroxyl sites). The reactions were performed for 24h under reflux conditions.

The resulting mesogenic polystyrene copolymers were recovered by extraction with DCM. The DCM layer was washed thoroughly with water and dried over anhydrous sodium sulphate. The sodium sulphate was removed by filtration and the filtrate was concentrated on a rotary evaporator to remove the DCM. The glassy polymer formed was dissolved in the small amount of DCM and precipitated in excess methanol. It has been observed that the starting hydroxyl polymer was soluble in methanol whereas the resulting mesogenic polystyrene was precipitating out in methanol. This is also an indirect evidence suggesting that the hydroxyl sites are replaced by azoprecursors. The precipitated polymer was filtered under suction and dried in a vacuum oven. The excess of unreacted bromo precursor was removed by soxhlet extraction in boiling methanol for 24 h.

The SEC analysis of the mesogenic polystyrenes shows the shift in the elution volume towards the higher molecular weight side with respect to the corresponding hydroxyl polymers. The M_n and PDI values obtained were based on linear polystyrene standards. In all the cases the SEC showed a single peak with some broadening of molecular weight distribution. These values are taken into consideration as they were based on the polystyrene standards. The molecular weights and the PDI observed are given in table 4.5.

Figure 4.8 shows the ^1H NMR spectrum of I-6-CN. It has been observed that the methylene group adjacent to the oxygen atom in the side chain shifts from the other aliphatic protons resonance and appears at 4.0 ppm. The aromatic region was too complex for individual assignment. Nevertheless, by comparing the integral area of the methylene proton resonance at 4 ppm with the combined integral area of the aromatic protons the degree of substitution can be determined.

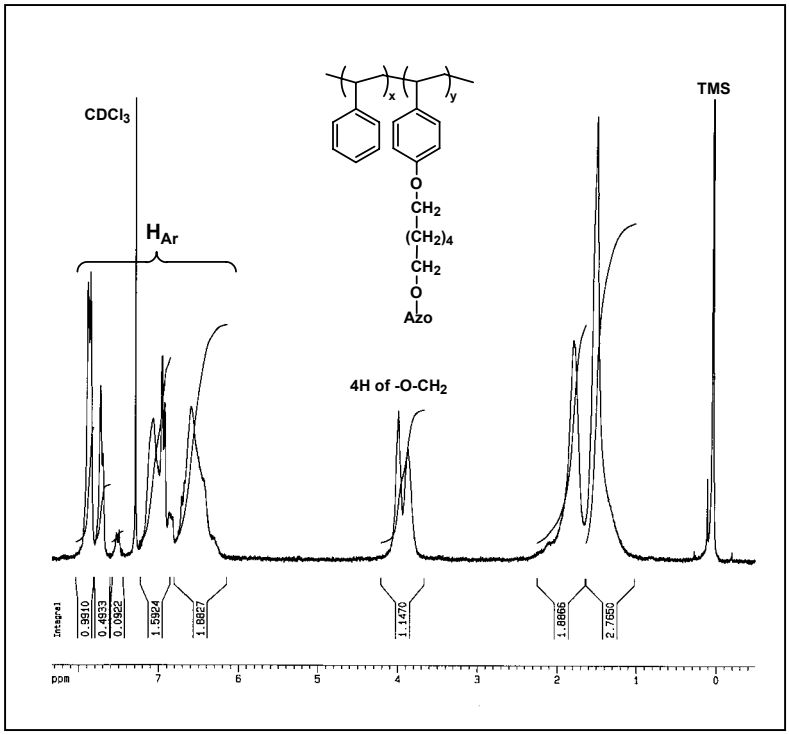

Figure 4.8 ^{1}H NMR spectrum of PS-*b*-P(CN-Azo-6)S in $CDCl_3$

In all the cases it was observed that the substitution was more than 95%. The ^{13}C-NMR spectrum of the mesogenic polystyrene was also too complicated for an individual assignment.

FT-IR analysis of these polymers was also employed to confirm the degree of substitution. The disappearance of the absorption around 3400 cm^{-1} characteristic of the template PS-*b*-PHS backbone polymer confirms the higher degree of functionalization. The comparative FT-IR spectra shown in figure 4.9 strongly support the above claim of quantitative substitution. The nitrile substituted mesogenic polystyrene showed the formation of an extra absorption peak at 2226 cm^{-1}, whereas in the case of F and CF_3 substituted mesogenic polymers a few new absorptions between 1200 - 1300 cm^{-1} were observed because of the C-F vibrations.

These mesogenic polymers were characterized by UV-visible spectroscopic analysis in the range of 250 nm to 700 nm. The ε_{max} values observed are in consistence with the concentration of the mesogenic blocks as determined by ^{1}H-NMR. Table 4.7 shows the ε_{max} and the percentage concentration of mesogenic blocks in the copolymer. The polymer having 67 % of the mesogenic block (by ^{1}H NMR) has the highest ε_{max} = 21000, whereas the polymer having 9:1 composition with 10% of the mesogenic block showed the lowest ε_{max} = 5700.

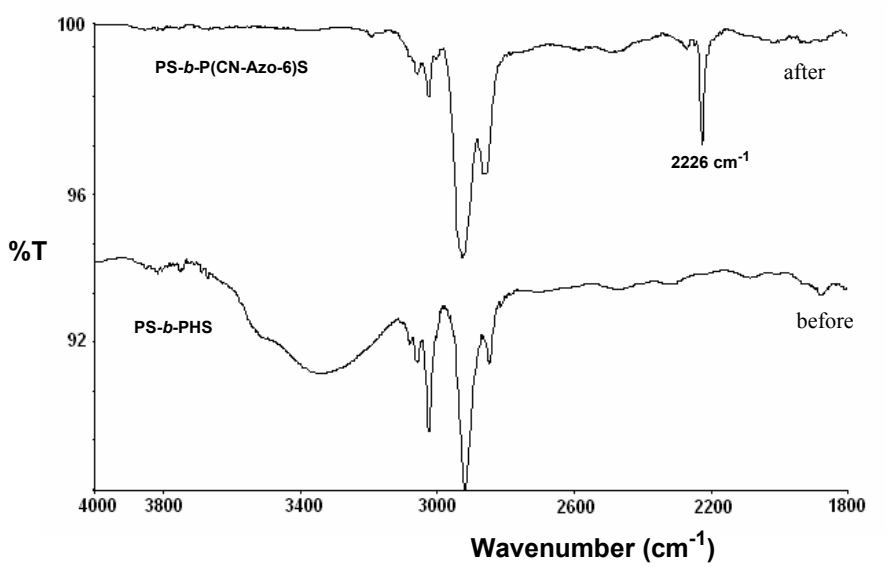

Figure 4.9 FT-IR spectra of PS-*b*-PHS before functionalization and after functionalization with the azomesogen**.**

The DSC analysis of the mesogenic block copolymers was performed with a heating rate of 3°C/min to study the liquid crystalline behavior. The polymers having more than 30% of mesogenic block were susceptible to show a step corresponding to the T_g due to the backbone PS followed by a single endothermic peak of melt transition (T_m) due to the azobenzene block. Figure 4.10 depicts the heating and cooling curves for (I-6-CN) a typical member of this series of the polymers.

Table 4.7 UV-visible data of mesogenic polystyrene block copolymer

Polymer	**% Mesogen**	**ε_{max} (l/cm * mol)**
II-6-CN	67	21000
I-6-CN	50	19000
III-6-CN	31	17000
IV-6-CN	10	5700

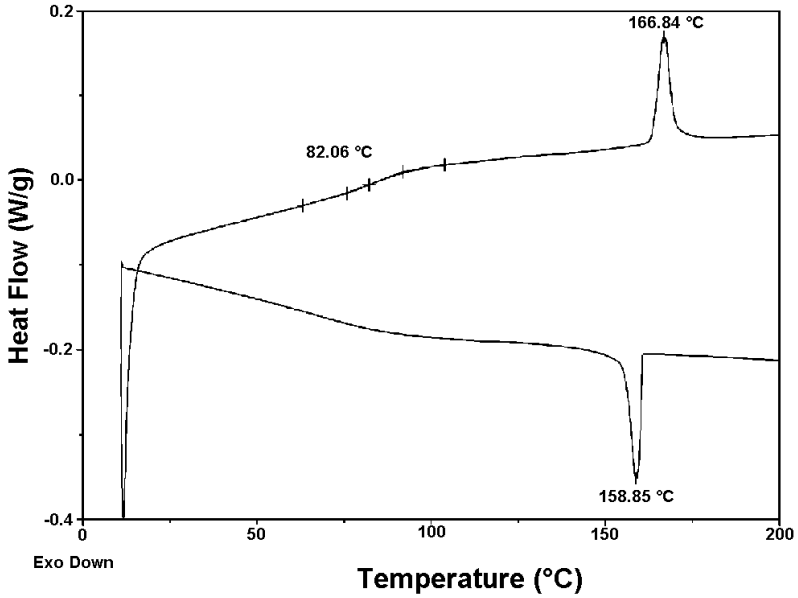

Figure 4.10 DSC chromatogram of I-6-CN with a heating and cooling rate of 3°C/min.

The mesogenic polystyrenes having a mesogenic block length of more than 30% in the copolymer had a remarkably lower T_g compared to its unsubstituted analogues. The T_g of PS-*b*-PBS (100°C) was decreased to 64°C after functionalization with azobenzene mesogens. This observation suggests that the presence of the alkoxy substituent in the para position of St causes the plasticizing effect due to the alkyl side chain and leads to a corresponding decrease in the T_g.

Furthermore, it has also been observed that the T_g of the polymer depended on the length of the alkyl spacer. The T_g of the mesogenic polymers decreases from 95 °C to 64 °C with an increase in side chain alkyl spacer length from 4 to 10, respectively. The nature of the DSC curve for all the polymers was similar. Figure 4.11 shows the overlay of the DSC chromatograms of the mesogenic polymers bearing spacer lengths 4, 6, 8 and 10. The detailed measurements of T_g, T_m, T_c and of the ΔH are given in table 4.8. The crystallization temperature of the polymers also decreases with the spacer length.

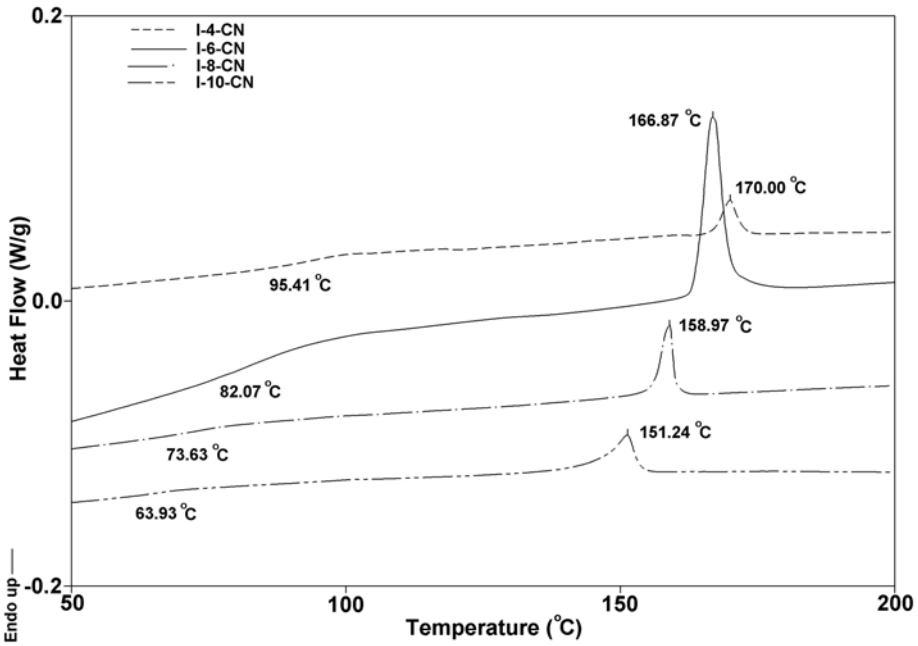

Figure 4.11 DSC overlay of the mesogenic polymers with spacer lengths 4 to 10

Table 4.8 DSC measurements of the mesogenic polystyrenes

Polymer	PS Content[a]	DSC			
	(%)	T_g (°C)	T_m (°C)	ΔH (J g^{-1})	T_c (°C)
I-4-CN	53	95	170	1.61	164
I-6-CN	53	82	166	2.78	159
I-8-CN	53	73	158	2.56	154
I-10-CN	53	64	151	3.05	145
II-6-CN	36	81	169	1.88	162
III-6-CN	69	101	n.o	n.o	n.o
IV-6-CN	90	98	n.o	n.o	n.o

[a] = based on PS-b-PBS, n.o = not observed, T_g, T_m, T_c stands for glass transition, melt transition and crystallization temperatures respectively.

On cooling (with a rate of 3°C/min) a sharp exothermic peak due to crystallization was observed. The crystallization temperature of the polymers also drops down from 164 °C to 145 °C with an increase in alkyl spacer length from 4 to 10. It may also be noted that the observed enthalpies of transition increases with the length of the spacer, which may be due to better decoupling of the mesogens from the main chain. The low values (1.61 – 3.05 J g^{-1}) observed for the enthalpies of the mesophase-isotropic transitions for these mesogenic

polymers suggest a low degree of order. However, in case of mesogenic polystyrene III and IV the percentage of PS in the block copolymer is more than 70%, which may suppress the observation of the formation of transitions in the polymer except T_g.

The polarizing optical microscope (POM) analysis of these mesogenic block copolymers was performed on a Leica (Germany) microscope equipped with a hot stage. The samples were investigated at their melting temperatures as observed by DSC. At isotropic temperatures the polymers form a fluid/viscous melt and undergo a transition from the mesophase to isotropic phase. But the very small domains observed below the clearing temperature do not allow a definitive classification of the mesophase.

4.4 Investigation of the Stability of Optical Anisotropy

The possibility to induce an anisotropy in the azobenzene containing polymeric materials by illumination with linearly polarized light is well known for a long time. It is due to the reorientation of the azobenzene units and their alignment into a direction perpendicular to the polarization of the light. This property makes them candidates for reversible optical data storage.

The optical anisotropy measurements were performed on thin films of polymer solution spin coated on a glass substrate (25 mg in 200 µl chloroform at 800 rpm). A linearly polarized argon laser beam with a wavelength of 488 nm was used to induce the anisotropy. Upon irradiation with plane-polarized light the azobenzene containing polymers undergo several trans-cis-trans photoisomerization cycles and reorient such that the long axis of the azobenzene mesogen remains perpendicular to the plane of the electric vector of the laser light. Figure 4.12 shows the reorientation mechanism and alignment of the azobenzene functionality.

The photoinduced birefringence is dependent on the mobility of the chromophore; the bulkiness of the azo chromophore plays an important role. Thus, the introduction of substituents on the azobenzene group may hinder its motion and either lower the level of photoinduced birefringence, or slow the process, or both.

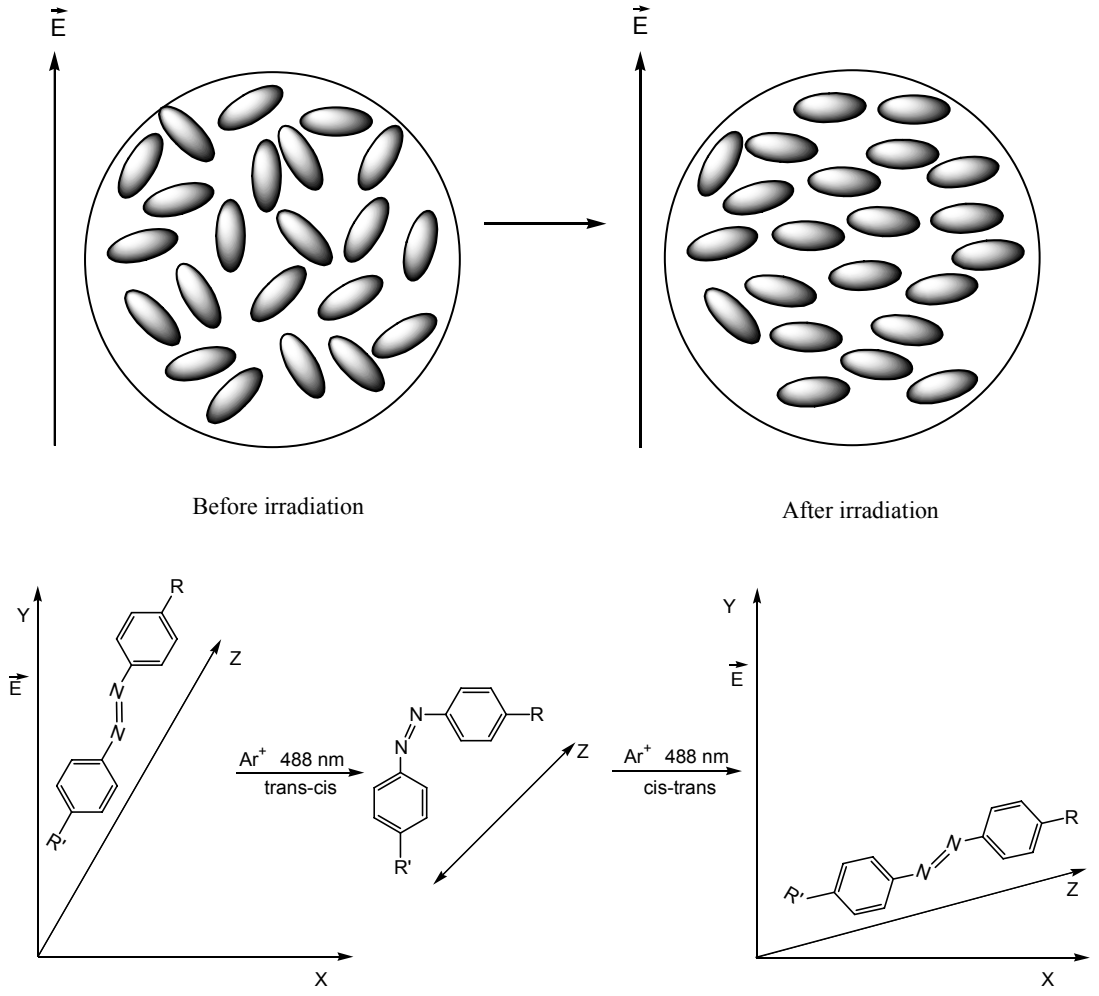

Figure 4.12 Photoisomerization cycle and alignment of an azobenzene molecule ($\vec{E}$: electric field vector of the polarized laser light)

As shown in figure 4.2 the strong π-π* absorption around 360 nm is characteristic of the trans conformation and a weak n-π* absorption at 450 nm is associated with the cis state of the azobenzene. In an ideal sample the induced orientation of the azobenzene has to remain constant for a period of years after switching off the laser.[3]

In order to investigate the stability of the induced anisotropy in the polymers thin films of the samples were irradiated with an argon ion laser and the stability of the recorded anisotropy is followed in darkness. Figure 4.13 shows the comparative plot of optical anisotropy stability of mesogenic polymers bearing different composition of St with different spacer length.

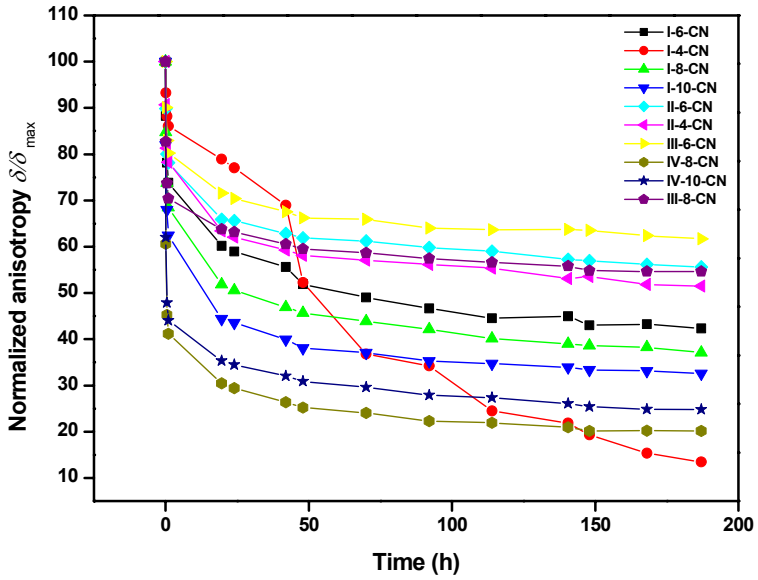

Figure 4.13 Decay of anisotropy (in darkness) as a function of time in different mesogenic PSs.

From the above plot it has been observed that the optical anisotropy of mesogenic polymers bearing relatively higher PS content and longer spacer length decreases much faster than that of polymers with lower PS content. More than 50% loss is observed within the first 24 h, and 25% of the recorded anisotropy was left after 8 days. In case of polymer series I having 50% of azo functionalized blocks the anisotropy reduces with increase in spacer length. As it is observed from the above figure the I-6-CN had a slightly higher anisotropy after 8 days than the I-8-CN and I-10-CN. Furthermore, the III-6-CN with 69 % PS in the block has the highest anisotropy left after 8 days. In order to investigate the effect of different parameters like the presence of light and the temperature on the stability of the recorded anisotropy, the polymers showing the highest stability of anisotropy in the darkness experiments were chosen and subjected to further analysis. Also the response of the azobenzene alignment with respect to time is measured.

4.4.1 Stability in the Presence of Light

In these experiments the polymer thin films are irradiated with an argon ion laser at 25°C and the decay of anisotropy in the presence of bright unpolarized light is measured as a function of time. The collimated light beam of a halogen lamp located at about 10 cm distance from the sample is used as a light source. During these measurements the investigated films were mounted on the hot stage in order to monitor the increase of the film temperature due to the illumination. We have observed that the temperature goes up to 50 ºC when the light

intensity was approximately 100 mW/cm^2 measured at the sample position. After irradiation a relaxation time of 30 min at 25 ºC with ambient light was allowed. The ratio of the photoinduced anisotropy at different time intervals to the anisotropy recorded at relaxation (δ_{30min}) was plotted as a function of time in figure 4.14.

The polymer III-6-CN has a slightly higher stability of the recorded anisotropy than the other three polymers. The same trend of stability was observed in the previous experiments in darkness.

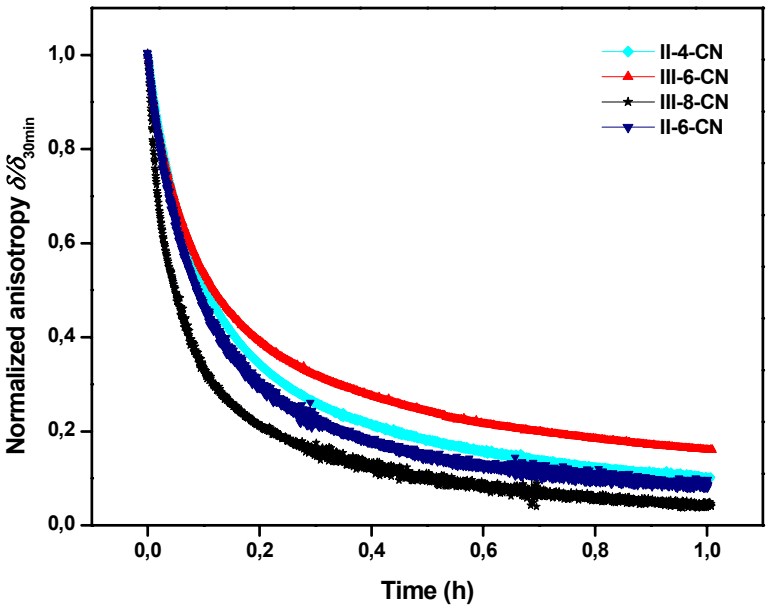

Figure 4.14 Comparison of anisotropy decay in the presence of light

In all the cases the stability drops to less than 50 % within 12 minutes. The measurements performed for 1h indicate that the decay of anisotropy continues and drops to less than 20% for all the samples.

4.4.2 Thermal Stability of Anisotropy

As a general rule, the increase of the temperature results in a loss of alignment in the amorphous polymers. When the temperature of the polymer is raised to isotropization temperature, all the alignment is lost.[16-21] This has been already confirmed on dyes dissolved in the polymer matrices, in the "hybrid" polymers (where the chromophore is bound or mixed in a variety of matrices) and in the polymers containing bound azo dyes. The stability of the photoinduced anisotropy, *i.e.*, the thermal behavior of the previously recorded anisotropy at

elevated temperatures in the above mentioned four polymers, was studied. The temperature of the films is increased with a constant heating rate of 3°C/min using a Linkam THMS600 hot stage connected to a temperature control block. This study not only indicates the maximum temperature the polarization recording can withstand without severe loss of information, but also relates to the stability of the birefringence at room temperature.

The following procedure was employed for the measurements of thermal stability

I. set the temperature to 25ºC and allow the sample to equilibrate thermally for 2 min
II. start the acquisition with 1 measurements per two seconds
III. allow for 30 sec before the argon ion laser is switched on to measure any residual or spontaneously induced anisotropy
IV. open the argon ion laser shutter and record for 30 sec at 700 mW/cm^2
V. close the shutter and wait 30 min for the initial relaxation of the anisotropy
VI. start heating from 25ºC to 150ºC at a heating rate of 3ºC/min (0.05ºC /sec).

The anisotropy data recorded as a function of time are converted to the temperature domain using the equation:

$$T(t) = (t - t_o) * \text{heating rate} + T_o$$

where, t_o is 30 min, heating rate 3ºC/min and T_o is 25ºC.

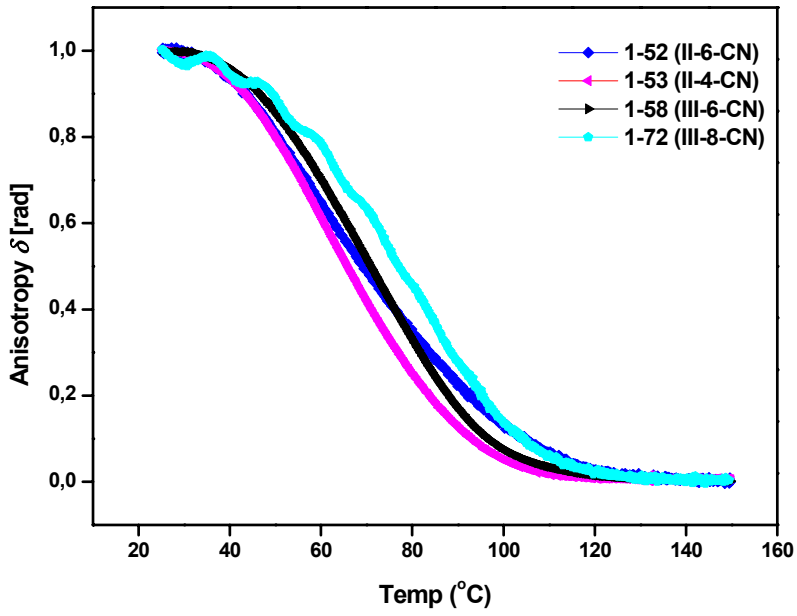

Figure 4.15 Behavior of the anisotropy induced in mesogenic PS at elevated temperatures

As illustrated in figure 4.15, in all four polymers the recorded anisotropy drops down with an increase of temperature. A closer look on the thermal stability plot shows that in the temperature range of 65-75 °C the anisotropy is lost to almost 50% in all the samples. Upon further heating the polymer films above their T_g the anisotropy was completely erased.

4.4.3 Response of Anisotropy

The increase of photoinduced anisotropy in thin films of the mesogenic polymers III-6-CN, II-6-CN, III-8-CN and II-4-CN were studied as a function of irradiation time. An irradiation time of 140 s was found sufficient to induce the anisotropy up to the saturation point for the laser intensity used (700 mW/cm^2). This is the time required for the macroscopic collective reorientation in the thin films of the polymer. In order to study the effect of different parameters on the alignment of azobenzene moieties in the polymers the growth rate of the photoinduced anisotropy was investigated. Among all these samples III-8-CN having 69% PS has the fastest response as compared to the other mesogenic PSs.

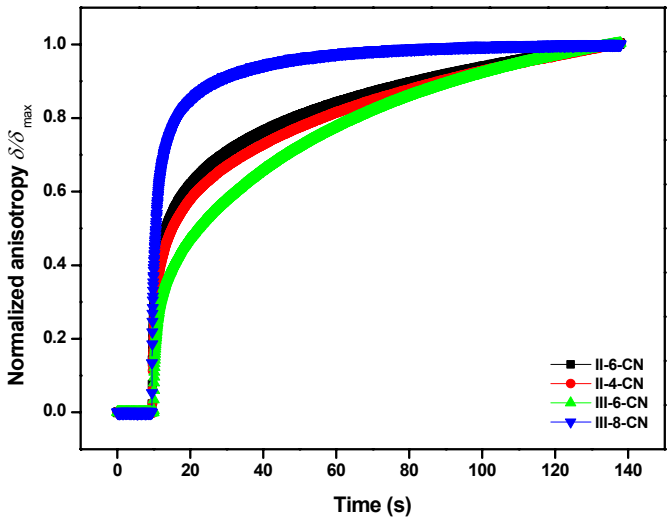

Figure 4.16 Growth of anisotropy in polymer thin films as a function of time at an intensity of 700 mW/cm^2.

Recently, Ramanujam et. al[22] have studied a series of side chain azobenzene containing polyesters and showed that the total energy required to induce a certain amount of anisotropy in a polymer film, is virtually constant over a wide range of laser intensities from

350 mW/cm^2 to more than 4000 mW/cm^2. Thus, increasing the intensity of the light used for the recording could reduce the response time.

4.5 Conclusions

A variety of SC-LC block copolymers with azobenzene functionalities have been prepared. The azobenzene precursors bearing different spacer lengths (4,6,8 and 10) were synthesized and characterized by various techniques. These precursors are then introduced as a pendant group on the PS-*b*-PHS copolymer by phase transfer catalysis reaction. The effect of PS composition and effect of spacer length on the properties of the final polymers is studied. The T_g of the polymers decreases with introduction of the azobenzene substituent and it further drops down with the increase in spacer length. The optical anisotropy measurements show that polymers of the type II and III having higher content of the azobenzene moieties are most stable in time. More than 50% of anisotropy left after 8 days in darkness. The temperature study shows that the induced anisotropy in the block copolymers decays with the increase in sample temperature and is erased completely at 140 °C. Furthermore, the macroscopic collective reorientation as a function of time in four different polymers is also investigated. It has also been observed that the fastest the response on recording, the fastest the decay on illumination with light (as with III-8-CN). From these observations no clear correlation between structure and the optical behavior of the polymer can be made.

Chapter V

Novel Fluorinated Polymer Materials Based on 2,3,5,6-tetrafluoro-4-methoxystyrene

Abstract

A novel route for the synthesis of fluorinated homopolymers as well as block copolymers has been described. 2,3,5,6-tetrafluoro-4-methoxystyrene (TFMS) has been prepared by nucleophilic substitution reaction between 2,3,4,5,6-pentafluorostyrene (FS) and sodium methoxide. This new monomer has been polymerized in bulk as well as in solution by Atom Transfer Radical Polymerization (ATRP) technique at 110 °C. Polymers with molecular mass (M_n) up to 17,000 with a relatively narrow polydispersity index (PDI) <1.3 have been prepared. The polymerization of TFMS is the fastest observed as compared to the other substituted styrene. Block copolymers with styrene (St) as well as FS have been prepared using PTFMS-Br as a macroinitiator under similar ATRP conditions. Block copolymers with different composition of TFMS and with different molecular weights and relatively narrow PDI have been achieved. The TFMS homo and block copolymers with PS have a better thermal stability and a lower solubility than PS. The polymers were formulated into thin films spin coated onto a glass surface with levels of 3 to 5wt. % solution in THF. Water contact angles (advancing) 115° and (receding) 101° were observed. In addition the XPS analysis of the PTFMS homopolymers as well as the block copolymers with St and FS showed fluorine enriched surfaces.

The methoxy site of PTFMS-Br has been functionalized with azobenzene containing bromo precursors. Furthermore, the derivatized polymer has additionally been employed as a macroinitiator for the block copolymerization with St. The polymers with azobenzene side chains form materials exhibiting liquid crystalline properties.

5.1 Introduction

Fluorinated polymers with varying fluorine content are materials that attract great attention due to a number of desirable properties such as high thermal, chemical, ageing and weather resistance and low surface energy. Moreover, thin film materials of fluorinated polymers with low permittivity or low dielectric constants,[1] low flammability, excellent inertness, low refractive index and low-loss optical wave guiding potential[2] are desirable properties for the (opto) electronic industry. Recently, copolymers containing both fluorinated oligomer segments and polyethylene glycol have shown excellent performance as electrolyte materials for lithium ion conductivity in batteries[3]. Thus, novel highly fluorinated monomers are of great scientific and technical interest.

Recently Hvilsted et. al demonstrated [4,5] the versatility of 2,3,4,5,6-pentafluorostyrene (FS) to be easily transformed by Atom Transfer Radical Polymerization[6] to polymers with controlled molecular weight characteristics. Both homopolymers (PFS) and block copolymers with PS could be prepared in a broad compositional range where the polydispersity index (PDI) in all instances was kept below 1.3. Compared to PS all these novel PFS based materials achieved both much higher thermal stability and significantly increased chemical resistance as reflected in inferior solubility in a large number of chemically different solvents. Another heavily fluorinated styrene, 2,3,5,6- tetrafluoro-4-methoxystyrene (TFMS), can be prepared from FS in a simple fashion. We here wish to report on the first polymerization of TFMS performed under ATRP conditions. Furthermore, we show how poly(2,3,5,6-tetrafluoro-4-methoxystyrene) (PTFMS) can be the basis of a number of novel materials by derivatization with azobenzene side chains. Such fluorinated polymers can serve as models for optical storage materials. Materials in which the azobenzene content can be reduced[7] are potential candidates for optical storage by holographic multiplexing. Another possibility is the design of new materials for optical wave guiding purposes.[2] Materials based almost entirely on fluorine substituted carbons are transparent in the NIR range used for optical data transmission. Additionally, the azobenzene part can be addressed by laser light[7] causing material birefringence changes in such a manner that optical wave guiding patterns can be formed.[8] Here also the azobenzene part can be highly fluorinated, since it is relatively easy to design the aromatic part fully fluorinated.

5.2 Experimental

5.2.1 Monomers.

FS (Aldrich) and St were passed through a ready-to-use, disposable prepacked inhibitor-remover column AL-154 (Aldrich).

Synthesis of TFMS : In what follows is a modified method of Hult et. al[2]. In a three-neck round bottom flask equipped with magnetic stirrer, addition funnel and reflux condenser, a solution of 25 g (128 mmol) FS in 100 ml dry MeOH was cooled down to 0 ^{o}C. To this a solution of 7.65 g (141.75mmol) of sodium methoxide in 50 ml dry MeOH was added slowly. The stirring was continued for 1 h and then brought to reflux for 19 h. The reaction mixture was poured in 400 ml of ice water and extracted with diethyl ether. The ether layer was dried over anhydrous sodium sulphate and filtered. The filtrate was concentrated on a rotary evaporator to give crude TFMS which was then distilled at 32-33 °C/1.3 mbar over calcium hydride and stored under nitrogen. Yield = 22.8 g (86%)

The structure of TFMS was confirmed by ^{1}H, ^{13}C and ^{19}F NMR and the purity was verified by OligoSEC.

^{1}H NMR ($CDCl_3$): δ = 5.8(d, 1H, ^{b}H), 6.0(d, 1H, ^{c}H), 6.59(dd, 1H, ^{a}H), 4.0(t, 3H, ^{d}H).

^{13}C NMR ($CDCl_3$):δ = 147(m), 143.15(m), 138.9(m), 137.1(m), 121.8(t), 110.4(m), 61.7(t)

^{19}F NMR (C_6F_6): δ = -156.15($2F_{ar}$), -142.01($2F_{ar}$)

For assignment of the NMR spectrum refer to figure 5.3.2.

5.2.2 Side-chain Precursors

The 6-bromohexyloxy-1-azobenzenes with different substitution were prepared as reported in chapter IV by modifying the reported procedure of Crivello.[9] Other reagents, CuBr, PhEBr, bipy, BBr_3 (all from Aldrich) were employed as received. All other chemicals were used after usual drying and/or distillation.

5.2.3 Polymerizations

ATRP of TFMS was carried out in bulk or in xylene solution (30 wt-% TFMS) in a Schlenk tube. In a typical experiment (PTFMS3-Br) the tube was charged with 0.072 ml (0.509 mmol) of PhEBr, 0.075g (0.509 mmol) of CuBr and 0.238 g (1.526 mmol) of bipy. TFMS, 5.0g (24.272 mmol) was added; the system was degassed 3 times and then heated to 110 ^{o}C under nitrogen. The homopolymers were precipitated in methanol and the yield was determined gravimetrically after vacuum drying. The block copolymers were obtained employing the styrenic macroinitiators in various concentrations of xylene and the same catalytic system.

Demethylation of homo- and block copolymers of TFMS was carried out using BBr_3 as deprotecting agent and chloroform as the solvent under nitrogen and reflux. The final molar ratio of $–OCH_3$:BBr_3 was 1:2. The degree of conversion of 4-methoxy groups was determined by ^1H NMR in DMSO-d_6.

5.2.4 Azobenzene Functionalization

The functionalization reactions are performed under phase transfer catalysis reaction conditions as mentioned in chapter IV and the resulting polymers were purified by Soxhlet extraction with CH_3OH.

5.3 Results and Discussion

5.3.1 Monomer Preparation and Polymerizations

TFMS was prepared in high yield (86%) by a nucleophilic replacement reaction on FS with sodium methoxide in methanol as shown in scheme 5.3.1 and purified by vacuum distillation as previously described.[2] The structure of the TFMS was confirmed by ^1H NMR, ^{13}C NMR and ^{19}F NMR spectroscopy. Neat TFMS can be polymerized in a conventional ATRP protocol at 110 ^oC by use of 1-phenylethyl bromide (PhEBr), CuBr and 2,2'-bipyridine (bipy). Under these conditions the heterogeneous polymerization proceeds very fast, in fact, 97% conversion can be achieved within 23 minutes. In comparison, FS under similar conditions took almost 100 min. to reach that level of conversion.[5] The results of a number of polymerizations performed in bulk and in xylene solution are listed in table 5.3.1. In the bulk polymerizations 5 g of monomer was polymerized employing different monomer to initiator ratios necessary to reach the target molecular mass.

In all experiments the initiator : CuBr : bipy was maintained as 1 : 1 : 3. The M_n was determined by ^{1}HMR (Figure 5.3.1) using the equation

$$M_n = DP * MW_{TFMS} + MW_{PhEBr} \qquad \text{eq (5.1)}$$

$$DP = 5H_d/3H_a$$

where, MW_{TFMS} and MW_{PhEBr} are the corresponding molecular weights and, H_a and H_d are areas of the methoxy and PhEBr aromatic protons, respectively.

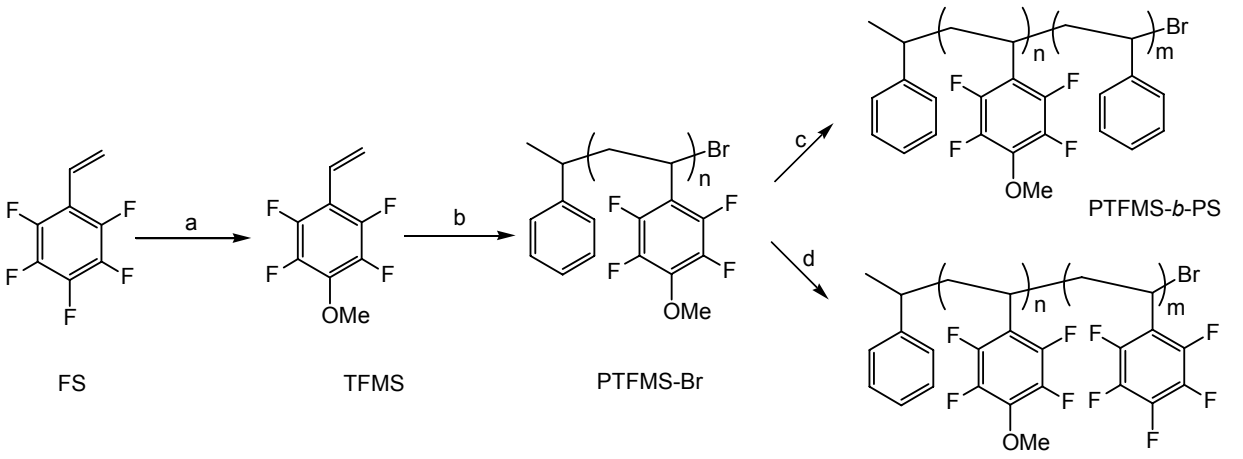

a) $NaOCH_3$, CH_3OH b) PhEBr, CuBr, bipy. 110°C

c) St, CuBr, bipy, xylene, 110°C d) FS, CuBr, bipy, xylene, 110°C

Scheme 5.3.1. Preparation and polymerization of TFMS and examples of block copolymerizations

Similarly, the bromine end group functionality, f_{Br}, could be estimated, however, only in case of the polymers with the lowest M_ns and it was between 0.75 and 0.88. Table 5.3.1 shows that M_ns up to 14,000 and 17,000 have been obtained both by bulk and solution polymerization. Furthermore, the PDI in all instances lies between 1.21 and 1.36, where in case of PFS [5] the PDI was generally lower, $\leq$1.2. The only explanation we can offer for the higher PDIs in case of PTFMS as well as the deviation of f_{Br} from unity is early termination.

Table 5.3.1. Polymer yield and molecular masses

Polymer	Time	Yield	M_n	NMR		SEC	
	min.	%	target [a]	Mn	f_{Br} [b]	M_n	PDI
PTFMS1-Br	10	93	2000	2900	0.88	3400	1.36
PTFMS2-Br	3	60	1500	3300	-	4400	1.21
PTFMS3-Br	15	67	10000	9700	-	8800	1.26
PTFMS4-Br	25	55	20000	12200	-	13700	1.30
PTFMS5-Br	20[c]	23	1000	2700	0.75	3100	1.22
PTFMS6-Br	110[c]	42	25000	11100	-	10500	1.13

[a] M_n, target = $[M]_0/[I]_0$ at 100% conversion; [b] $f_{Br} = 3H_c/H_b$, where H_c and H_b are the areas of >CHBr and $-CH_3$, respectively; [c] in 30% xylene solution.

The structure of the resulting PTFMS-Br as shown in scheme 5.3.1 was elucidated by ^1H, ^{13}C and ^{19}F NMR spectroscopy. The particular ^1H spectrum shown in Figure 5.3.2

originates from a sample with a low degree of polymerization (DP = 13) thus allowing the initiator residue to be easily recognized.

In a series of experiments samples were withdrawn after increasing time and subjected to analyses of conversion by ^{1}H NMR as exemplified in figure 5.3.2 and to molecular weight determination by size exclusion chromatography (SEC) as depicted in figure 5.3.3. Based on the conversion data the first order plot in figure 5.3.4 can be constructed. The plot implies the controlled ATRP of TFMS. Figure 5.3.4 additionally shows the same features for the ATRP of FS and St.

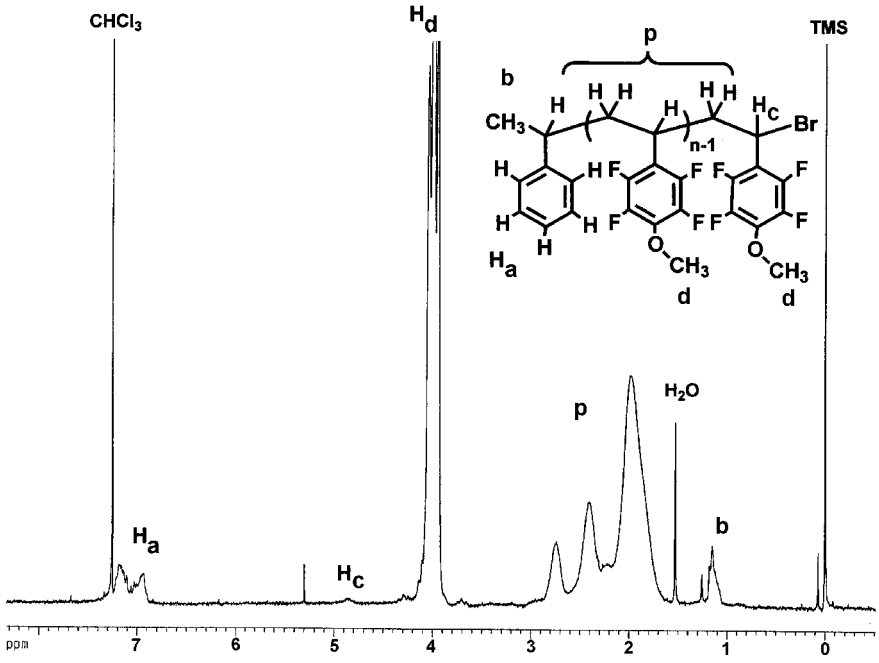

Figure 5.3.1 ^{1}H NMR spectrum of PTFMS1-Br

From the derived straight lines the apparent rate coefficients, $k_p^{app} = -d\ln[M]/dt$, listed in table 5.3.2 were calculated. With reference to these data it is evident that the replacement of the St aromatic hydrogen's with 5 electron-withdrawing fluorine's greatly enhances the rate of polymerization of FS as compared to that of St. However, substituting the 4-F in FS with an electron-donating methoxy group enhances the rate of polymerization of TFMS even further as compared to that of FS. Previously, the enhancing rate effect has been observed[9] in ATRP of substituted styrenes by introducing one electron-withdrawing substituent such as 3-CF_3 or 4-CF_3, whereas the electron-donating 4-OCH_3 had a slight retarding effect as also listed in table 5.3.2; a single F (4-F) only had a neglectable effect. Thus, in the light of these earlier findings the apparent synergistic substitution of four F electron-withdrawing atoms and

the one electron-donating 4-OCH_3 group in TFMS is beneficial in terms of enhancing the rate of polymerization which was surprising and unexpected. However, higher k_p or k_{eq} or lower solubility of Cu(II) can not be disregarded.[6,10] This unusual rate enhancing synergy is the subject of further and more theoretical studies.

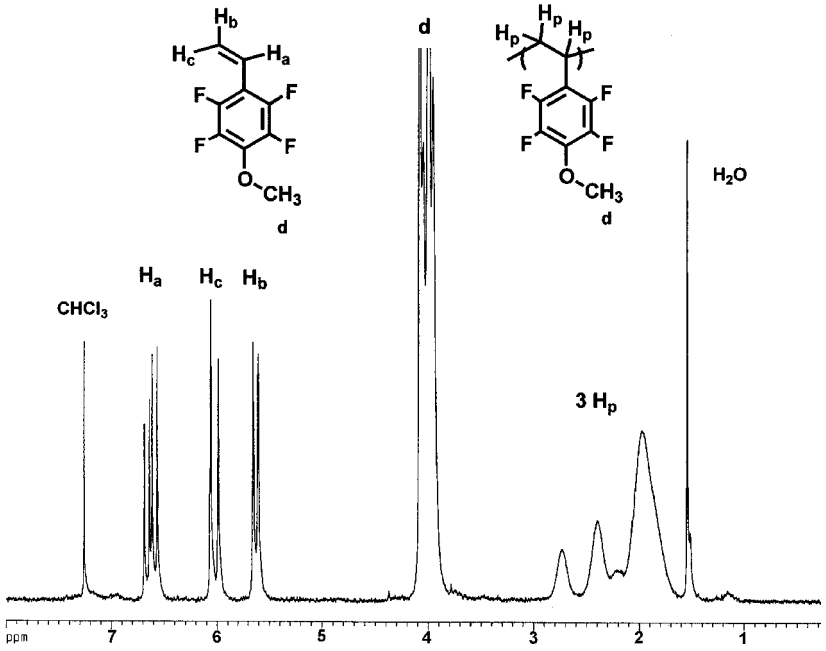

Figure 5.3.2. ^{1}H NMR of a crude sample for calculation of the monomer conversion

Table 5.3.2. Apparent rate coefficients in ATRP of substituted styrenes

Substitution	$k_p^{app} * 10^4 (s^{-1})$	**Solvent**	**Reference**
2,3,5,6-F_4-OCH_3	6.9	none	this work
2,3,4,5,6-F_5	3.0	none	5
None	1.41	none	this work
3-CF_3	1.44	DPE[a]	9
4-CF_3	1.25	DPE[a]	9
None	0.44	DPE[a]	9
4-F	0.39	DPE[a]	9
4-OCH_3	0.21	DPE[a]	9

[a] *DPE : diphenyl ether, $[M]_0$ = 4.37 g, $[M]:[PhEBr]_0:[CuBr]:[bipy]_0$ = 100:1:1:3 at 110°C*

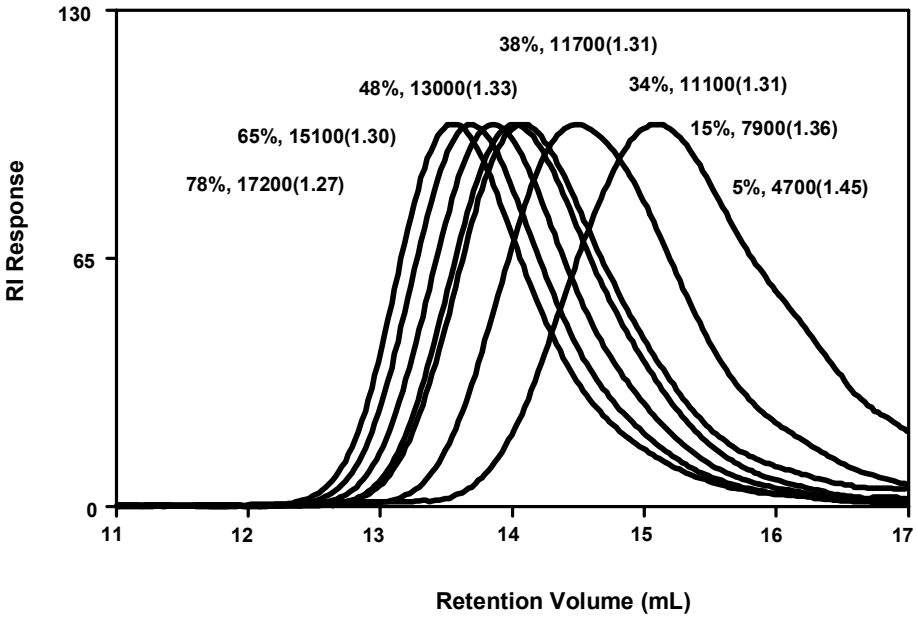

Figure 5.3.3. SEC traces of PTFMS (M_n, target 20,800) as a function of increasing conversion in % to each trace has been added the calculated M_n and the PDI

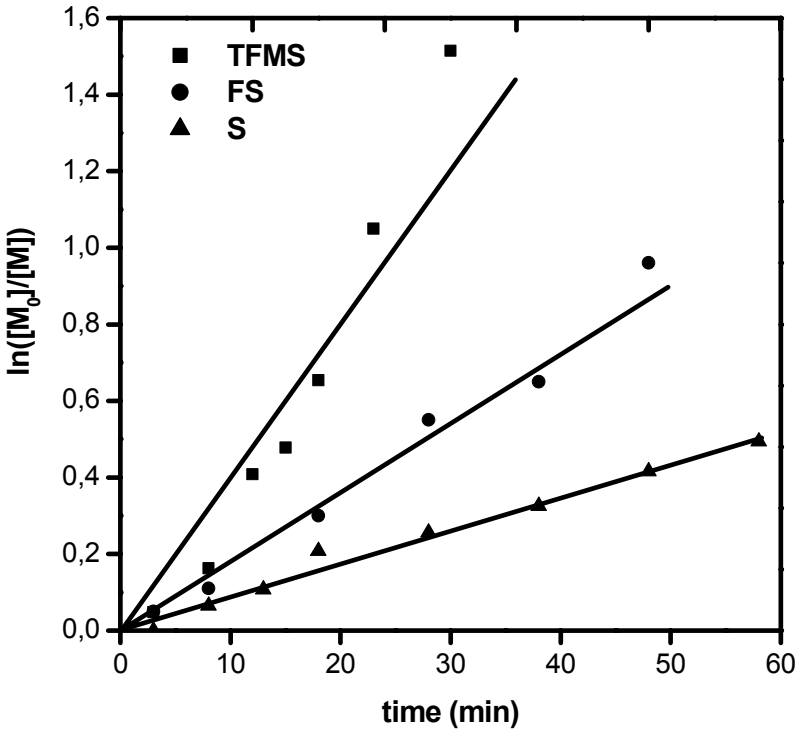

Figure 5.3.4. First order plot for ATRP of TFMS, FS, and St at 110 ºC, [M]:[PhEBr]:[CuBr]:[bipy] = 100:1:1:3

The development of M_n and PDI as a function of conversion is shown in figure 5.3.5. However, the molecular weights of PTFMS determined by the PS calibration are higher than the theoretical ones suggesting that a significant amount of radicals are terminating in the very beginning of the ATRP. Support for this behavior is the higher PDI of PTFMS polymers as compared to those of PFS [5] ≈1.2 and PS [9] ≈1.1. Figure 5.3.3 also shows how the molecular weights develop with conversion. The initial M_w/M_n of PTFMS is 1.45 that decreases to 1.27 with increasing conversion. PTFMS employed as macroinitiators and discussed in a subsequent section also tend to provide block copolymers with low molecular weight tailing indicating that termination reactions occur throughout the homopolymerization of TFMS.

5.3.2. Block Copolymerization of PTFMS with St or FS

Several of the recovered PTFMS-Br samples were used as initiators for ATRP in xylene solution of both FS and St, respectively. This approach afforded preparation of novel block copolymers as seen in scheme 5.3.1. PFS-Br and PS-Br likewise prepared by ATRP were in the same manner employed as macroinitiators for the preparation of block copolymers with the complementary monomers as listed in table 5.3.3. Nevertheless, the preferred synthetic pathway for block copolymers of TFMS and FS is the one starting from PTFMS-Br instead of PFS-Br due to the significantly better solubility in xylene of the former. No preference is needed due to solubility considerations in case of block copolymer synthesis involving PTFMS-Br or PS-Br.

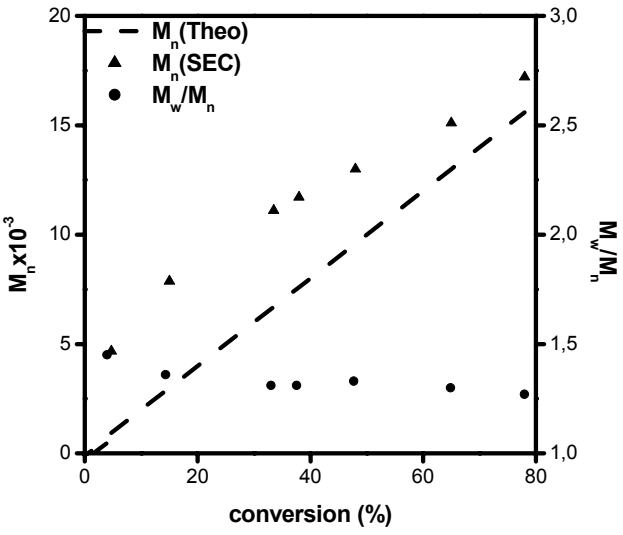

Figure 5.3.5 Molecular weights and polydispersities of PTFMS as a function of conversion for ATRP at 110°C, [M]:[PhEBr]:[CuBr]:[bipy] = 100:1:1:3

Table 5.3.3. Block copolymers and the seeding macroinitiators

Polymer	PTFMS Wt-%	PFS Wt-%	PS Wt-%	$M_{n,\,SEC}$	PDI	$M_{n,\,NMR}$	T_g °C
PTFMS1-Br	100			2,900	1.36	2,900	41
PTFMS1-*b*-PS	10[a]		90[a]	34,000	1.32	34,000	90
PTFMS3-Br	100			8,800	1.26	9,700	90
PTFMS3-*b*-PFS	64[a]	36[a]		12,600	1.20	13,800	95
PFS-Br		100		11,400	1.21	13,000	95
PFS-*b*-PTFMS	71[a]	29[a]		35,000	1.40	39,300	90
PFS-*b*-PS		42[a]	58[a]	21,000	1.32	27,000	101
PS-Br			100	16,500	1.11	-	100
PS-*b*-PTFMS	57[a]		43[a]	35,000	1.54	38,400	99
PS-*b*-PFS		21[a]	79[a]	19,400	1.16	20,900	92

[a] *by ^1H NMR*

The composition of the block copolymers as determined by ^1H NMR (equation 5.1) could be varied in a fairly large range while still maintaining the relatively narrow PDIs. Since the procedure is not sequential addition of monomers but in fact performed in two separate steps great design freedom is offered for both blocks. The content of Table 5.3.3 is by no means comprehensive and only in case of the PTFMS-Br the achievable molecular weight range is indicated (more PTFMS block copolymers are listed in Table 5.3.5). It should furthermore be stressed that M_n (SEC) and the corresponding PDI are only indicative. These values are obtained directly from the PS calibration and reported without any corrections. However, when the PS-Br was used as initiator the absolute M_n was determined by a combination of PS-Br molecular weight obtained from the PS calibration and the comonomer ratio derived from ^1H NMR. It can be seen from Table 5.3.3 that some discrepancy between the indicative M_n(SEC) and M_n(NMR) are found. The wt.% of PS/PFS and M_n(NMR) are calculated for the block copolymers by equation 5.2 and 5.3 respectively.

Wt % Composition of PS / PFS in the block copolymer is calculated as

$$\%\ PS = \frac{1H_{ar} * 104}{[(1H_{ar} * 104) + (1H_{OMe} * 206)]} * 100 \qquad \text{eq (5.2)}$$

where, H_{ar} and H_{OMe} are the integral areas of St and methoxy protons respectively in ^1H NMR. And 104 & 206 are the formula weight of the St and TFMS monomers, respectively.

Therefore, by taking into account the observed wt% of PS and PTFMS the M_n of the block copolymer was determined by ^1H NMR as follows:

$$M_n\,(NMR) = \frac{M_n\,(SEC)\ of\ MI}{wt\ \%\ of\ MI\ in\ block\ copolymer} * 100 \qquad \text{eq (5.3)}$$

where, MI is the starting macroinitiator.

5.3.3 Thermal Properties of PTFMS and its Block Copolymers

Generally, the glass transition temperature, T_g, as also listed in table 5.3.3 is basically independent of whether the phenyl is substituted (PTFMS) or non-substituted (PS). On the other hand, the molecular weight is important, such that short chain samples have lower T_gs. A similar behavior was observed previously for PFS and PS.[5] Finally, it is noted that the implied flexibility of block length design is considered important for future applications as further elaborated in a subsequent section.

The thermal stability of PTFMS was investigated by thermogravimetry (TGA) in N_2 atmosphere and compared to those of PFS [5] (M_n = 11,400) and PS (M_n = 14800) as depicted in figure 5.3.6. PTFMS (M_n = 12,700) has a slightly higher thermal stability than PS as evident from the TGA traces. However, the thermal stability is inferior to that of PFS. A close inspection of the thermogramme also reveals that an approx. 8 wt-% residue is left at 550 °C suggesting that the methoxy group is thermolabile. Also the block copolymer, PTFMS-*b*-PS (M_n = 16,100, 50 wt-% PTFMS), with 50 wt-% PTFMS leaves a small residue at the end of the analyses. In comparison, PFS and PS are seen to leave vertically no residues under the same experimental conditions. Most likely the loss of methoxy renders formation of tetrafluorophenyl radicals forming highly fluorinated, fused aromatic structures.

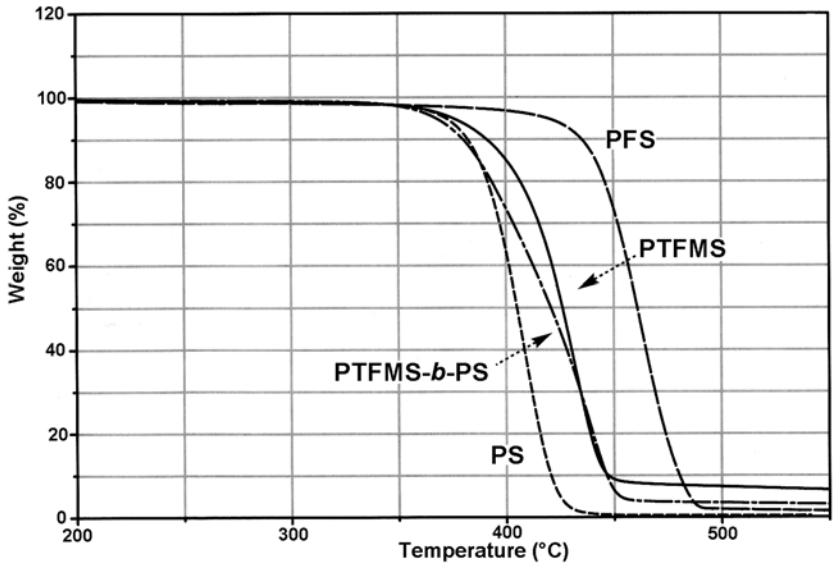

Figure 5.3.6. Thermal stability of PTFMS, PTFMS-*b*-PS, PFS and PS determined by TGA in N_2 by heating at a rate of 5 °C/min

5.3.4 Solubility Parameters of PTFMS Homopolymers

Solubility of polymers to a first approximation inversely reflects chemical resistance. The solubility* of PTFMS was determined in a number of common chlorinated, oxygen containing or aromatic solvents as listed in table 5.3.4 that also contains comparative information on PFS and PS. From table 5.3.4 it is evident that the introduction of 4-OCH_3 enhances the solubility of PTFMS as compared to that of PFS in the investigated solvents with the exception of fluorobenzene. However, the general solvent resistance is still significantly higher than that of PS. Most likely the polarizability of fluorobenzene significantly better matches that of the pentafluorophenyl moiety of PFS than those of both phenyl residues in PTFMS and PS and thus accounts for this significant difference in solubility.

Table 5.3.4. Solubility of PTFMS, PFS and PS in common solvents, g polymer in 1 g solvent

Solvent	PTFMS	PFS[a]	PS
Chloroform	0.206	0.027	>0.7[b]
Methylene chloride	0.148	0.009	>0.9[b]
Tetrahydrofuran	0.218	0.125	>0.9[b]
Methyl ethyl ketone	>0.9	0.143	>0.9[a]
Xylene	0.321	0.113	>1.3[a]
Fluorobenzene	0.194	0.413	0.106

[a] *Ref. (5);* [b] *Ref. (12)*

** Solubility experiments were performed with the help of K. Jankova (DTU, Denmark)*

5.3.5 Surface Properties of PTFMS and its Block Copolymers

The surfaces of the PTFMS6-Br and several other block copolymers of FS and St with PTFMS were examined by XPS. In these surface spectroscopic experiments the sample of interest is irradiated with an AlK_α X-ray source and the kinetic energy of the emitted photoelectrons is recorded. The PTFMS6-Br homopolymer exhibits a relative atomic composition towards the surface: 61% C, 29% F, and 10% O, whereas the block copolymer PTFMS3-*b*-PFS having almost the same block length exhibits: 62% C, 30%F and 8% O even though the second block was also a highly fluorinated styrene. On the other hand the PTFMS-*b*-PS block copolymer [M_n = 22500, 59 Wt.% PTFMS] shows a surface composition of 65% C, 22% F and 13% O respectively. This observation evidences that the PTFMS block segregate and tend to go towards the surface.

The contact angle measurements with water droplet towards airside were performed with the sessile airdrop technique. The advancing angles and receding angles observed for PTFMS6-Br are 115° and 101°, respectively. These angles were slightly higher than the contact angles measured for PFS[2] homopolymer (adv. 108° and rec. 97°). The only explanation which supports this observation is that the surface tension depends on the constituent group and decreases in the order of $CH_2 > CH_3 > CF_2 > CF_3$.[11] Hence the presence of the -OCH_3 group has some influence on the contact angle. Furthermore, the contact angle measurement for the block copolymers shows the inverse relation with PS content in the block. The PTFMS1-b-PS has the advancing contact angle 97 ° almost the same as that of observed for normal PS.

5.3.6 Demethylation Reaction

Conversion of the p-methoxy sites in PTFMS and PTFMS based block copolymers to the corresponding p-hydroxyl analogues appeared very attractive. Basically, a significant change of the hydrophobic character of both homo- and block copolymers by a considerable introduction of hydrophilic sites is to be expected. Secondly, and not less important, a viable route to functional scaffold polymers also appears through potential derivatization by reactions on the hydroxyl sites. The target was reached after several unsuccessful attempts with known deprotecting agents. Thus, both trimethylsilyl iodide[13] that works for the deprotection of poly(*p*-methoxystyrene) or concentrated hydrobromic acid [14] which similarly functions for poly(*p-tert*-butoxystyrene) failed in the case of PTFMS. On the other hand, the reported procedure [2] for the demethylation of TFMS to the corresponding hydroxyl compound by use of boron tribromide (BBr_3) was adopted for the synthesized homo- and block copolymers.

The degree of deprotection was subsequently improved with a molar ratio of -OCH_3 : BBr_3 of 1:2. In the best case 97 % of the methoxy groups of PTFMS could be removed as demonstrated by ^{1}H NMR. Furthermore, in this case no influence on either M_n or PDI was noticed (PTFHS5-Br, Table 5.3.5). The consequence of demethylation of block copolymers with PS and one example of subsequent functionalization is elaborated below.

5.3.7 Functionalization Reaction with Azobenzene Precursors

The strategy for preparation of azobenzene side-chain block copolymers that could have interesting applications for optical storage of information through polarization holography [7] is outlined in Scheme 5.3.2. Initially, route **I** was undertaken in which the plan

Table 5.3.5. Demethylation and intermediates to the azo-functionalized block copolymer, routes I and II in scheme 2

Route I	Route II	M_n	PDI	OH[a] %	T_g °C	T_{LC-I}[b] °C	ΔH J/g
PTFMS1-Br		3,400	1.36		41		
PTFMS1-*b*-PS		34,000	1.32		96		
PTFMS1-*b*-PS		15,000	1.82	n.a.[c]	n.a.[c]		
	PTFMS5-Br	2,300	1.28		51		
	PTFHS5-Br	2,300	1.26	97	116		
	PTF(azo-CN)S5-Br	6,200	1.37		67	126	63
	PTF(azo-CN)S5-*b*-PS	11,400	1.65		93	n.i.[d]	n.i.[d]
	PTFMS3-Br	8,800	1.26		90		
	PTFHS3-Br	8,500	1.25	93	114		
	PTF(azo-CN)S3	27,000	1.58		80	163	4.2
	PTF(azo-F)S3	25,000	1.79		126	203	
	PTF(azo-CF3)S3	29,000	1.57		108	148	4.6

[a]By ^{1}H NMR; [b]mesophase to isotropic transition; [c]not analyzed; [d]not possible to identify

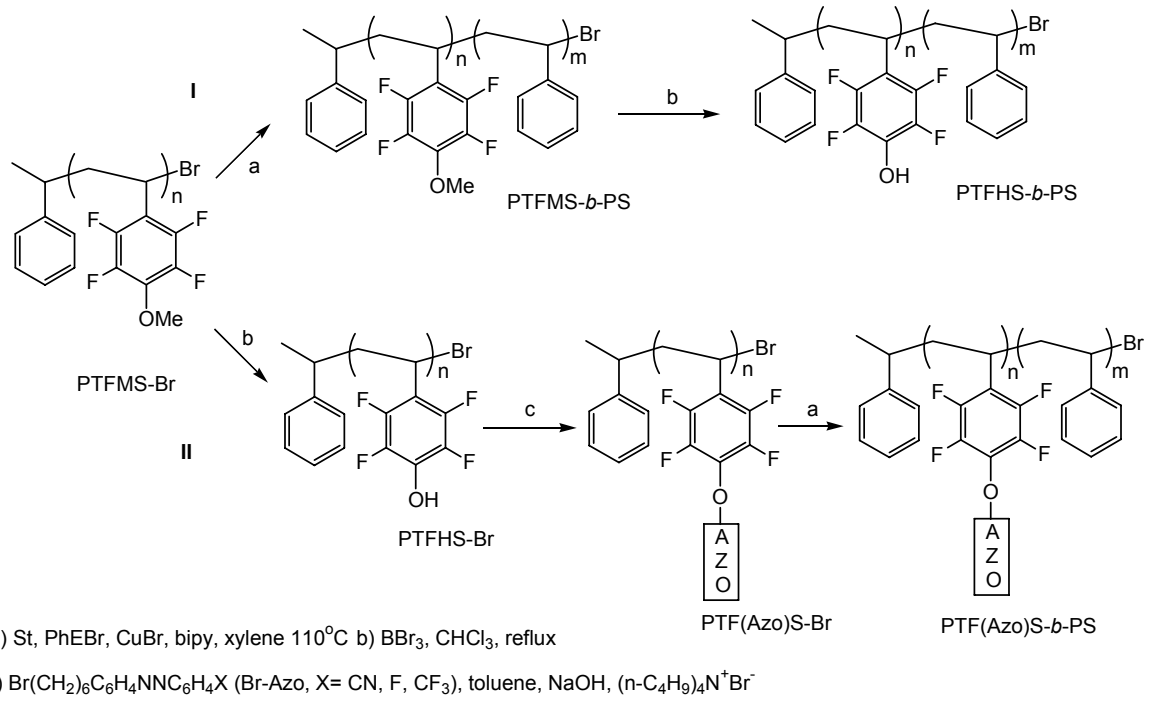

Scheme 5.3.2. Demethylation and intermediates to azobenzene side-chain block copolymers

was to prepare PTFHS-*b*-PS and then react suitable azobenzene side-chain precursors on the hydroxyl sites. However, in this case some apparent degradation occurred as observed by both a significant reduction in M_n associated with some broadening of PDI. On the other hand, supporting control experiments performed under demethylation conditions with BBr_3 on narrow molecular weight PS standards prepared by anionic polymerization and thus composed of only hydrocarbon fragments clearly demonstrated that PS partially degraded under these conditions. It was therefore concluded that the PS block of the copolymers was degraded but not the PTFHS block by the BBr_3 treatment. As a consequence the second route (**II**) was adopted. That no degradation of the PTFHS-Br homopolymers occur is verified by the results reported in table 5.3.5 where PTFHS5-Br and PTFHS3-Br show no sign of changes of neither M_n nor PDI. The next step, reaction of the azobenzene side chains (AZO) onto the hydroxyl sites by alkylation under phase transfer conditions, resulted in a slight increase in PDI. Finally, the PS block was formed through ATRP with some broadening in PDI. However, this broadening is probably acceptable since the idea is to achieve microphase separation and form small liquid crystalline azobenzene domains in the amorphous PS phase. Already the difference between the fluorinated and the normal phenyl blocks of polystyrene is expected to induce a phase separation and the azobenzene derivatization likely enhances the expected microphase separation. The thermal transitions as detected by DSC indicate that all azobenzene derivatized polymers have developed a mesophase of varying broadness

depending on both the block length and the substituent on the azobenzene. The determined enthalpy values of the formed mesophases could indicate the mesophases to be of a smectic type.[15]

5.4 Conclusions

Neat TFMS polymerizes very fast in a conventional ATRP protocol at 110 °C. Under identical conditions PTFMS is produced faster than PFS. The polymerization is relatively well controlled with M_ns up to 17,000 and corresponding PDIs generally below 1.3. The recovered PTFMS can function as ATRP macroinitiator for both FS and S producing block copolymers while maintaining the controlled ATRP characteristics. In fact, block copolymers in all combinations of these three monomers have been prepared based on the macroinitiator concept. Homo- and block copolymers of PTFMS impart both better thermal stability and chemical resistance than that of PS, however, not to the same extent as that of PFS. On the other hand, the presence of the 4-methoxy group in PTFMS has been exploited for the possible demethylation that allows for post-polymerization reactions. The resulting hydroxyl functionality has been utilized for alkylations with different azobenzene side chains. Furthermore, the azobenzene derivatized polymers retain ATRP reactivity that has been employed in the preparation of an azobenzene PS block copolymer.

These new fluorinated materials can open up some potential application for novel optical materials. The azobenzene side-chain materials can serve as models for optical storage materials since the block lengths can be adjusted and ultimately the absorptivity can be controlled to make thick holographic materials potentially capable of holographic multiplexing to be prepared. However, because of the optimization of the standard conditions to synthesize these new materials we ended up with only few milligrams of sample which was not sufficient for optical investigations.

Chapter VI

Synthesis of Novel Fluorinated Styrene Monomers for ATRP: Homopolymerization as well as Block Copolymerization with Styrene and Pentafluorostyrene

Abstract

It is well known that fluorine is a good leaving group in activated aromatic nucleophilic substitution reactions in which the presence of nucleophile and substrate nature strongly influence the relative mobility.[1] Highly fluorinated styrene monomers 2,3,5,6-tetrafluoro-4-(2,2,3,3,3 pentafluoropropoxy) styrene [TF(F_5)S] and 2,3,5,6-tetrafluroro-4-(2,2,3,3,4,4,5,5,6,6,7,7,8,8,8 pentadecafluorooctaoxy) styrene [TF(F_{15})S] were prepared by reacting 2,3,4,5,6-pentafluorostyrene (FS) with respective perfluorinated alcohols under reflux conditions. The structures of TF(F_5)S and TF(F_{15})S were characterized by FT-IR, ^{1}H, ^{13}C and also ^{19}F NMR techniques.

Here we would like to report on the ATRP of these new highly fluorinated styrene monomers. The TF(F_5)S and TF(F_{15})S were homopolymerized in bulk as well as in xylene solution using phenylethylbromide (PhEBr) as an initiator and Cu(I)Br/bipy as a catalyst system at 110 °C. This results in fast polymerization and high conversions to polymers with relatively narrow PDI. TF(F_5)S polymers with great variation of molecular weights in the range of 6300 to 30,000 have been prepared. The polymerization can also be performed at temperatures down to 70 °C. The isolated polymers of TF(F_5)S have been utilized as macroinitiators for the block copolymerization with St or FS. Block copolymers with styrene (St) content from 70 to 90% have been synthesized. The limited solubility of PTF(F_{15})S restricts its use as a macroinitiator. Therefore, the block copolymers of TF(F_{15})S are based on a PS macroinitiator.

The PTF(F_5)S, PTF(F_{15})S and their block copolymers have high numbers of fluorines that can affect the surface properties of polymers. The contact angles of the polymer films were measured using a water droplet, which shows contact angles up to 122°. Both, the X-ray photoelectron spectroscopy (XPS) and contact angle measurement techniques showed that the fluorinated blocks segregate and are preferentially enriched at the surface. DSC analysis of PTF(F_5)S and PTF(F_{15})S shows lower glass transition temperatures (T_g) than for polypentafluorostyrene (PFS) and polytetrafluoromethoxystyrene (PTFMS). The block copolymers reflect a two-phase morphology. It has been observed that the PTF(F_5)S and PTF(F_{15})S polymer exhibit a lower thermal stability than PFS.

6.1 Introduction

Fluorinated polymers have found wide use in materials science due to their distinctive properties like good thermal stability and high chemical resistance. As a result they have numerous commercial applications as for example, in microelectronic packaging, for low-energy surfaces, optical wave-guides and biomaterials.[2-4] Perfluorinated copolymers are well studied due to their unique behavior in membrane science and surface modification. Miyata et. al [5] have synthesized pervaporation membranes by using fluorinated copolymers of PFS-*g*-PDMS, which are very effective in the separation of very low concentrations of benzene from waste water. In semifluorinated side chain polymers the fluorinated side chains possess a higher level of organization and exhibit a self-assembly process at surfaces.[6]

Recently Hvilsted[7] and coworkers have shown that fully fluorinated and partly fluorinated styrenes can be easily polymerized in a controlled manner by ATRP with relatively narrow molecular weight distribution.[7-9] So far the perfluorinated styrene polymers reported are based on functionalization in the post-polymerization reaction. However, to our knowledge side chain perfluorinated styrene monomers and their polymerization by ATRP has not been reported so far. Also, highly fluorinated polymers have typically very low solubility in most organic solvents, which limits the use of these materials. Grafting or block copolymerizing them with nonfluorinated blocks like PS can overcome this problem.

6.2 Experimental

6.2.1 Materials

Pentafluoropropane-1-ol and pentadecafluorooctane-1-ol (ABCR Chemicals, Germany) were used as received. St and FS (Aldrich) were passed through a ready to use, disposable pre-packed inhibitor remover column. Tetrahydrofuran was distilled prior to use over sodium metal under a stream of dry nitrogen. Cu(I)Br, 1-phenylethylbromide and bipyridine (all from Aldrich) were used as received. All the reactions described were carried out in an inert atmosphere. Xylene is degassed with a stream of nitrogen and distilled over calcium hydride and stored under nitrogen atmosphere.

6.2.2 Synthesis of 2,3,5,6-tetrafluoro-4-(2,2,3,3,3-pentafluoropropoxy) styrene [TF(F_5)S] and 2,3,5,6-tetrafluoro-4-(2,2,3,3,4,4,5,5,6,6,7,7,8,8,8-pentadecafluorooctaoxy) styrene [TF(F_{15})S]

In what follows is a modified method of Burdon[10] and Hult.[11] In a three-neck round bottom flask equipped with magnetic stirrer, addition funnel and reflux condenser, a solution

of 13 g (67 mmol) FS in 50 ml dry THF was cooled down to 0°C. To this a solution of 12.67g (74 mmol) of fluorinated sodium 1-propoxide in 100 ml THF was added slowly. The stirring was continued for 1 h and then brought to reflux for 19 h. The reaction mixture was poured in 400 ml of ice water and extracted with diethyl ether and distilled at 56 °C/1.3 mbar over calcium hydride and stored under nitrogen. Yield = 17.5 g (80%)

^{1}H NMR ($CDCl_3$): δ = 5.7(d, 1H, ^{2}H), 6.05(d, 1H, ^{3}H), 6.65(dd, 1H, ^{1}H), 4.6(t, 2H, $^4H_2$).

^{13}C NMR ($CDCl_3$): δ = 147 (m), 142.8 (m), 138.65 (m), 134.8 (m), 122.7(t), 121.3 (t), 116.14 (m), 112.5 (m), 69.5 (t)

^{19}F NMR (C_6F_6): δ = -155.12($2F_{ar}$), -141.26($2F_{ar}$), -121.73(2F), -80.75(3F)

Following the same procedure and using fluorinated sodium 1-octaoxide TF(F_{15})S was also synthesized in 85% yield and distilled at 94 °C/1.3 mbar.

^{1}H NMR ($CDCl_3$): δ = 5.65(d, 1H, ^{2}H), 6.05(d, 1H, ^{3}H), 6.6(dd, 1H, ^{1}H), 4.7(t, 2H, ^{4}H).

^{19}F NMR (C_6F_6): δ = -155.15($2F_{ar}$), -141.36($2F_{ar}$), -123.33($2F^7$), -120.19($2F^6$), -119.77($2F^3$), -119.01($4F^{4,5}$), -117.92($2F^2$), -78.25($3F^8$)

6.2.3 Polymerization Procedure

The polymerizations were performed in a dry Schlenk tube. In a typical experiment the tube was charged with 3.5 g (10.8 mmol) monomer, 0.126 g (0.68 mmol) PhEBr, 0.107 g (0.75 mmol) Cu(I)Br and 0.319 g (2.041 mmol) bipyridine were added. Oxygen was removed by three freeze-pump-thaw cycles and then the Schlenk tube heated at 110°C under nitrogen. The polymers were precipitated in methanol and dried under vacuum. The yield was determined gravimetrically. These homopolymers were further employed as macroinitiators for block copolymerizations with St and FS in xylene solution by analogy with the St polymerization.

6.3 Results and Discussion

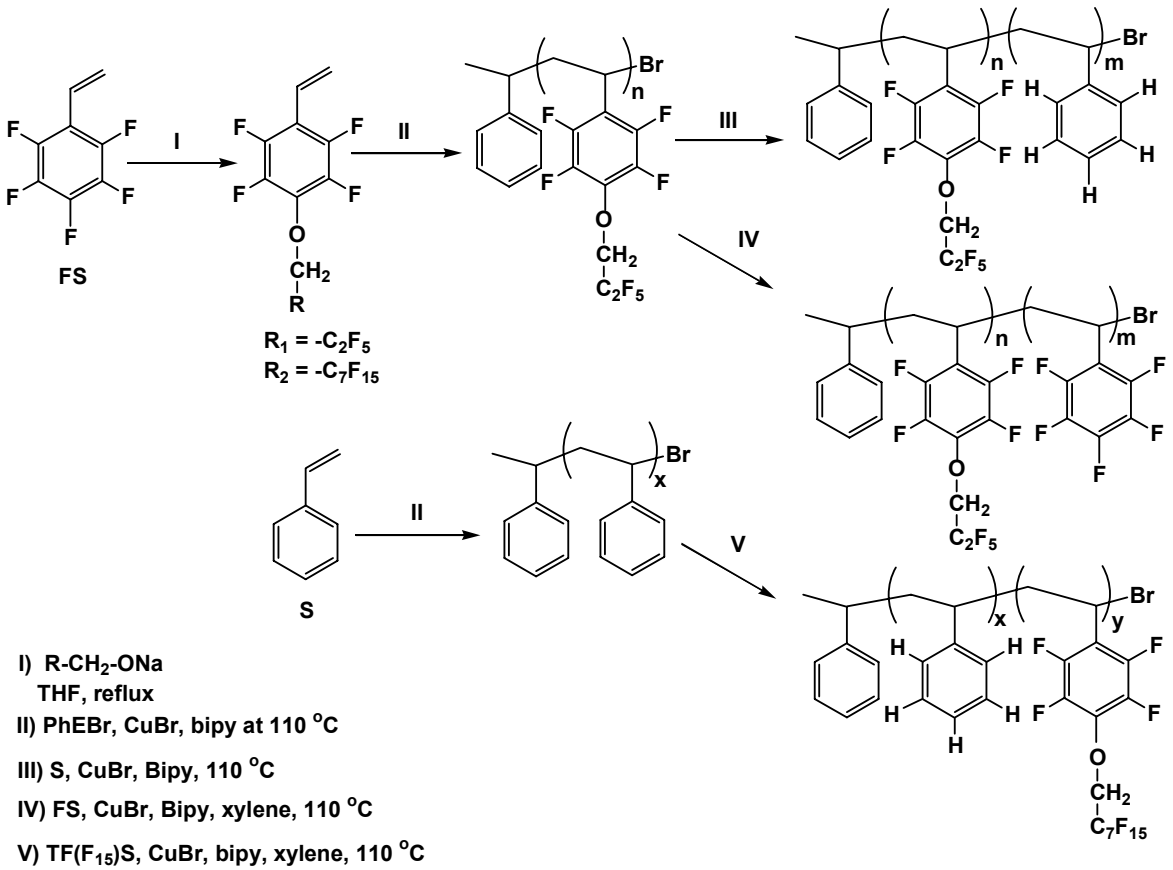

Scheme 6.3.1 Synthesis of monomers and their homopolymerization as well as block copolymerization with St and FS

6.3.1 Monomer Synthesis

Scheme 6.3.1 presents the synthesis of the monomers TF(F_5)S and TF(F_{15})S and their homopolymerization as well as their block copolymerizations with St or FS. The detailed procedure for the synthesis of TF(F_5)S and TF(F_{15})S is given in the experimental section. The monomers were synthesized by nucleophilic substitution reaction in high yield (80 and 85%) and purified by vacuum distillation at 56°C and 94°C respectively at 1.3 mbar. The structures of the monomers were confirmed by ^{1}H, ^{13}C and ^{19}F NMR spectroscopy. The FT-IR spectrum shows the formation of strong bands at 1200 cm^{-1} and 1103 cm^{-1} due to the presence of side-chain aliphatic fluorines.

Furthermore, the absence of the peak at 3400 cm^{-1} evidences that no pentadecafluorooctane-1-ol has been left as depicted in figure 6.3.1.

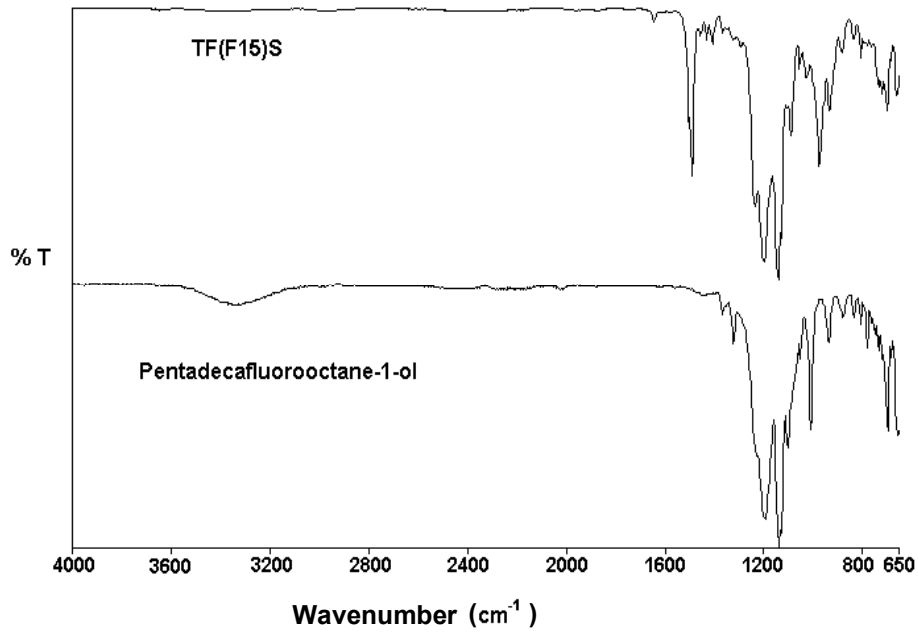

Figure 6.3.1 Comparative FT-IR spectrum of pentadecafluorooctane-1-ol and TF(F_{15})S

Figure 6.3.2 shows the ^{1}H NMR spectrum of TF(F_5)S. The triplet due to the side-chain methylene protons of the corresponding perfluorinated alcohol is shifted from 4 ppm to 4.6 ppm in TF(F_5)S and TF(F_{15})S monomers. The splitting of side chain methylene protons is due to the coupling with the fluorine substituent of the neighboring carbon atom. The ^{19}F NMR spectrum explains the presence of four sets of fluorines in the case of TF(F_5)S, whereas in the case of TF(F_{15})S eight different peaks have been observed as illustrated from figure 6.3.3 (a) and (b).

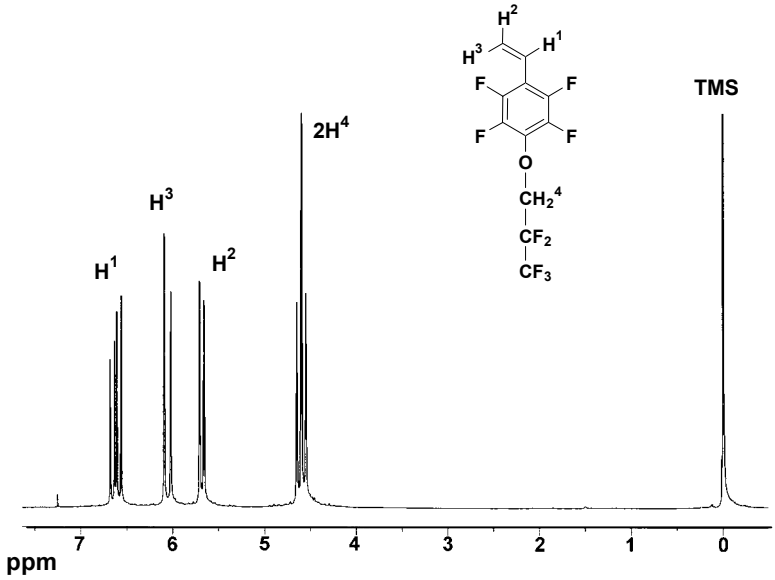

Figure 6.3.2 ^{1}H NMR spectrum of TF(F_5)S

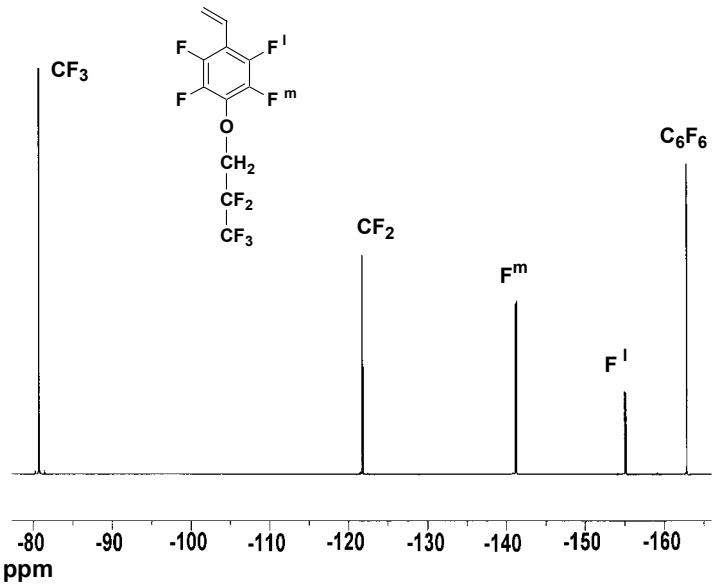

Figure 6.3.3 a) ^{19}F NMR spectrum of TF(F_5)S ($CDCl_3$-C_6F_6)

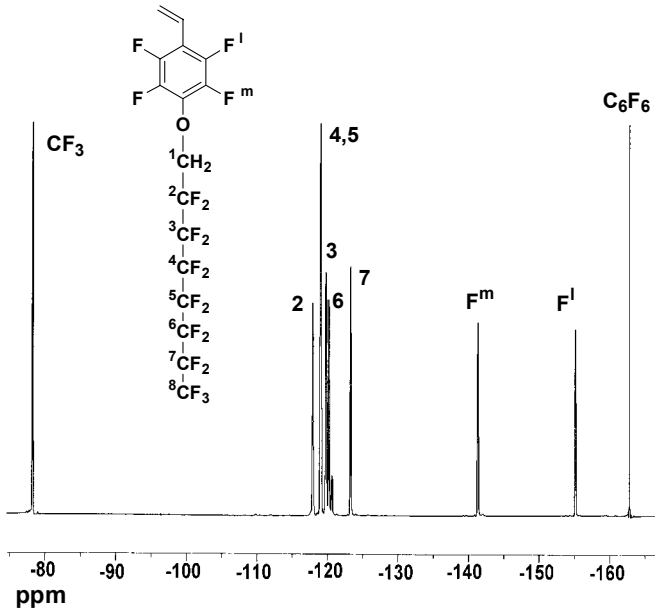

Figure 6.3.3 b) ^{19}F NMR spectrum of TF(F_{15})S ($CDCl_3$-C_6F_6)

6.3.2 Homopolymerization as well as Block Copolymerization of TF(F_5)S and TF(F_{15})S

3.5 g of TF(F_5)S was polymerized in bulk under ATRP conditions using 1-phenylethyl bromide as an initiator and Cu(I)Br and bipyridine as catalyst system at 110^{o}C. 86% conversion has been accomplished using these conditions. The results of homopolymerizations of TF(F_5)S performed in bulk or in xylene solution are listed in table 6.3.1. All the polymerizations were performed by keeping the initiator:CuBr:bipy ratio at 1:1.1:3.

Table 6.3.1 Homopolymerization of TF(F_5)S, TF(F_{15})S and St in bulk or in xylene solution

Polymer	Time (min)	M_n(target)	M_n(NMR)	SEC		Yield (%)	T_g (°C)
				M_n	PDI		
PTF(F_5)S1-Br	10	5000	6700	6300	1.30	86	34
PTF(F_5)S2-Br	20	20000	15300	18400	1.09	77	60
PTF(F_5)S3-Br[a]	20	20000	-	16900	1.08	58	56
PTF(F_5)S4-Br	23	36000	-	25400	1.20	69	62
PTF(F_{15})S1-Br	120	50000	28500	-	-	74	26
PTF(F_{15})S2-Br	60	10000	9700	-	-	70	16
PS1-Br	135	5000	-	4000	1.26	77	81
PS2-Br	420	10000	-	9700	1.18	84	87

[a] *30% in xylene solution*

The polymerizations were also carried out at 70°C and 90°C, which confirmed that increasing the temperature leads to a faster polymerization. Table 6.3.2 shows the effect of temperature on the polymerization of TF(F_5)S. The reaction carried out at 70°C needs almost 3 h to reach the 47% conversion, whereas the reactions performed at 90°C and 110 °C lead to 65% and 69% conversion within 75 min and 23 min, respectively, under identical conditions. Furthermore, the molecular weight distribution observed at lower temperatures was slightly broader as the reaction time was longer. This suggests that the radical termination is suppressed at higher temperatures when the polymerization rate is faster. The M_n was also calculated from the ^{1}H NMR spectrum by comparing the integral of the initiator with the main chain protons of the polymer as shown in figure 6.3.4. The TF(F_5)S polymerization by conventional radical initiator using AIBN resulted in a polymer with relatively high molecular weight and a broad PDI (1.60). Nevertheless, the polymerization performed at 70°C had

quantitative conversion but no control with respect to molecular weight and PDI could be observed.

Table 6.3.2 Effect of temperature and initiator on the polymerization of TF(F_5)S

Polymer	Temp(°C)	Time(min)	Yield(%)	SEC	
				M_n	M_w/M_n
PTF(F_5)S4-Br	110	23	69	25400	1.20
PTF(F_5)S5-Br	90	75	65	23900	1.28
PTF(F_5)S6-Br	70	180	47	30000	1.37
PTF(F_5)S7-Br[#]	70	30	86	145900	1.60

M_n(target) 36000, $[M]_o$ = 1g, [#] AIBN as a initiator

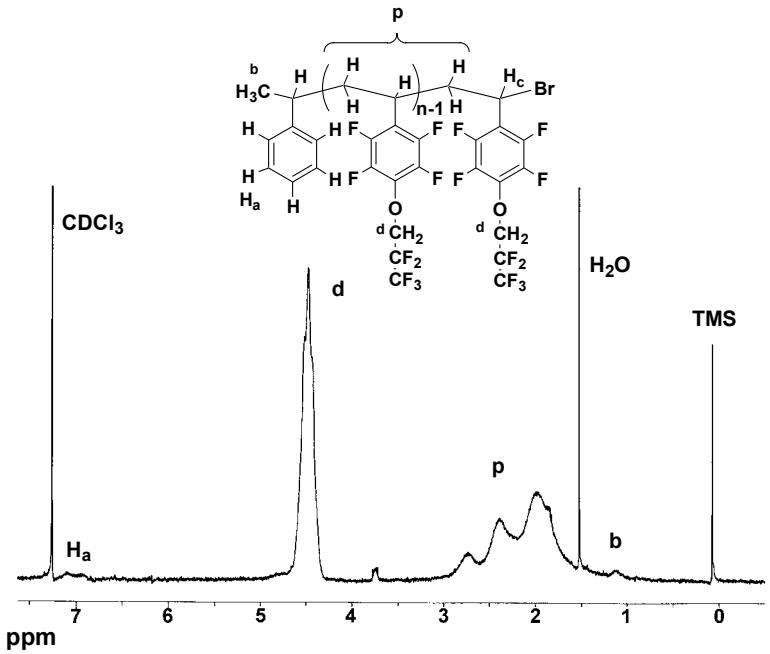

Figure 6.3.4 ^{1}H NMR spectrum of PTF(F_5)S2-Br ($CDCl_3$)

In case of the TF(F_{15})S polymerization using the ATRP protocol and the same initiator and catalyst system at 110 °C resulted in 74 % yield within 2 h when the target molecular weight was 50000. It has been also observed that the PTF(F_{15})S polymers formed were insoluble in common organic solvents other than fluorinated solvents. The ^{1}H NMR spectra of the TF(F_{15})S polymers were measured in a mixture of C_6F_6 and $CDCl_3$ (3:1 v/v). The molecular weights were calculated by comparing the integral area of the side chain aliphatic

methylene protons of the perfluorinated substituent with the aromatic protons from the initiator fragment as illustrated in figure 6.3.5.

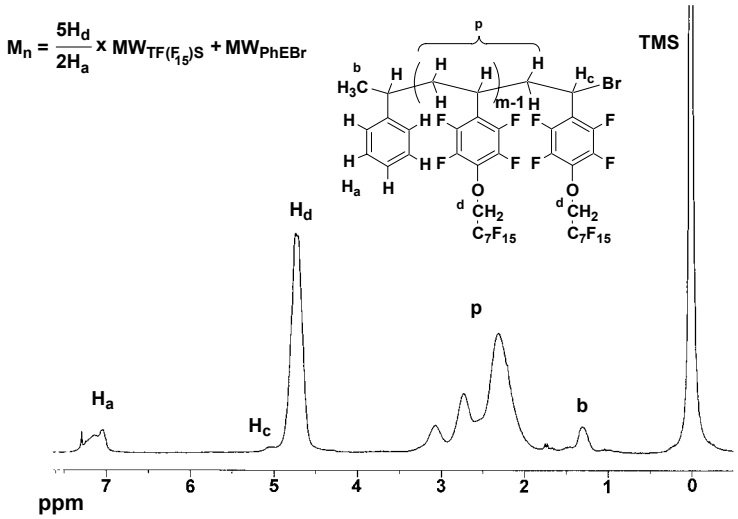

Figure 6.3.5 ^{1}H NMR spectrum of PTF(F_{15})S2-Br (3:1 mixture of C_6F_6 and $CDCl_3$)

PTF(F_5)S-Br polymers were employed as macroinitiators for the synthesis of block copolymers with St and FS in xylene solution. A great variation of block copolymers in the range from 50% to 90% PS were prepared. The composition of the PS was calculated from the ^{1}H NMR spectra. Figure 6.3.6 shows the SEC overlays of block copolymers, which evidence the shift in elution volume as compared to the macroinitiator, implying the formation of copolymers rather than a mixture of two different polymers.

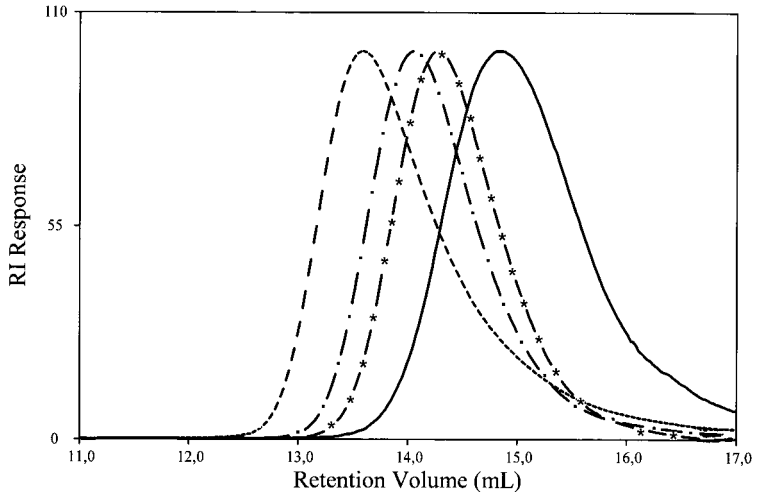

Figure 6.3.6 SEC overlays of PTF(F_5)S1-Br & block copolymers as a function of PS content

PTF(F_5)S1-Br(6300, 1.30) PTF(F_5)S1-*b*-PS (10800, 1.20)
PTF(F_5)S1-*b*-PS (12400, 1.23) PTF(F_5)S1-*b*-PS (14800, 1.37)

As the polymerization rate of fluorinated styrene is much faster than its unsubstituted analogue[7] 90% of the FS can be incorporated within 4.5 h whereas it took 8 h to incorporate 90% of St under similar conditions. The results are given in table 6.3.3. A PTF(F_{15})S was soluble only in fluorinated solvents, hence the block copolymers of TF(F_{15})S were prepared by using PS as a macroinitiator.

Table 6.3.3 Block copolymerization of PTF(F_5)S-Br /PTF(F_{15})S-Br with S and FS

Polymer	Time (h)	M_n (target)	Xylene (ml)	Yield (%)	SEC		% S or FS (mol)	T_g (°C)
					M_n	PDI		
PTF(F_5)S1-*b*-PS	4	25000	1	5	10800	1.20	70	31,75
PTF(F_5)S1-*b*-PS	8	50000	1	5	12400	1.23	79	30,95
PTF(F_5)S1-*b*-PS	17	100000	1	9	14800	1.37	89	n.o,93
PTF(F_5)S1-*b*-PFS	4.5	50000	1	55	34700	1.34	88	n.o,96
PS2-*b*-PTF(F_5)S	9	67000	3	48	19900	1.30	51	92, 53
PS1-*b*-PTF(F_{15})S	4	50000	2	69	6800	1.30	36	72,34
PS2-*b*-PTF(F_{15})S	4	9500	2	63	11600	1.24	90	87, n.o

temperature =110 ℃

Two different block copolymers with 36 and 90% St content (by ^{1}H NMR spectroscopy) have been synthesized in xylene solution. By introduction of the PS into the block copolymers PS-*b*-PTF(F_{15})S was soluble in THF and $CDCl_3$. The SEC analysis of the PS-*b*-PTF(F_{15})S polymers shows a relatively narrow PDI and the shift in elution volume confirms the formation of a block copolymer.

6.3.3 Thermal Properties

All the samples were first heated to a temperature higher than the glass transition temperature (T_g) and the DSC data reported are from the second heating cycle. The T_gs of the TF(F_5)S and TF(F_{15})S homopolymers were comparatively lower than the corresponding PS and PFS. This observation can be explained by the plasticizing effect of the alkoxy side-chain substitute on the *para* position of the fluorostyrene, which may lead to a corresponding decrease in the glass transition temperatures. On the contrary the effect of molecular weight on T_g of the TF(F_5)S and TF(F_{15})S polymers as illustrated in table 6.3.3 showed that the polymers with lower molecular weight posses lower T_g and vice versa. Table 6.4.1 shows that the glass transition temperatures of the *para*-substituted fluorostyrene homopolymers decrease as the bulk or length of the *para*-substituent of St increases. The block copolymers having

different compositions of PS and fluorinated blocks, reveal a two-phase morphology and show two different glass transition temperatures for the individual blocks. A typical DSC run is shown in figure 6.4.1. In the block copolymers containing 90% PS/PFS, it was difficult to observe the T_g of the fluorinated block.

As predicted TF(F_{15})S homopolymers showed lower T_gs than PFS, PTFMS, PS and PTF(F_5)S.

Table 6.4.1 Contact angles and glass transition temperatures of St and p-substituted styrene homopolymers

Polymer	**M_n(SEC)**	**PDI**	**T_g (°C)**	**Contact Angle (°)**	
				Adv	**Rec**
PS-Br	16500	1.11	100	95	80
PFS-Br[a]	16000	1.18	98	108	97
PTFMS-Br[b]	16700	1.25	94	115	101
PTF(F_5)S-Br	16900	1.09	62	117	105
PTF(F_{15})S-Br	28500[c]	-	26	122	104

[a] = Ref. 7, [b] = Ref. 9, [c] = M_n by ^1H NMR (C_6F_6-$CDCl_3$),

The TGA analysis of the fluorinated polymers indicates that PTF(F_5)S and PTF(F_{15})S polymers have lower thermal stability than PFS. Figure 6.4.2 shows the TGA overlays of the PFS, PTFMS, PS, PTF(F_{15})S and PTF(F_5)S polymers.

A previous study on PFS[7] and PTFMS[9] revealed that they have a higher thermal stability than PS, but it has been observed that these side-chain fluorinated polymers [PTF(F_5)S and PTF(F_{15})S] have a lower thermal stability than PS. This observation suggests the labile nature of the bulky substituent of fluorinated styrene.

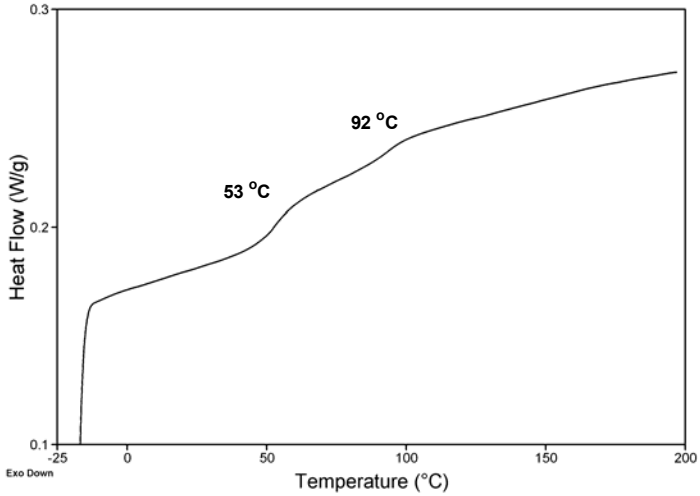

Figure 6.4.1 DSC run of PS2-*b*-PTF(F_5)S with a heating rate of 10°C/min

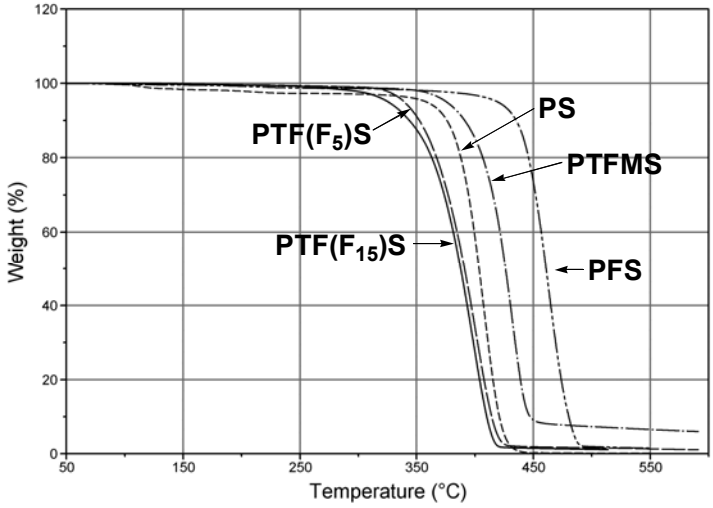

Figure 6.4.2 TGA curves of PTFMS, PS, PFS, PTF(F_5)S and PTF(F_{15})S in N_2 atmosphere with a heating rate of 5 °C/min.

6.3.4 Surface Properties

The surface property measurements of the homopolymers as well as the block copolymers were carried out by XPS and contact-angle measurements. The PTF(F_5)S, PTF(F_{15})S and their block copolymers were expected to exhibit a considerable degree of hydrophobicity. This has been evidenced by the measurement of water contact angles, which are 117° and 122°, respectively, for PTF(F_5)S and PTF(F_{15})S.

Table 6.5.1 Contact-angle measurements using water droplets on a film surface of the fluorinated polymers

Polymer	%PS[a]	XPS data (%)		(F/C)*100	Contact Angle [deg]	
	(mol)	F	C		Adv	Rec
PTF(F_5)S1	0	46.2	48.3	95.7	117	105
PS2-*b*-PTF(F_5)S	51	43.4	50.0	86.8	113	102
PTF(F_5)S1-*b*-PS	70	37.7	57.7	65.3	111	104
PTF(F_5)S1-*b*-PS	79	38.6	54.4	70.9	109	100
PTF(F_5)S1-*b*-PS	89	31.3	63.3	49.4	105	99
PS	100	-	-	0	95	80
PS1-*b*-PTF(F_{15})S	36	54.7	42.7	128.1	119	103
PS2-*b*-PTF(F_{15})S	90	36.7	61.4	59.77	111	102
PTF(F_{15})S	0	57	40.1	142.1	122	104

[a] by NMR

Table 6.5.1 lists the percentage of fluorine and carbon observed at the surface by XPS measurements and the contact angle calculated for a water droplet. In case of the block copolymers the % F and the water contact angle decreases from 50 to 90% with an increase in St content. The PTF(F_5)S-*b*-PS block copolymer containing 89% PS shows 31% F at the surface whereas the PS-*b*-PTF(F_{15})S block copolymer having 90% PS has 37% F at the surface.

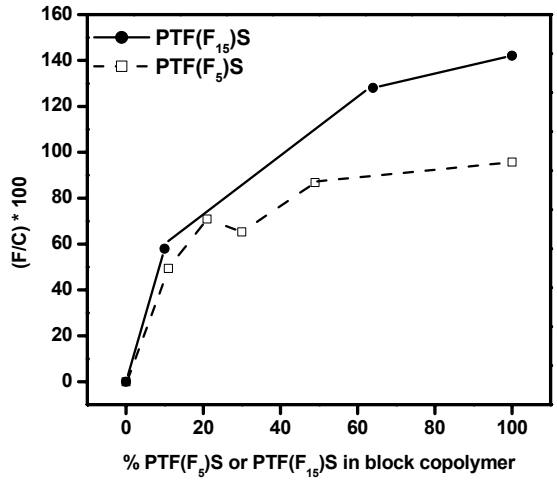

Figure 6.5.1 Plot of % PTF(F_5)S or PTF(F_{15})S in block copolymers against F/C-ratio at the surface by XPS

The water contact angle for PTF(F_5)S-*b*-PS and PS-*b*-PTF(F_{15})S copolymers having 89 and 90% PS was 105° and 111°, respectively. Figure 6.5.2 shows the plot of contact angle as a function of PS content in the block copolymers. However, the XPS measurement of 2,3,5,6-tetrafluoro-4-methoxystyrene polymers showed only 28% F at the surface.

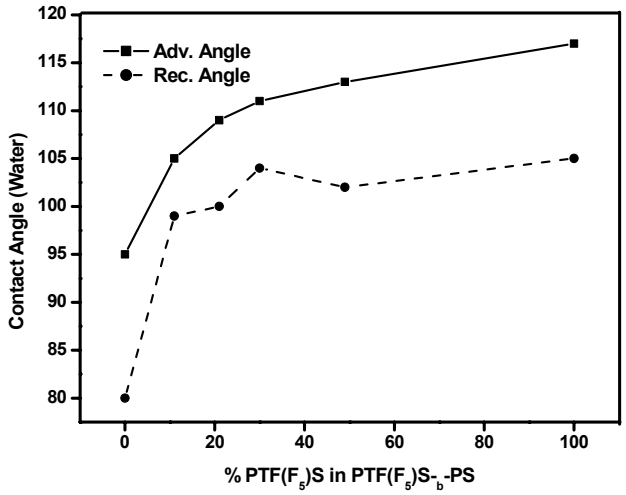

Figure 6.5.2 Plot of % PTF(F_5)S in block copolymers against contact angle (H_2O)

These results suggest that the hydrophobicity of the homopolymers and block copolymers is dependent on the length of the fluorinated side chain and the amount of fluorinated blocks. Introduction of the longer fluorinated side chains resulted in highly hydrophobic fluorine enriched surfaces predicted by higher contact angles and XPS measurements.

6.4 Conclusions

Highly fluorinated styrenic monomers TF(F_5)S and TF(F_{15})S were synthesized in high yields and polymerized by controlled ATRP. The resulting polymers are suitable for hydrophobic non-stick coatings. The polymerization of TF(F_5)S can be carried out at lower temperatures down to 70°C. The homopolymer of TF(F_5)S was used as a macroinitiator for block copolymerization with St and FS. The block copolymers have a two-phase morphology as shown by DSC. The TGA analysis of the homopolymers showed the labile nature of the fluorinated alkyl side chain. The homopolymers as well as the block copolymers containing F_5 and F_{15} side chains showed fluorine enriched surfaces. The XPS and contact-angle measurements on the block copolymer films as a function of PS content show that the polymers bearing a F_{15} side chain have more fluorine enriched at the surface than the F_5 side chain analogue and possess higher water contact angles. These results suggest that in the copolymers the fluorinated blocks segregate and enriched at the surface thereby creating a highly hydrophobic surface.

Chapter VII

Engineering End-functional Low Energy Surface PS Through Molecular Design: - Synthesis of Fluorinated and non-Fluorinated Initiators for ATRP

Abstract

This chapter deals with the synthesis of fluorinated and non-fluorinated initiators for the copper mediated ATRP of St and FS. The aliphatic fluorine containing (F-15) and non-fluorine containing (H-17) 1-octanol are transformed into the brominated initiators by esterification reaction and employed for the polymerization of St and FS. Other initiators like pentafluorobenzylbromide [F-5Br], benzyl bromide [BzBr], 1-phenylethylbromide [PhEBr] and phenyl(4-carboxy)ethyl bromide [Ph(COOH)E-Br] were also used for ATRP of the St. PS with six different end groups and with different molecular weights in the range of 1500 – 19000 with relatively narrow PDI were prepared. The molecular weights (M_n) of the fluorinated and non-fluorinated chain end polymers were determined by SEC as well as by ^1H NMR spectroscopy. The glass transition (T_g) temperatures were also analyzed using DSC. The contact-angle measurements on thin films of the polymer with a water droplet showed that the PSs having a perfluorooctyl end group possess higher advancing (108°) and receding angles (97°) for water than the other end functional PSs. This is also evidenced by XPS analysis indicating surface enrichment in the aliphatic fluorinated chain end polymer compared to the aromatic chain ends.

7.1 Introduction

Many physical as well as chemical properties of polymers are dependent on their surface structure and on the chemical composition. In this respect fluorinated polymers are well studied due to their great chemical resistance and their high thermal stability. These interesting properties made them applicable in electronics and coatings of substrates such as textiles, papers, leather, wood etc. Furthermore, the use of these polymers provides low-energy oil or chemical repellant surfaces.[1-5]

The grafting reaction and living polymerization are well known methods for fluorine incorporation in a polymer. The microstructure of the fluorine containing groups determines the surface properties of the polymers. Thus, controlling the distribution of fluorine atoms within the polymer the properties of the material can be altered. Living anionic,[6] living cationic,[7] group transfer polymerization,[8] condensation polymerization[9] are the common methods to prepare well defined fluorinated polymers. But all these techniques have their disadvantages such as precise reaction conditions or polar monomers and so on.

Fluorine containing monomers are relatively expensive, which limits their commercial use. In order to achieve the desirable properties, the fluorine content in the polymers and placement of the fluorine containing segments within the polymer are very important. Polymers having terminal fluorine segments are more efficient than with middle fluorine segments to alter the properties of the polymers.[6]

The end groups of the polymer also have great influence on the behavior of the material. In order to study the effect of chain end group on the thermal as well as surface properties of polymers different functional initiators were employed for designing St polymers by ATRP technique. The ATRP is a recent and most versatile technique[10,11] for the synthesis of well-defined polymers. This technique combines the control available from living polymerization and the versatility and robust character of the free radical process. The ATRP also gives a good control over the compositions, the functionalities and permits the use of different functional initiators and macroinitiators. The macroinitiator strategy is a convenient tool to prepare block copolymers with well controlled block lengths. This method involves the isolation and the purification of the first block polymer and its subsequent use as a macroinitiator.

7.2 Experimental

7.2.1 Materials

Pentadecafluorooctane-1-ol (ABCR Chemicals, Germany), 1-phenylethylbromide, benzyl bromide, 1-octanol, dimethylamino pyridine (DMAP), bromoisopropylbromide (all from Aldrich) were used as received without further purification. The St and FS (Aldrich) were passed through a ready to use, disposable pre-packed inhibitor remover column and distilled over calcium hydride prior to use. All other solvents or chemicals were used as received if not otherwise stated separately.

7.2.2 Synthesis of 2-bromo-2-methyl-propionic acid-(2,2,3,3,4,4,5,5,6,6,7,7,8,8,8 – pentadecafluorooctyl) ester (F-15Br initiator)

The synthetic pathway used for preparation of brominated initiators is shown in scheme 7.1.

2 g (7.49 mmol) of pentadecafluorooctane-1-ol and 60 ml of dry THF were suspended in a three-neck round bottom flask equipped with a magnetic needle and an addition funnel. To this mixture 1.6 ml (11.24 mmol) triethyl amine, 100 mg DMAP and 1.4 ml (11.27 mmol) bromoisopropylbromide were added slowly with continuous stirring. The reaction was performed at room temperature for 20h. The suspension was filtered and THF was removed by a rotary evaporator. The colored liquid formed is diluted with diethyl ether and the ether layer was washed extensively with saturated $NaHCO_3$ solution, 1M HCl and finally with distilled water. The ether layer was dried over Na_2SO_4 and the solvent was removed on a rotary evaporator to leave a yellowish liquid. The observed yield was 97%.

FT-IR: ν(C=O) absorption at 1753 cm^{-1}

^{1}H NMR ($CDCl_3$) δ (ppm from TMS): 2 (s, 6H, 2 $^{a,b}C\underline{H_3}$), 4.6 (t, 2H, -O-$^{1}C\underline{H_2}$)

^{19}F NMR ($CDCl_3$) δ (ppm from C_6F_6): -77.5 (-$^{8}CF_3$), -116.1 (-$^{2}CF_2$), -118.6 (-$^{3}CF_2$-$^{4}CF_2$-), -119.4 (-$^{5}CF_2$), -119.9 (-$^{6}CF_2$), -122.8 (-$^{7}CF_2$).

The preparation of the other initiator H-17Br was performed using the corresponding 1-octanol following the similar procedure as above to give the corresponding bromoester.

H-17Br

FT-IR: ν(C=O) absorption 1734 cm^{-1}

^{1}H NMR ($CDCl_3$) δ (ppm from TMS): 4.2 (t, 2H, -O-C$\underline{H_2}$), 1.95 (S, 6H, -C(C$\underline{H_3}$)$_2$), 1.7 (m, 2H, OCH_2-C$\underline{H_2}$), 1.3 (m, 10H, 5C$\underline{H_2}$), 0.98(t, 3H, -C$\underline{H_3}$)

The phenyl(4-carboxy)ethyl bromide [Ph(COOH)E-Br] was synthesized by Katrine Wienberg (DTU, Denmark) using 4-ethylbenzoic acid and was used as such for polymerizations.

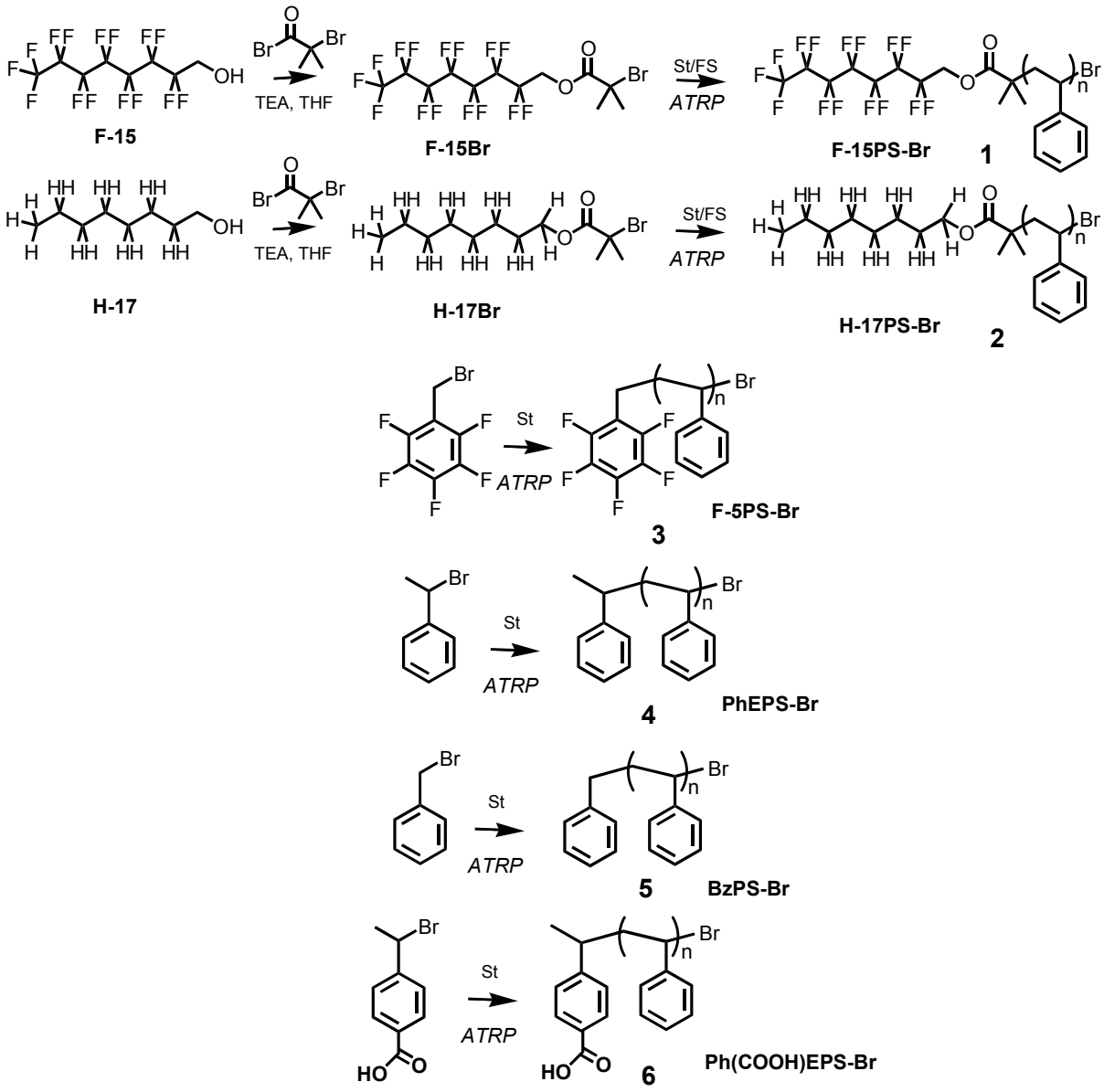

Scheme 7.1 General scheme employed for the synthesis of initiators and the polymerization reactions.

7.2.3 ATRP of St and FS

In a typical experiment 3 g (28.8 mol) of St, 0.1647 g (0.3 mmol) of F-15Br initiator, 0.0473 g (0.33 mmol) of CuBr, 0.140 g (0.9 mmol) of bipyridine and a magnetic needle were placed in a Schlenk tube. The system was deoxygenated by three freeze-pump-thaw cycles using dry nitrogen and the polymerization was initiated by immersing the tube in a preheated oil bath at 110 °C. The polymer was precipitated in methanol and the yield was determined gravimetrically. The polymerizations of St or FS using other initiators were also performed by the similar procedure.

7.3 Results and Discussion

7.3.1 Synthesis of Fluorinated and non-Fluorinated Initiators

The fluorinated (F-15Br) and non-fluorinated (H-17Br) initiators were synthesized by an esterification reaction. The perfluoroalkyl octanol was used to synthesize a fluorinated initiator (F-15Br) by reacting with the α-bromoisobutyryl bromide.[12,13] The general route followed for the synthesis is mentioned in scheme 7.1. The corresponding fluorinated ester was recovered by extracting the reaction mixture with diethyl ether. The ether layer was dried over sodium sulphate and evaporated on the rotary evaporator to give a yellowish liquid. The initiator was well characterized before employing for the polymerization reactions. The FT-IR spectrum of the ester shown in figure 7.3.1 indicates the new absorption at 1753 cm^{-1} due to the ester carbonyl vibration. The absorption at 3343 cm^{-1} corresponding to the vibration of the hydroxyl group of the respective alcohol precursor has completely disappeared indicating that the alcohol has been converted quantitatively to the bromo ester.

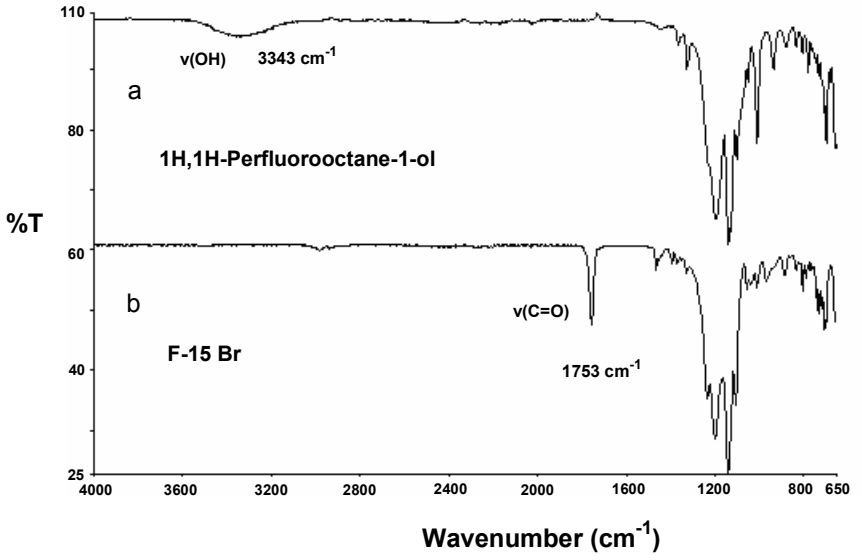

Figure 7.3.1 FT-IR spectrum of 1H,1H-perfluorooctane-1-ol a) before esterification and b) after esterification.

The ^{1}H and ^{19}F NMR spectra of F-15Br were performed using $CDCl_3$ as a solvent. The ^{1}H NMR spectrum shows two resonances, a sharp singlet at 2 ppm corresponding to two methyl groups and a triplet at 4.6 ppm due to the methylene group. The methylene proton couples with the adjacent fluorine and appears as a triplet. Furthermore, the comparison of the integral area confirms the presence of only F-15Br.

The ^{19}F NMR spectrum has well separated resonances as assigned in figure 7.3.2 and supports the claim that all alcohol is converted to the corresponding bromo ester. The assignments are based using hexafluorobenzene as an internal standard.[14] The ^{19}F NMR spectrum also indicated that the average number of CF_2 units is 6 and it strongly supports the structure of F-15Br shown in scheme 7.1.

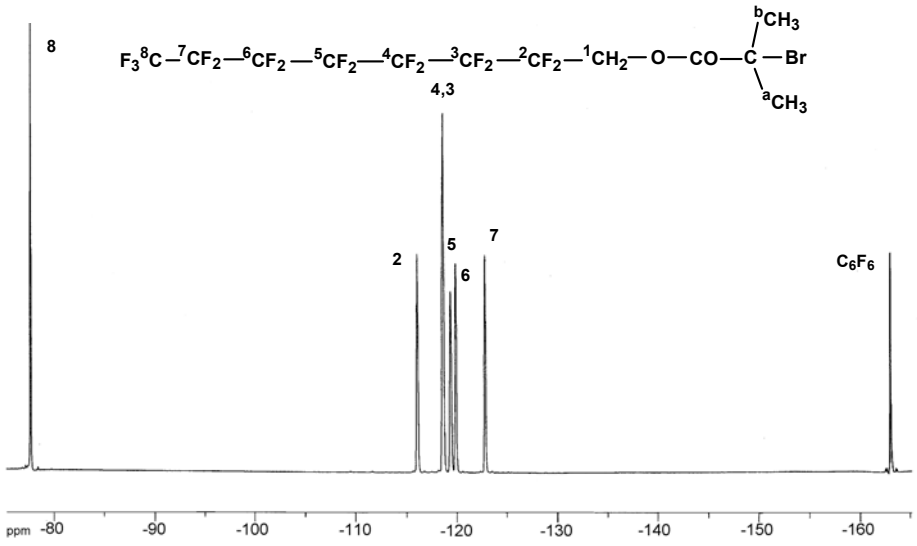

Figure 7.3.2 ^{19}F NMR spectrum of F-15Br

The synthesis of the H-17Br was performed by the same analogy using 1-octanol as starting compound. The ^{1}H NMR and FT-IR analysis of H-17Br were used to confirm that no traces of the corresponding alcohol precursor or bromo acid were left. Figure 7.3.3 shows the FT-IR spectrum of the bromo ester of 1-octanol. The other initiators F5-Br, Bz-Br, PhE-Br were used as received. The Ph(COOH)E-Br was synthesized* by bromination of 4-ethylbenzoic acid using bromine solution in the presence of AIBN at 130 °C in chlorobenzene.

** Ph(COOH)E-Br was synthesized by Katrine Wienberg, DTU, Denmark.*

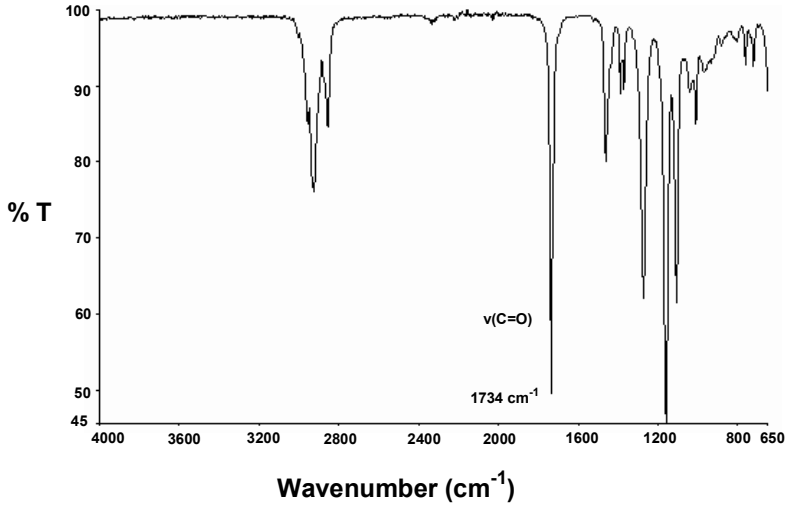

Figure 7.3.3 FT-IR spectrum of bromoester of 1-octanol (H-17Br)

7.3.2 Polymerization of St and FS

The polymerization reactions were performed at 110°C using the above mentioned initiators and Cu(I)Br/bipy as a catalyst system in bulk as well as in solution. The polymerizations were continued until the stirrer stopped due to the high viscosity of the reaction mixture. When the target molecular weight was 5000, the F-15Br initiator needed 2 h to lead to 81% conversion of St whereas the H-17Br initiator took 3 h to reach up to 80 % conversion. These observations indicate that the presence of fluorine in the initiator moiety also has some influence on the rate of polymerization. The same trend has been observed when F-5Br and BzBr were used as initiators for styrene polymerization. By this method the polymers with low fluorine content have been synthesized. In these compounds the fluorine containing aliphatic or aromatic moiety is left as a terminal segment. Furthermore, by using these initiators and the ATRP protocol the amount of fluorine in the polymer was controlled by maintaining the ratio between the fluorine containing initiators and the St.

The polymerizations using Ph(COOH)E-Br were performed in xylene solution as well as in bulk. This initiator was synthesized by α-bromination of 4-ethylbenzoic acid. The presence of a carboxylic acid end group at the chain end allows the functionalization of these polymers even in the post-polymerization reaction. When the styrene polymerizations were performed with Ph(COOH)E-Br as initiator in xylene solution using CuBr/bipy as a catalyst system targeting M_n = 5000 it took 20h to reach 48% conversion. Polymers with a molecular weight range between 1500 and 10000 with PDIs $\leq$1.2 have been synthesized.

Although in all the cases the M_n increased linearly with time, the observed molecular weights were slightly lower than the theoretical values for few cases of polymerization. This observation suggests the good control over the molecular weight. By using other initiators (e.g

F-5Br, BzBr and PhEBr) polymers with different molecular weights of 2000 to 17000 and PDIs <1.4 have been synthesized.

The presence of the signals from the initiator fragment in the ^{1}H NMR spectrum of F-15Br and H-17Br initiated polymers permitted the calculation of the degree of polymerization and thus the molecular weight of the PS. The M_ns observed by SEC were in good agreement with the M_ns observed by ^{1}H NMR as shown in figure 7.3.4 (a) and (b).

When the M_ns were relatively higher, it was difficult to exploit the area of the -O-CH_2- in F-15PS. These F-15Br and H-17Br initiators were also employed for the polymerization of FS. Hvilsted[15] et. al recently have shown that FS polymerizes relatively faster than St under ATRP conditions. The polymers of FS with relatively low PDI and the molecular weights ranging from 3000 to 8000 were synthesized under the same conditions as employed for PS. The table 7.3.1 and 7.3.2 depict the M_n and PDI observed for PFS. In these cases the M_ns determined by NMR were also in close agreement with the values obtained by SEC analysis.

Table 7.3.1 Polymerization data and glass transition temperatures of F-15 PFS

No.	M_n (Target)	M_n (SEC)	PD	Time min	Yield (%)	T_g (°C)	M_n (NMR)
1	2550	3000	1.17	25	91	63	2750
2	5550	4000	1.18	30	95	76	4150
3	10550	6700	1.17	30	90	85	7500

$[M]_o$ = 1 g; [I] : [CuBr] : [bipy] = 1 : 1.1 : 3

Table 7.3.2 Polymerization data and glass transition temperature of H-17 PFS

No.	M_n (Target)	M_n (SEC)	PD	Time min	Yield (%)	T_g (°C)	M_n (NMR)
1	2280	3900	1.30	10	76	75	3850
2	5280	6200	1.34	18	91	88	-
3	10280	7700	1.22	30	87	94	-

$[M]_o$ = 1 g; [I] : [CuBr] : [bipy] = 1 : 1.1 : 3

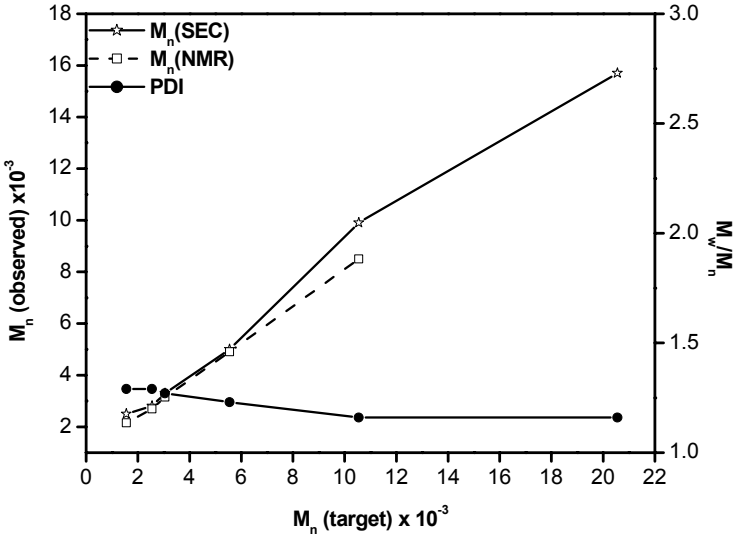

a

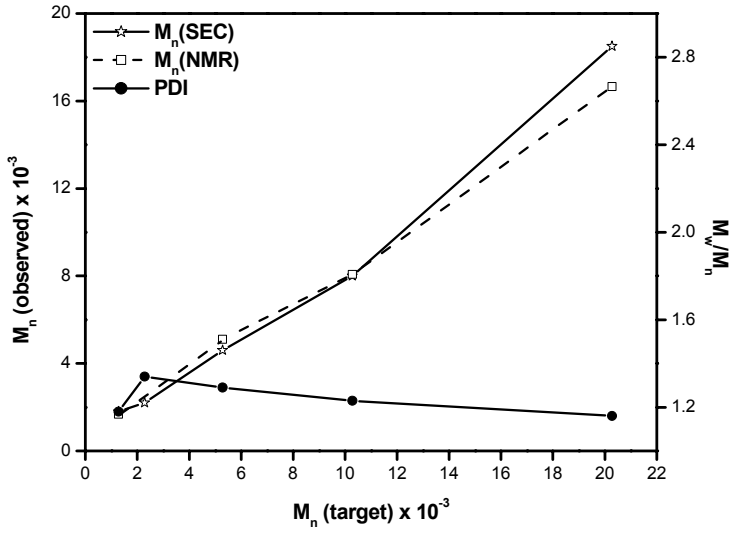

b

Fig 7.3.4 Plots of M_n (target) vs M_n observed by SEC and NMR and PDI of PS a) F-15 PS b) H-17 PS

7.3.3 Thermal Properties

The glass transition temperature (T_g) of a polymer is an important property, which has great influence on the molecular mobility. Various factors directly or indirectly affect the T_g of a polymer. The molecular weight of polymers is one of the important criteria, which has a proportional relation with T_g up to a certain molecular weight. The bulk and the type of the side group are also another factors which influence the T_gs of the polymer. As an example it can be appreciated by comparing the T_g of PS with that of poly(α-methylstyrene). Here the presence of the methyl group of α-methylstyrene hinders the free rotation of the C-C bond of the chain backbone resulting in an increase of T_g.

Five different types of initiators were employed for the polymerization of St, which provides different end groups to the polymer chain. The polymers with low M_n are synthesized to study the effect of end group, because in the high molecular weight polymers the end group has minor influence on the T_g. Figure 7.3.5 shows the plots of M_n against the T_g of the PS synthesized by using F-15Br and H-17Br initiators. The fluorine containing materials are well known for their high thermal stability. The presence of F-15 side chain has a great influence on the T_g of PS as it is observed by comparing with its non-fluorinated PS analogue. Table 7.3.3 lists the T_gs of F-15 PS and H-17 PS with increasing M_n.

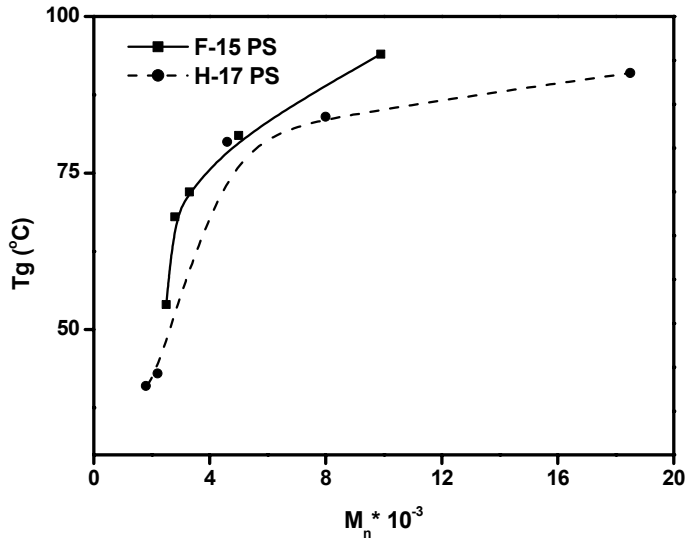

Figure 7.3.5 Plot of T_g against the M_n (SEC) for F-15 PS and H-17 PS

The T_g of F-15 PS increases from 42°C for a PS with M_n of 2200 to 91°C for M_n 9900, whereas in case of H-17 PS the increase is from 41°C with M_n 1800 to 91°C for M_n 18500.

Table 7.3.3 The M_n, PDI and T_g observed for F-15 PS and H-17 PS.

No.	F-15 PS			H-17 PS		
	M_n	PDI	T_g(°C)[a]	M_n	PDI	T_g(°C)[a]
1	2200	1.19	42	1800	1.28	41
2	2500	1.29	54	2100	1.45	43
3	2800	1.29	68	4600	1.29	77
4	3300	1.27	72	8000	1.23	84
5	5000	1.23	81	18500	1.16	91
6	9900	1.16	91			

[a] Heating/cooling rate of 3°C/min

Kajiyama et al[16] have studied the effect of four different end groups on the surface molecular motion of PS films. They have shown that the end group has a great influence on the T_g at the surface of the polymer film rather than in the bulk.

The T_gs were more apparently shifted to a higher temperature with an increase of M_n in all the cases. In case of the F-5Br and Bz-Br initiated PS it has been observed that the effect on T_g was not so prominent.

The PhEBr initiated PS have slightly higher T_g than the Bz-Br initiated PS. This observation suggests that the presence of the methyl group at the α-position of the chain end phenyl may hinder the free rotation and results in an increase in the T_g of PhE-PS.[17]

The Ph(COOH)E-Br initiated polymers have the highest T_gs compared to the other end group PS. Figure 7.3.6 shows the comparative plot of T_g against the M_n of the PS having different end groups. This high T_g is may be due to the intermolecular hydrogen bonding of carboxylic acid groups which ultimately results in increase of the apparent molecular weight of Ph(COOH)E-PS. Alternatively, it can also be due to the network formation of PS chains which results in the decrease of surface molecular motion. Thus, it seems reasonable to conclude that the T_gs of the Ph(COOH)E-PSs were higher than those of the other end group PSs.

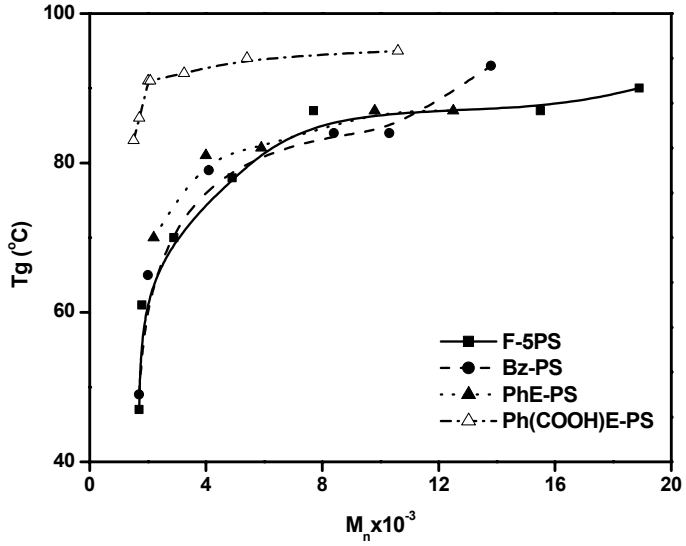

Figure 7.3.6 Comparative plot of T_g against M_n of the F-5PS, Bz-PS, PhE-PS and Ph(COOH)E-PS

7.3.4 Contact Angle Measurements

In order to study the surface behavior of the PSs synthesized by fluorine containing initiators, the thin films of these fluorine end functional PSs were studied by contact angle measurements with a water droplet. The polymers were dissolved in THF and the solution was passed through an alumina column to remove the residual Cu catalyst used during polymerization. The thin films of these purified polymers are then spin coated on a glass surface (3-5 %) and dried overnight at 30 °C under vacuum before they were used for the measurements. The results obtained are summarized in table 7.3.4 and 7.3.5.

Table 7.3.4 Contact angle (water) measured for the F-5 PS

No	M_n (SEC)	PDI	Contact angle (deg)	
			Adv	Rec
1	1700	1.19	99	87
2	1800	1.28	98	87
3	2900	1.28	98	85
4	4900	1.24	97	84
5	15500	1.16	96	84
6	18900	1.15	96	83

Table 7.3.5 Contact angle (water) measured for the F-15 PS

No	M_n (SEC)	PDI	Contact angle (deg)	
			Adv	Rec
1	2240	1.19	108	97
2	2500	1.29	107	95
3	2800	1.29	108	96
4	3300	1.27	106	93
5	5000	1.23	104	93
6	9900	1.16	100	88
7	15700	1.16	98	87

The contact angle measurements showed advancing angle values in the range of 98°-108° for F-15 PS and 96° - 99° for F-5 PS under the same conditions. The receding values were in the range of 87°-97 ° and 83°-87° for F-15 PS and F-5 PS, respectively.

The degree of contact angles decreases with increasing molecular weight in both the cases as illustrated from figure 7.3.7 (a) and (b). Moreover, the F-15PS always showed higher contact angles than the F-5 PS. However, F-15 PS (entry 2 from table 7.3.5) with M_n 2500 showed a higher contact angle than F-5 PS (entry 3 from table 7.3.4) having M_n 2900. This observation suggests that the fluorinated alkyl chains are more susceptible to enrich the surface and result in formation of hydrophobic surfaces. In case of F-5 PS the effect was only in the low molecular weight polymers ($M_n < 2000$). Beyond that, the contact angles observed were similar to those of the normal PS. A similar trend has been observed for the receding angles. The receding angles were in the range of 97° - 87° for F-15 PS and 87° - 83° for F-5 PS. Thus, the alkyl fluorinated chain ends appear more effective than the aromatic fluorinated chain ends.

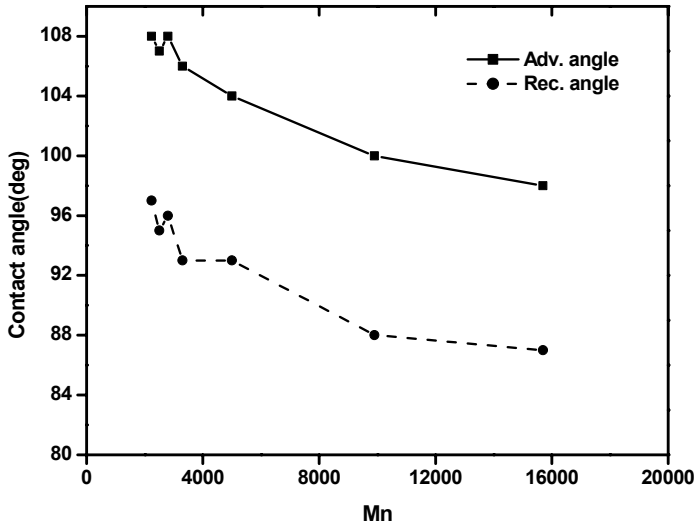

a

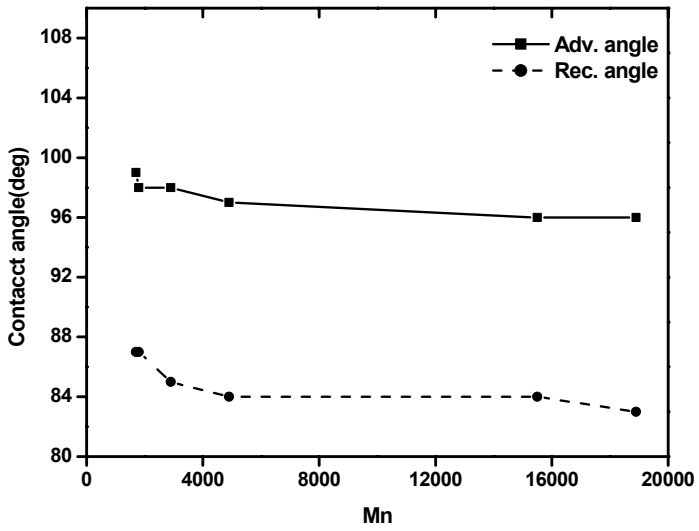

b

Figure 7.3.7 Plot of M_n against contact angle of water droplet a) F-15 PS b) F-5 PS

7.3.5 XPS Analysis

The surface composition as a function of the molecular weight of F-5 PS and F-15 PS was measured by XPS. It has been observed that the atomic percentage ratios of F/C at the surface of F-15 PS are higher than those of F-5 PS. The F/C ratio in both the series decreases with an increase in M_n of the PS as depicted in figure 7.3.8. In the polymers F-5 PS (entry 3 from table 7.3.4) with M_n of 2900 and F-15 PS (entry 3 from table 7.3.5) with M_n of 2800 have 3.3% and 15.1% fluorine, respectively, towards the surface.

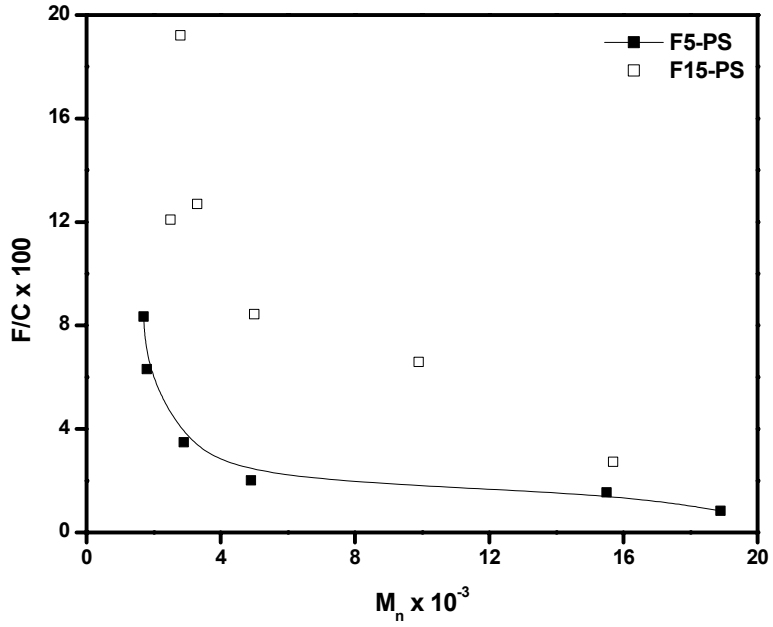

Figure 7.3.8 Plot of M_n against the F/C ratio observed by XPS towards the surfaces of F-5 PS and F-15 PS.

Surprisingly, a low F/C ratio was attained in F-15 PS (entry 1 table 7.3.7) having an M_n of 2500. This was definitely higher than that of F-5 PS but comparatively lower than that of the polymer (entry 2 from table 7.3.7) having M_n of 2800. Furthermore, a descending trend in F/C ratio was observed with the increase in M_n of the PS. These observations support the previous claim of the surface enrichment that the fluorine substituted aromatic end group is usually less effective than that of the aliphatic fluorine containing terminal group.

The molecular size of the F-5Br and F-15Br initiator moiety in high molecular weight PS is may be too small to cover the surface area and thereby the fluorine enrichment decreases towards the surface. On the other hand, in low molecular weight F-15 PS (M_n <

5000) the C_8F_{15} group is sufficient to cover the surface area estimating from the observed F-C ratio in XPS.

Table 7.3.6 weight percentage of F, O and C observed at the surface of F-5 PS by XPS

No.	M_n (SEC)	PDI	XPS		
			F(%)	O(%)	C(%)
1	1700	1.19	7.3	3	87.5
2	1800	1.28	5.7	2.5	90.3
3	2900	1.28	3.3	1.2	94.8
4	4900	1.24	1.9	2.3	94.4
5	15500	1.16	1.5	1.0	97.1
6	18900	1.15	0.8	1.5	96.3

Table 7.3.7 weight percentage of F, O and C observed towards the surface of F-15 PS by XPS

No.	M_n (SEC)	PDI	XPS		
			F(%)	O(%)	C(%)
1	2500	1.29	10.4	2.8	86.0
2	2800	1.29	15.1	4.3	78.6
3	3300	1.27	10.4	4.0	81.9
4	5000	1.23	7.3	4.2	86.5
5	9900	1.16	6.0	2.1	91.0
6	15700	1.16	2.4	5.9	87.6

7.4 Conclusions

The chain end functionalized polystyrenes with F-5Br, F-15Br, H-17Br, PhEBr, BzBr and Ph(COOH)E-Br initiators were successfully synthesized by the ATRP technique. The polymers obtained were in the range of M_n from 1500-19000 and with PDI $\leq$ 1.3. In case of F-15 PS, H-17 PS and PhE-PS the end groups of the polymer were employed to calculate the molecular weight of the polymers. In general the M_n (NMR) and M_n (SEC) observed were in good agreement. The DSC analysis of these end functional polymers showed the highest T_gs for PS having a benzoic acid end group. The fluorine end groups also had a slight effect on the T_gs as observed by a comparative study of the F-15Br and H-17Br initiated polystyrenes. Furthermore, the comparison of F-5 PS and F-15 PS showed that the aliphatic chain end polymers possess slightly higher T_g than the aromatic chain ends. The PSs synthesized by using aliphatic and aromatic fluorinated initiators showed fluorine enrichment at the surface of the polymer film depending on the number and type of fluorinated groups and on the molecular weight of the functional polymer. In general the degree of surface enrichment is found to decrease with an increase in molecular weight and also the aliphatic fluorinated chain ends were more susceptible to enrich in the surface than the aromatic fluorinated chain ends.

References

Chapter I

1. Reinitzer, F. *Monatsh*, **1888**, *9*, 421.
2. Lehmann, O. *Z. Phys. Chem*., **1889**, *4*, 462.
3. a) Lehmann, O. *Ann. Physik*., **1908**, *25*, 852 b) Lehmann, O. *Ann. Physik*, **1908**, *27*, 1099.
4. Liquid crystalline polymers, *Cambridge solid state science series*, by Donald, AM and Windle, AH. **1992** p 108.
5. Gray, GW. *Molecular Crystals*, **1966**, *1*, 333.
6. Dave, JS; Dewar, MJS. *J. Chem. Soc*., **1954**, 4616.
7. Dave, JS; Dewar, MJS. *J. Chem. Soc*., **1955**, 4305.
8. Kuhfuss, HF; Jackson, WJ. *US pats*., 3,778,410 [**1973**] and 3,804,805 [**1974**].
9. Roviello, A; Sirigu, A. *Macromol. Chem*., **1979**, *180*, 2543.
10. Eich, M; Wendorff, JH; Reck, B; Ringsdorf, H. *Makromol. Chem., Rapid Commun*., **1987**, *8*, 59.
11. Delaire, JA; Nakatani, K. *Chem. Rev*., **2000**, *100*, 1817.
12. Ichimura, K. *Chem. Rev*., **2000**, *100*, 1847.
13. Kryder, MH. *Annu. Rev. Mater. Sci*., **1993**, *23*, 411.
14. Finkelmann, H; Ringsdorf, H; Wendorff, HJ. *Makromol. Chem*., **1978**, *179*, 273.
15. Ichimura, K. *Appl. Phys. Lett*., **1993**, *63*, 449.
16. Todorov, T; Nikolova, L; Tomova, N. *Appl. Opt.,* **1984**, *23*, 4309.
17. Eich, M; Wendorff, JH. *Makromol. Chem., Rapid Commun.,***1987**, *8*, 467.
18. Eich, M; Wendorff, JH. *J. Opt. Soc. Am. B,* **1990**, *7*, 1428.
19. Stumpe, J; Muller, L; Kreysig, D; Hauck, G; Koswig, HD; Ruhmann, RD; Rubner, J. *Makromol. Chem., Rapid Commun.,* **1991**, *12*, 81.
20. Wiesner, U; Reynolds, N; Boeffel, C; Spiess, HW. *Makromol.Chem., Rapid Commun.,* **1992**, *92*, 403.
21. Ivanov, S; Yakovlev, I; Kostromin, S; Shibaev, V; Lasker, L; Stumpe, J; Kreysig, D. *Makromol. Chem., Rapid Commun.,* **1991**, *12*, 709.
22. Nikolova, L; Todorov, T; Ivanov, M; Andruzzi, F; Hvilsted, S; Ramanujam, PS. *Appl. Opt.,* **1996**, *35*, 3835.
23. Holme, NCR; Ramanujam, PS; Hvilsted, S. *Appl. Opt.,* **1996**, *35*, 4622.
24. Holme, NCR; Ramanujam, PS; Hvilsted, S. *Opt. Lett.,* **1996,** *21,* 902.

25. Holme, NCR; Nikolova, L; Ramanujam, PS; Hvilsted, S. *Appl. Phys. Lett.,* **1997**, *70*, 1518.
26. Ringsdorf, H; Schmidt, HW. *Makromol. Chem*., **1984**, *185*, 1327,
27. Talroze, RV; Kostromin, SG; Shibaev, VP; Plate, NA. *Makromol. Chem. Rapid Commun*., **1981**, *2*, 305.
28. Ringsdorf, H; Zentel, R. *Makrolmol. Chem*., **1982**, *183*, 1245.
29. Finkelmann, H. *Mol. Cryst. Liq. Cryst*., **1982**, *89*, 23.
30. Ringsdorf, H *Makromol.Chem. Rapid Commun*., **1982**, *3*, 745.
31. Hirao, A; Koide, G; Sugiyama, K. *Macromolecules,* **2002**, *35*, 7642.
32. Percec, V; Lee, M. *Journal of Material Science- Pure appl chem*., **1992**, *29*, 723.
33. Matyjaszewski, K; Xia, J. *Chem. Rev*., **2001**, *101*, 2921.
34. Maarten, K; Martin, M. *Macromol. Chem. Phys.,* **1997**, *198*, 2163.
35. Szwarc, M; Levy, M; Milkovich, R. *J. Am. Chem. Soc.,* **1956**, *78*, 2657.
36. "Controlled / living radical polymerization" Progress in ATRP, NMP and RAFT. *Matyjaszewski K Ed.; ACS symposium series*, **2000**, 768.
37. Hawker, CJ. *J. Am. Chem. Soc*., **1994**, *116*, 11185.
38. Georges, MK; Veregin, RPN; Kazmaier, PM; Hamer, GK. *Macromolecules*, **1993**, *26*, 5316.
39. Braun, D. *Macromol. Symp*., **1996**, *111*, 63.
40. Curran, DP. *Synthesis* **1988**, 489.
41. Kharasch, MS; Jensen, EV. *Science,* **1945**, *102*, 128.
42. Ando, T; Kato, M; Kamigaito, M; Sawamoto, M. *Macromolecules*, **1996**, *29*, 1070.
43. Wang, JS; Matyjaszewski, K. *Macromolecules*, **1995**, *28*, 7901.
44. Patten, TE; Xia, J; Abernathy, T; Matyjaszewki, K. *Science,* **1996***, 272*, 866.
45. Kato, M; Kamigaito, M; Sawamoto, M; Higashimura, T. *Macromolecules,* **1995**, *28*, 1721.
46. Xue, L; Agarwal, US; Lemstra, PJ. *Macromolecules,* **2002**, *35*, 8650.
47. a) Xia, J; Matyjaszewski, K. *Macromolecules*, **1997**, *30*, 7697. b) Xia, J; Scott, GG; Matyjaszewski, K. *Macromolecules*, **1998**, *31*, 5958.
48. Haddleton, M; Jasieczek, CB; Hannon, MJ; Shooter, AJ. *Macromolecules*, **1997**, *30*, 2190.
49. Jian, Q; Matyjaszewski, K. *Macromolecules*, **1997**, *30*, 5643.
50. Wang, XS; Jackson, RA; Armes, SP. *Macromolecules*, **2000,** *33,* 255.
51. Jankova, K; Hvilsted, S. *Macromolecules*, **2003**, *36*, 1753.

52. Gao, B; Chen, X; Ivan, B; Kops, J; Batsberg, W. *Macromol. Rapid Commun*., **1997**, *18*, 1095.
53. Xia, J; Johnson, T; Gaynor, S; Matyjaszewski, K; Desimone, J. *Macromolecules*, **1999**, *32*, 4802.
54. Binancas, S; Acar, AE; Mathias, LJ. *Journal of Polymer Science: Part A: Polymer Chemistry*, **2002**, *40*, 334.
55. Jung, D; Park, IJ; Choi, YK; Lee, S; Park, HS; Ruhe, J. *Langmuir*, **2002**, *18*, 6133.
56. Matyjaszewski, K; Wang, J; Grimaud, T; Shipp, DA. *Macromolecules*, **1998**, *31*, 1527.
57. Haddleton, DM; Heming, AM; Kukulj, D; Duncalf, DJ. *Macromolecules*, **1998**, *31*, 2016.
58. Feng, XS; Pan, CY. *Journal of Polymer Science: Part A Polymer Chemistry***, 2001,** *39*, 2233.
59. Matyjaszewski, K; Patten, TE; Xia, J. *J. Am. Chem. Soc*., **1997**, *119*, 674.
60. Matyjaszewski, K; Nakagawa, Y; Jasieczek, CB. *Macromolecules*, **1998**, *31*, 1535.
61. Plunkett, RJ. *U. S. Pat.,* US 2230654.
62. Kung, E; Lesser, AJ; McCarthy, TJ. *Macromolecules*, **2000**, *33*, 8192.
63. Bunyard, WC; Romack, TJ; DeSimmone, JM. *Macromolecules*, **1999**, *32*, 8224.
64. Miyata, T; Yamada, H; Uragami, T. *Macromolecules*, **2001**, *34*, 8026.
65. Zisman, WA. *Contact Angle, Wettability, and Adhesion,* Advances in Chemistry Series *43*, Am. Chem. Soc.: Washington DC, **1964**.
66. Sugiyama, K; Nemoto, T; Koide, G; Hirao, A. *Macromol. Symp*., **2002**, *181*, 135.
67. Arnold, ME; Nagai, K; Freeman, BD; Spontak, RJ; Betts, DE; DeSimone, JM; Pinnau, I; *Macromolecules*, **2001**, *34*, 5611.
68. Andruzzi, L; Chiellini, E; Galli, G; Li, X; Kang, SH; Ober CK. *J. Mater. Chem*., **2002**, *12*, 1684.
69. Park, IJ; Lee, SB; Choi, CK. *Macromolecules*, **1998**, *31*, 7555.
70. Park, IJ; Lee, SB, Choi, CK. *J. Appl. Polym. Sci*., **1994**, *54*, 1449.

Chapter III

1) Delaire, JA; Nakatani, KA. *Chem. Rev*., **2000,** *100*, 1817.
2) Simon, H. *Today's chemist,* **2001**, *10*, 15.
3) Ikeda, T; Shin, H; Durga, KB; Seiji, K; Shigeo, T. *Macromolecules*, **1990**, *23*, 36.
4) Ikeda, T; Tsutsumi, O. *Science,* **1995**, *208*, 1873.

5) Eich, M; Wendorff, JH. *J. Opt. Soc. Am. B*, **1990**, *7*, 1428.
6) Hvilsted, S; Ramanujam, PS. *Monatshefte für Chemie,* **2001,** *132*, 45.
7) Eich, M; Wendorff, JH; Ringsdorf, H; Schmidt, HW. *Makromol. Chem*., **1985**, *186*, 2639.
8) Eich, M; Wendorff, JH; Reck, B; Ringsdorf, H. *Makromol. Chem. Rapid Commun.,* **1987**, *8*, 59.
9) Tsutsumi, O; Tahkeshi, S; Ikeda, T; Giancarlo, G. *J. Phys, Chem., B,* **1997**, *101*, 1332.
10) Ikeda, T; Sasaki, T; Ichimura, K. *J. Am. Chem. Soc.,* **1994**, *116*, 625.
11) Walther, M; Finkelmann, H. *Prog. Polym. Sci*., **1996**, *21*, 951.
12) Pugh, C; Kiste, AL. *Prog. Polym. Sci*., **1997**, *22*, 601.
13) Fischer, H; Poser, S. *Acta Polym*., **1996**, *47*, 413.
14) Pragliola, S; Ober, CK; Mather, PT; Joen HG. *Macromol. Chem. Phys*., **1999**, *200*, 2338.
15) Kasko, AM; Heintz, AM, Pugh, C. *Macromolecules,* **1998**, *31*, 256.
16) Matyjaszewski, K; Xia, J. *Chem. Rev*., **2001**, *101*, 2921.
17) Ringsdorf, H. *Makromol.Chem*., **1984**, *185*, 1327.
18) Wangs, JS; Matyjaszewski, K. *Macromolecules,* **1995**, *28*, 7901.
19) Kato, M; Kamigaito, M; Sawamoto, M; Higashimura, T. *Macromolecules,* **1995***, 28*, 1721.
20) Sykes P. *Mechanisms in Organic Chemistry 6th edition pp 146.*
21) Rau, H. *In Photochemistry and Photo Physics*, *Rabek, JF. Ed.; CRC Press: Boca Raton*, **1990**; Vol. II, Chapter 4, 119.
22) Rau, H; Luddecke, E. *J. Am. Chem. Soc.,* **1982**, *104*, 1616.
23) a) Marianne Pedersen, *PhD thesis*, **1997**. b) Lycka, A; Snobl, D; Machacek, V; Vecera, M. *Organic Magnetic Resonance*, **1981**, *15*, 390.
24) Harwood, LM; Moody, CJ. *Experimental organic chemistry: Principles and Practice, Blackwell scientific publications, Oxford*, **1989**.
25) Barrett, AGM; Hamprecht, D; James, RA; Ohkubo, M; Procopiou, PA; Toledo, MA; White, AJP; Williams, DJ. *J. Org. Chem*., **2001**, *66*, 2187.
26) Beers, KL, Matyjaszewski K. *J. of Macromol. Sci.- Pure Appl. Chem*., **2001**, *A38*, 731.
27) Jankova, K; Hvilsted, S. *Macromolecules*, **2003**, *5*, 1753.

Chapter IV

1. Mao, G; Wang, J; Clingman, SR; Ober, CK; Chen, JT; Thomas, EL. *Macromolecules*, **1997**, *30*, 2556.
2. Bignozzi, MC; Ober, CK; Laus, M. *Macromol. Rapid Commun*., **1999**, *20*, 622.
3. a) Delaire, JA; Nakatani, K. *Chem. Rev*., **2000,** *100*, 1817. b) Ichimura, K. *Chem. Rev*., **2000,** *100*, 1847.
4. Andruzzi, L; Altomare, A; Ciardelli, F; Solaro, R; Hvilsted, S; Ramanujam, PS. *Macromolecules*, **1999**, *32*, 448.
5. Natansohn, A; Xie, S; Rochon, P. *Macromolecules,* **1992**, *25*, 5531.
6. Ho, MS; Natansohn, A; Rochon, P. *Macromolecules*, **1996**, *29*, 44.
7. Ramanujam, PS; Hvilsted, S; Ujhelyi, F; Koppa, R; Lorincz, E; Erdei, G; Szarvas, G. *Synthetic Metals,* **2001**, *124*, 145.
8. Crivello, JV; Deptolla, M; Ringsdorf, H. *Liq. Cryst.,* **1988,** *3*, 235.
9. SE, K; Miyawaki, K; Hirahara, K; Takano, A; Fujimoto, T. *J. Polymer Sci. Part A: Poymer Chemistry*, **1998**, *36*, 3021.
10. Jannasch, P. *Macromolecules,* **2000**, *33*, 8604.
11. Mechanism in organic chemistry by Peter Sykes 6th edition pp 146.
12. Lycka, A; Snobl, D; Machacek, V; Vecera, M. *Organic Magnetic Resonance*, **1981**, *15*, 390.
13. Chen, XY; Jankova, K; Kops, J; Batsberg, W. *Journal of Polymer Science : Part A: Polymer chemistry*, **1999**, *37*, 627.
14. Qui, J; Matyjaszweski, K. *Macromolecules,* **1997**, *30*, 5643.
15. Higashimura, T; Kojima, K; Sawamoto, M. *Makromol. Chem., Suppl***., 1989,** *15*, 127.
16. Mateev, V; Markvosky, P; Nikolova, L; Todorov, T. *J. Phys.Chem.,* **1992**, *96*, 3055.
17. Bohm, N; Materny, A; Steins, H; Muller, MM; Schottner, G. *Macromolecules,* **1998**, *31*, 4265.
18. Song, OK; Wang, CH; Pauley, MA. *Macromolecules,* **1997**, *30*, 6913.
19. Hore, D; Natansohn, A; Rochon, P. *Can. J. Chem.,* **1998**, *76*, 1648.
20. Holme, NCR; Ramanujam, PS; Hvilsted, S. *Appl. Opt.,* **1996**, *35*, 4622.
21. Natansohn, A; Rochon, P. *Chem. Rev*., **2002**, *102*, 4139.
22. Nedelchev, LL; Matharu, AS; Hvilsted, S; Ramanujam, PS. *Applied optics*, in press.
23. Hvilsted, S. Unpublished results.

Chapter V

1) Han, LM; Timmons, RB; Lee, WW; Chen, YC; Hu, Z. *J. Appl. Phys*., **1998**, *84*, 439.
2) Pitois, C; Wiesmann, D; Lindgren, M; Hult, A. *Adv. Mater.,* **2001,** *13***,** 1483.
3) Gavelin, P; Jannasch, P; Wesslen, B. *J. Polym. Sci. Part A: Polym. Chem*., **2001**, *39*, 2223.
4) Jankova, K; Hvilsted, S. Book of Abstracts, IUPAC Intern. Symposium on Ionic Polymerization (IP´2001), Crete, Greece, October **2001**, p. 145.
5) Jankova, K; Hvilsted, S. *Macromolecule*s, **2003**, *36*, 1753.
6) Coessens, V; Pintaur, T; Matyjaszewski, K. *Prog. Poly. Sci*., **2001**, *26*, 337.
7) Hvilsted, S; Andruzzi, F; Kulinna, C; Siesler, HW; Ramanujam, PS. *Macromolecules,* **1995**, *28*, 2172-2183; Berg, RH, Hvilsted, S; Ramanujam, PS. *Nature,* **1996,** *383*, 505.
8) Sahlen, F; Geisler, T; Hvilsted, S; Holme, NCR; Ramanujam, PS; Petersen, JC. *Mat. Res. Soc. Symp. Proc.,* **1999,** *561***,** 57.
9) Crivello, JV; Deptolla, M; Ringsdorf, H. *Liq. Cryst.,* **1988,** *3*, 235.
10) Qiu, J; Matyjaszewski, K. *Macromolecules,* **1997,** *30***,** 5643.
11) Zisman, WA. *Contact Angle, Wettability, and Adhesion,* Advances in Chemistry Series 43, Am. Chem. Soc.: Washington DC, **1964**
12) Suh, KW; Clarke, DH. *J. Polym. Sci. Part-A1.,* **1967**, *5***,** 1671.
13) Xiang, M; Jiang, M. *Macromol. Rapid Commun.,* **1995,** *16***,** 477.
14) Se, K; Miyawaki, K; Hirahara, K; Takano, A; Fujimoto, T. *J. Polym. Sci. Part A Polym.Chem.,* **1998,** *36***,** 3021.
15) Hvilsted, S. Unpublished results.

Chapter VI

1. a] Liu, F; Ding, J; Li, M; Day, M; Robertson, G; Zhou, M. *Macromol. Rapid Commun.* **2002,** *23*, 844. b] Moreno-Manas, M; Spengler, J. *Tetrahedron* **2002**, *58*, 7769.
2. Yamabe, M. *Makromol. Chem. Macromol. Symp.* **1992**, *64*, 11.
3. Chapman, TM; Marra, KG. *Macromolecules* **1995**, *28*, 2081
4. Kim, J; Lee, W; Kang, J; Kwon, S; Kim, J; Lee, J. *Macromolecules* **2001**, *34*, 7817.
5. Miyata, T; Yamada, H; Uragami, T. *Macromolecules* **2001,** *34*, 8026.
6. Wang, J; Ober, CK. *Macromolecules* **1997**, *30*, 7560.
7. Jankova, K; Hvilsted, S. *Macromolecules* **2003**, *36*, 1753.

8. Hvilsted, S; Borkar, S; Abildgaard, L; Ventisislava, G; Siesler, HW; Jankova, K. *Polymer Preprints* **2002,** *43(2)*, 26.
9. Hvilsted, S; Borkar, S; Siesler, HW; Jankova, K. *Controlled Radical Polymerization ACS Symposium Series,* **2003**, *854*, 236.
10. Burdon, J; Westwood, WT. *J. Chem. Soc.,(C)* **1970**, *2*, 1271
11. Pitois, C; Wiesmann, D; Lindgren, M; Hult, A. *Advanced Materials* **2001**, *13*, 1483.

Chapter VII

1. Hunt, MO; Belu, AM; Linton, RW; DeSimone, JM. *Macromolecules*, **1993**, *26*,4854.
2. Affrossman, S; Hartshorne, M; Kiff, T; Pethrick, RA; Richards, RW; *Macromolecules,* **1994**, *27*, 1588.
3. Elman, JF; Johs, BD; Long, TE; Koberstein, JT. *Macromolecules,* **1994**, *27*, 5341.
4. Affrossman, S; Bertrand, P; Hartshorne, M; Kiff, T; Leonard, D; Pethrick, RA; Richards, RW. *Macromolecules,* **1996**, *29*, 5432.
5. Sugiyama, K; Hirao, A; Nakahama, S. *Macromol. Chem. Phys*., **1996**, *197*, 3149.
6. Hirao, A; Koide, G; Sugiyama, K. *Macromolecules*, **2002**, *35*, 7642.
7. Kwon, OS; Kim, YB; Kwon, SK; Choi, BS; Choi, SK. *Macromol. Chem. Physc.*, **1993**, *194*, 251.
8. Krupers, M; Moller, M. *Macromol Chem. Phys.,* **1997**, *198*, 2163.
9. Liu, F; Ding, J; Li, M; Day, M; Robertson, G; Zhou, M. *Macromol. Rapid commun*. **2002**, *23*, 844.
10. Wang, JS; Matyjaszewski, K. *Macromolecules*, **1995**, *28*, 7901.
11. Patten, TE; Xia, J; Abernathy, T; Matyjaszewki, K. *Science,* **1996***, 272*, 866.
12. Jankova, K; Chen, X; Kops, J; Batsberg, W. *Macromolecules,* **1998**, *31*, 538.
13. Ashford, EJ; Naldi, V; O'Dell, R; Billingham, NC; Armes, SP. *Chem. Comm*., **1999**, *14*, 1285.
14. Proton and Fluorine Nuclear Magnetic Resonance Spectral Data **1988** edition, Edited by Varian Instruments Ltd. Tokyo, Japan and Japan Halon Co. Ltd. Tokyo, Japan.
15. Jankova, K; Hvilsted, S. *Macromolecules*, **2003**, *36*, 1753.
16. Kajiyama, T; Satomi, N; Yokoe, Y; Kawaguchi, D; Tanaka, K; Takahara, A. *Macromol. symp*., **2000**, *159*, 35.
17. Gowariker, VR; Viswanathan, NV; Sreedhar, J. 'Polymer Science' New Age International (P) Limited Publishers, India, **1999**.

Curriculum Vitae

Name	Sachin Borkar	
Date of Birth and Place	July 26th 1975 in Pune, India	
Education		
Primary School	06/81 – 05/87	Dr. B. A. Vidyalaya School, Pune, India
Secondary School	06/87 – 06/90	Maharashtra Vidyalaya School, Pune, India
Higher Secondary School	07/90 – 06/92	Fergusson College, Pune, India
Bachelor of Science (Chemistry)	07/92 – 05/95	University of Pune, Pune, India
Master of Science (Organic Chemistry)	06/95 – 06/97	University of Pune, Pune, India
Graduate research assistant	07/97 – 12/00	National Chemical Laboratory, Pune, India
PhD Thesis	Since 01/01 Dept. of Physical Chemistry, University of Duisburg-Essen/Prof. H. W. Siesler Dept. of Physical Chemistry, University of Duisburg-Essen/Prof. M. Ulbricht Danish Polymer Centre, Technical University of Denmark/Prof. S. Hvilsted	